Inaugural dissertation

for

obtaining the doctoral degree

of the

Combined Faculty of Mathematics, Engineering and Natural Sciences

of the

Ruprecht - Karls - University

Heidelberg

presented by

Melinda Ahmels, M.Sc.

born in: Darmstadt

Oral examination: 30.05.2023

*Mastomys coucha* as preclinical model

to study macrophage-assisted DNA repair

and cross-protecting L2 based vaccination

in the same animal

Referees: Prof. Dr. Martin Müller

Prof. Dr. Frank Rösl

“The difference in winning & losing is most often, not quitting.”

- *Walt Disney* -

# Table of contents

# Summary

Non-melanoma skin cancer (NMSC) is the most commonly diagnosed skin cancer in Caucasians and develops at UV-exposed areas of the body. Particularly the development of SCCs is favoured by infection with human papillomaviruses (HPVs). HPVs have been shown to alter the immune response to prevent apoptosis of infected cells. L1-VLP-based vaccines have already been licensed to protect against high-risk HPVs, but these are limited in their cross-protection against cutaneous types. To study the impact of PV infections on both innate and adaptive immunity in detail, an immunocompetent animal model is required. *Mastomys coucha* represents such a natural preclinical model to study the development of NMSC. After infection with the species-specific *Mastomys natalensis* papillomavirus (MnPV) the animals develop benign skin tumours. During chronic UV exposure, MnPV-infected *Mastomys* develop SCCs in which *Trp53* was found to be frequently mutated, potentially influencing DNA repair mechanisms after UVB irradiation. It has been reported that macrophages are able to increase DNA repair efficiency by secreting HB-EGF (heparin-binding epidermal growth factor-like growth factor). Based on these results, the innate immune system and its influence on DNA repair mechanisms after UV irradiation were investigated in the present study. Indeed, HB-EGF was shown to increase DNA repair efficiency in *Mastomys* fibroblasts, independent of the *Trp53* status. In addition, the oncogene MnPV E7 was observed to upregulate the expression of the cytokine MCP-1 (monocyte chemoattractant protein-1) after UV irradiation, suggesting that macrophage migration and activation may be stimulated. MnPV E7 further increases expression of pro-inflammatory cytokines after UV irradiation, which resembles a chronic inflammation in persistent infection. To investigate which signalling pathways are regulated after irradiation and HB-EGF treatment, proteomic analyses were performed. The molecular changes after 24 hours were limited, suggesting that the proteins responsible for the morphologically detectable effects had already returned to their normal levels. However, the upregulation of matrix metalloproteinase-3 (MMP-3) by stimulating the MAPK/ERK-signalling pathway was observed in p53-deficient cells. This protein, which is able to cleave the preform of HB-EGF, could lead to a positive feedback loop. In the second part of this thesis, the two HPV L2-based vaccines (HPV16 RG1-VLP and CUT-PANHPVAX) were tested in *Mastomys coucha* for their cross-protection against MnPV, in comparison to a mock control or MnPV L1-VLPs. Both L2-based vaccines provided protection *in vivo*, as the viral load in hair bulbs of vaccinated animals was lower compared to those of unprotected animals. In addition, cross-reactive antibodies against MnPV L2 could be detected for both vaccines, which also had a cross-neutralising effect against MnPV pseudoviruses *in vitro*. This study proves that next-generation L2-based vaccines are able to protect against PV infections even for different genera.

# Zusammenfassung

Nicht-melanozytärer Hautkrebs (NMSC) ist der am häufigsten diagnostizierte Hautkrebs bei Kaukasiern und entwickelt sich an UV-exponierten Stellen des Körpers. Besonders die Entwicklung von SCCs wird durch eine Infektion mit humanen Papillomviren (HPV) begünstigt. Es wurde gezeigt, dass HPVs die Immunantwort verändern und die Apoptose infizierter Zellen verhindern. Zum Schutz gegen Hochrisiko-HPVs sind L1-VLP-basierte Impfstoffe bereits zugelassen, bieten jedoch nur einen begrenzten Kreuzschutz gegen kutane Typen. Um die Auswirkungen von PV-Infektionen auf die angeborene und adaptive Immunität im Detail zu untersuchen, ist ein immunkompetentes Tiermodell erforderlich. *Mastomys coucha* stellt ein solches natürliches, präklinisches Modell zur Untersuchung der Entwicklung von NMSC dar. Nach Infektion mit dem artspezifischen *Mastomys natalensis* Papillomavirus (MnPV) entwickeln die Tiere gutartige Hauttumore. Bei chronischer UV-Bestrahlung entwickeln MnPV-infizierte *Mastomys* SCCs, bei denen häufig eine Mutation von *Trp53* festgestellt wurde, die möglicherweise die DNA-Reparaturmechanismen nach UVB-Bestrahlung beeinflusst. Es konnte gezeigt werden, dass Makrophagen in der Lage sind, die Effizienz der DNA-Reparatur zu erhöhen, indem sie HB-EGF (heparin-binding epidermal growth factor-like growth factor) sezernieren. Auf der Grundlage dieser Ergebnisse wurden in der vorliegenden Studie das angeborene Immunsystem und sein Einfluss auf die DNA-Reparaturmechanismen nach UV-Bestrahlung untersucht. In der Tat konnte gezeigt werden, dass HB-EGF die DNA-Reparatur-Effizienz in Mastomys-Fibroblasten unabhängig vom *Trp53*-Status erhöht. Darüber hinaus wurde beobachtet, dass das Onkogen MnPV E7 nach UV-Bestrahlung die Expression des Zytokins MCP-1 (monocyte chemoattractant protein-1) erhöht, was darauf hindeutet, dass die Migration und Aktivierung von Makrophagen stimuliert werden könnte. Zudem erhöht MnPV E7 die Expression von pro-inflammatorischen Zytokinen nach UV-Bestrahlung, was einer chronischen Entzündung bei persistierender Infektion ähnelt. Um zu untersuchen, welche Signalwege nach Bestrahlung und HB-EGF-Behandlung reguliert werden, wurden Proteomanalysen durchgeführt. Die molekularen Veränderungen nach 24 Stunden waren begrenzt, was darauf hindeutet, dass die für die morphologisch nachweisbaren Effekte verantwortlichen Proteine bereits wieder auf ihre normalen Werte zurückgegangen waren. Allerdings wurde in p53-defizienten Zellen eine Hochregulierung von Matrix-Metalloproteinase-3 (MMP-3) durch Stimulierung des MAPK/ERK-Signalwegs beobachtet. Dieses Protein, das in der Lage ist, die Vorform von HB-EGF zu spalten, könnte zu einer positiven Rückkopplungsschleife führen. Im zweiten Teil dieser Arbeit wurden die beiden HPV L2-basierten Impfstoffe (HPV16 RG1-VLP und CUT-PANHPVAX) in *Mastomys coucha* auf ihre Kreuzprotektion gegen MnPV im Vergleich zu einer Mock-Kontrolle oder MnPV L1-VLPs getestet. Beide L2-basierten Impfstoffe boten *in vivo* Schutz, da die Viruslast in den Haarwurzeln der geimpften Tiere im Vergleich zu denen der ungeschützten Tiere geringer war. Darüber hinaus konnten für beide Impfstoffe kreuzreaktive Antikörper gegen MnPV L2 nachgewiesen werden, die auch *in vitro* eine kreuzneutralisierende Wirkung gegen MnPV-Pseudoviren hatten. Diese Studie beweist, dass Impfstoffe der nächsten Generation auf L2-Basis in der Lage sind, vor PV-Infektionen zu schützen, auch bei verschiedenen Gattungen.

# 1. Introduction

## 1.1. Infection and cancer

The cases of cancer increased during the last years and are supposed to do so continuously. Cancer develops due to uncontrollable proliferation of cells leading to outgrowth and invasive displacement of healthy tissue [1]. Investigations on molecular level over the last decades revealed that the uncontrolled proliferation is caused by mutations in the genome of tumour cells [2]. Those mutations can lead to loss or overexpression of proteins, which result in pathway dysfunction or even inactivation [3-5]. So far, different options of cancer treatment are available [6, 7]. Besides surgical removal of tumours, chemotherapy and radiotherapy [8, 9], immune therapies have been developed to prevent and treat cancer diseases [10-12].

Cancer is favoured by risk factors such as genetic predispositions, sun exposure, alcohol consumption, smoking and obesity, respectively [13]. Furthermore, previous studies have shown that among other pathogens *Helicobacter pylori*, hepatitis B-virus and human papillomaviruses (HPV) contribute to cancer development in 13% of cases worldwide [14]. So far, additional viruses have been identified to support the development of cancer such as, human T-lymphotropic virus-1 (HTLV-1), hepatitis C virus as and the Kaposi's sarcoma herpesvirus (KSHV) [15].

## 1.2. Papillomaviruses

The first proof that HPV is a major risk factor for the development of cervical cancer could be shown in 1984 by the detection of HPV in tumour cells [16, 17].

Until today, over 200 different types of HPV have been described [18]. Based on their sequence HPVs are classified into the genera alpha, beta, gamma, mu and nu. They infect human epithelial cells, more accurately basal keratinocytes. While β-HPVs and γ-HPVs infect cutaneous squamous epithelia, α-HPVs infect mucosal sites and are related to anogenital cancers (cervical, anal, penile, vulvar, vaginal) [19]. The mucosal HPV types are further categorized as "high-risk" or "low-risk" types depending on their ability to contribute to the development of cancer [19].

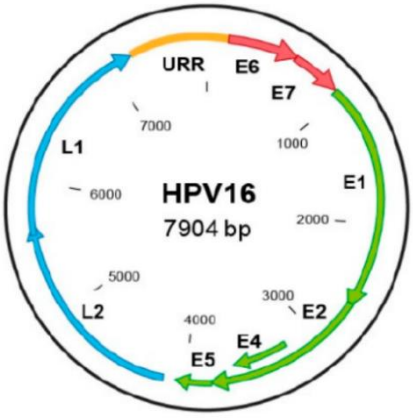


**Fig. 1.2.1 Genomic organization of human papillomavirus 16.** HPVs consists of 8 kb and different open reading frames (ORFs) (shown in solid bars). The expression of the early genes (E1, E2, E4, E6 and E7) changes over the viral life cycle. The late genes (L1 and L2) encode for proteins encapsulating the viral DNA. The figure is adapted from [188].

So far, 12 high-risk HPV types (HPV 16, 18, 31, 33, 35, 39, 45, 51, 52, 56, 58 und 59) have been rated as carcinogenic by the World Health Organisation (WHO) and International Agency for Research on Cancer (IARC) [20].

Papillomaviruses are small, non-enveloped double-stranded DNA viruses with a size about 8 kb and eight or nine genes that are divided into early (E) and late (L) gene regions (Fig. 1.2.1). The early regions encode the early proteins E1-E7, which are synthesized throughout the whole viral life cycle [21]. L1 and L2 code for viral capsid proteins encapsulating the viral DNA with L2 being hidden inside the virion. For virus entry, epithelial traumata are needed, resulting in exposure of the basement membrane on which heparan sulfate proteoglycans (HSPGs) are located. After binding of the L1 major capsid protein to those HSPGs, conformational changes of the capsid proteins are induced. This reveals the N-terminus of the L2 protein, which is then cleaved by furin leading to the exposure of a secondary receptor binding site of L1 [22]. This cleavage site is conserved among all PVs and cleavage is required for infection [22, 23].

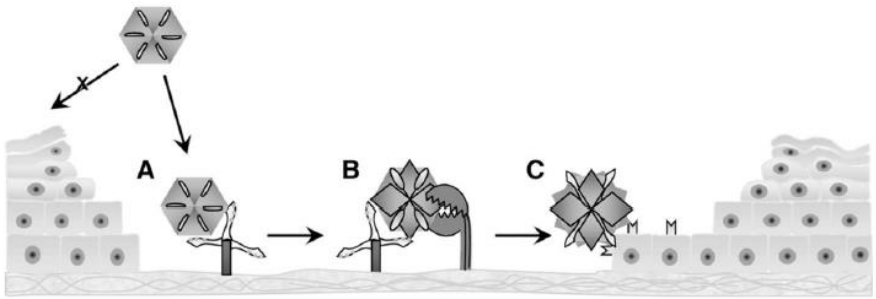


**Fig. 1.2.2 Binding of virions to extracellular sites.** Basement membrane is exposed upon epithelial trauma. The virions bind to heparan sulfate proteoglycans (HSPGs) presented on the basement membrane. (**A**) After binding *via* the L1 major capsid protein, conformational changes are induced exposing the furin cleavage site of the L2 protein. (**B**) Upon cleavage, a region of L1 is exposed which binds to an unidentified receptor (**C**). The figure is adapted from [187].

After infection, the viral genome is transported to the nucleus of the host cell and persists as episomal DNA [24, 25]. However, HPVs have also the capability to integrate their DNA into the host genome [26]. The viral life cycle is divided into two stages: a non-productive and a productive one. During the non-productive stage the viral gene expression is low, 50-100 copies of viral DNA per cell can be detected [27]. In the maintenance phase, the E2 oncoprotein contributes to the synchronous replication of the viral episomal DNA and the host genome, while the helicase E1 is required for efficient viral DNA replication [28]. Infected cells undergo differentiation leading to a productive viral cycle.

Proliferation of infected cells is stimulated by E5, E6 and E7. Both, high- and low-risk HPV E6 can bind p53, but in high-risk HPVs, the oncoprotein forms a complex with p53 and induces ubiquitination. In that way, E6 prevents premature cell death by degradation of p53 [29, 30]. This mechanism allows resistance of the host cell to apoptosis and increased chromosomal stability. Additionally, the binding of the retinoblastoma (Rb) protein and the transcription factor E2F can be disrupted by E7. Due to this mechanism, S-phase promoting gene transcription is activated [31]. HPV16 E5 targets different transmembrane proteins (e.g., epidermal growth factor receptor (EGFR) and colony-stimulating factor-1 (CSF-1)) resulting in mitogenic stimulation by complex formation [32]. By targeting pathways in the host cell related to apoptosis,

cell cycle and proliferation, HPV oncogenes enable persistent infection of the host cell and directly contribute to carcinogenesis.

## 1.3. HPV infection and non-melanoma skin cancer

The most frequently diagnosed cutaneous cancer in Caucasians is non-melanoma skin cancer (NMSC) [33]. The major risk factor for the development of NMSC is UV light [34]. NMSC can be classified into basal cell carcinomas (BCCs) [35] and squamous cell carcinomas (SCCs) [36]. The development of both tumour types is favoured by UV light, but in the case of SCCs, β-HPV infections play an important role in carcinogenesis [37]. While α-HPVs are sexually transmitted, infection with β-HPVs occurs during early childhood by skin to skin contact [38]. So far, more than 40 β-HPVs have been identified in the skin of healthy individuals [39]. HPV5 and HPV8 are the first discovered and therefore mostly investigated β-HPVs [40, 41]. Previous studies describe the induction of cutaneous SCCs via 'hit-and-run' mechanism [42]. This hypothesis states that papillomaviruses play an important role in the initiation of skin cancer development but disappear when the host cells have acquired enough mutations to be able to grow uncontrolled.

UV irradiation primarily induces cyclobutane pyrimidine dimers (CPDs), DNA intra-strand crosslinks [43]. Those crosslinks are repaired cell cycle dependently through nucleotide excision repair (NER) or the Fanconi anaemia (FA) pathway [44], but can also result in DNA double-strand breaks (DSBs) due to replication fork collapse [45]. To ensure that the UV light-exposed cells are still able to proliferate, HPVs can interfere with DNA repair mechanisms [50]. While E6 of high-risk α-HPVs degrades the protein p53 [46], the "guardian of the genome", β-HPVs E6 have developed different mechanisms to affect p53-related pathways. For example, E6 of the HPVs 17, 38 and 92 can bind and stabilise p53 supporting its transcriptional activity [47-49]. Another mechanism described for HPV5, HPV8 and HPV38 E6 leads to the destabilisation of p53 contributing to continued proliferation [30]. Furthermore, studies have shown that β-HPV E6 directly interacts with DNA damage repair mechanisms [50].

Furthermore, E7 influences proliferation and avoidance of apoptosis by targeting the protein Rb, a tumour suppressor. HPV38 E7 inactivates pRb in keratinocytes, leading to uncontrolled G to S phase transition [51]. This interplay with the intracellular network of infected cells enables PVs to enhance viral replication and further support carcinogenesis.

## 1.4. HPV and the immune system

Not only DNA repair but also immunological escape mechanisms are targets of HPV oncogenes to support survival of infected cells.

The immune system is divided into two main components: the innate and the adaptive immune system [52]. The innate immune system is the body's first line of defence against pathogens, it responds quickly and non-specifically to a wide variety of pathogens [53]. In contrast, the adaptive immune system is a more specialised and sophisticated mechanism that develops over time as the body encounters and responds to specific pathogens [54, 55]. It involves the activation of lymphocytes, which produce antibodies and other immune molecules that target and eliminate specific pathogens [55].

HPVs aim to avoid clearance by the immune system and to favour persistent infection. Therefore, HPVs have developed several strategies: besides downregulation of chemokine (C-C motif) ligand 20 (CCL20), which stimulates migration of epidermal Langerhans cells [56, 57], HPVs can interfere with cytokine expression by targeting toll-like receptors (TLRs), their expression as well as their signalling pathways [58, 59]. TLRs play an important role in the innate immune system by recognition of pathogen-associated molecular patterns (PAMPs) and following regulation of expression of inflammatory cytokines [58, 60, 61]. Besides targeting recognition receptors, HPV oncoproteins downregulate the NF-κB signalling pathway promoting the persistence of the HPV infection [62]. Furthermore, cytokines such as IL-1β, which usually acts in pro-inflammatory responses, has been shown to be degraded by HPV16 E6 forming a complex with ubiquitin ligase E6-AP in keratinocytes [63]. By maintaining a viral reservoir with low replication numbers in the host, HPVs are able to avoid the detection by the immune system [64]. During the productive stage, the virus takes advantage of the outer layer of the epithelium, which shows low density of antigen presenting cells and therefore enable high viral replication and generation of viral proteins without triggering the immune response [64].

So far, several HPV strategies have been described to reprogram the local immune system by infected cells and leading to chronic inflammation favouring carcinogenesis. To prevent the carcinogenesis, vaccines have been licensed priming the adaptive immune system against HPV infection.

## 1.5. HPV vaccines

In 2007, the bivalent vaccine Cervarix® (against HPV16/18) was licensed while in 2006 the quadrivalent Gardasil® (against HPV6/11/16/18) and 2015 the further developed Gardasil-9® were licensed in Europe, protecting against nine HPV types (HPV6/11/16/18/31/33/45/52/58) [65]. Successful protection against HPV infection was proven by 87% efficacy of bivalent and quadrivalent vaccines against HPV16/18 in HPV-naïve women [66]. For the development of the vaccines, HPV L1 major capsid protein is expressed either in yeast (Gardasil®) or insect cells (Cervarix®) [67]. The recombinant L1 protein can self-assemble to virus-like particles (VLPs), which do not contain viral DNA and the L2 protein and are therefore non-infectious.

Those VLPs effectively trigger B-cell immunological response and therefore the adaptive immune system [68]. VLPs composed of L1 induce high neutralizing antibody titres, but protection and efficacy are restricted to the included types [69]. Limited cross-protection of the bivalent and the quadrivalent vaccine could be proven only for closely related HPV types (HPV31, HPV33 and HPV45). To induce cross-reactivity and therefore protection against more PV types, vaccines have been developed based on the minor capsid protein L2. Those vaccines showed the ability to induce genotype cross-neutralizing antibodies in animal PV models providing efficient protection against papillomavirus-induced infection [70-73]. This phenomenon can be explained by the highly conserved epitopes in the N-terminus of L2 between aa 11-200 [73, 74]. One epitope is the RG1 epitope of HPV16 L2 (aa 17-36). Immunisation with a vaccine based on RG1 resulted in broad cross-neutralisation activity against other papillomavirus types [75]. Antibody titres raised against the L2 monomer are relatively low compared to type-specific VLP-induced antibody titres [76]. To enhance neutralizing antibody titres different strategies have been pursued: e.g., besides inserting epitopes in a L1 surface loop [77], bacteriophages have been used as scaffold for L2 epitope display [78, 79].

However, newly developed L2 based vaccines need to be tested carefully by *in vitro* as well as *in vivo* studies. The challenge here is to find a suitable, immunocompetent preclinical model, in which the viral life cycle and cross-reactivity can be observed and investigated.

## 1.6. Animal models for the investigation of HPV and carcinogenesis

To investigate the role of β-HPV in carcinogenesis, the most widely used *in vivo* models are transgenic (tg) mouse models. These models allow the expression of the complete early region of the virus or individual viral oncogenes. In most cases, these genes are expressed under control of a keratin promoter to ensure that the expression is restricted to the cells of interest. For instance, Schaper *et al.* could show in their HPV8 tg model, expressing the early gene region under the keratin 14 promotor, that single- or multifocal benign tumours develop in the skin [80]. Using HPV8 E6 tg mice, tumours were not only induced by UVR or wounding but also developed spontaneously comparable with transgenic mice with the complete early region (CER) (HPV8-CER) [81]. Furthermore, it could be observed that the repair of thymine dimers took longer in HPV8 E6 positive animals compared to wildtype mice [82] resulting in the development of tumours. Investigation of HPV38 E6/E7 tg mice showed enhanced proliferation of the skin, but no spontaneous development of tumours during their life span. Only after two-stage carcinogenic treatment, the animals developed *inter alia* squamous cell carcinomas while this effect was not observed in non-transgenic animals [83]. Those models enable to investigate the roles of the different oncogenes *in vivo* but lack the possibility to observe the whole viral life cycle.

To fill this gap, the animal model *Mastomys coucha* (Fig. 1.6.1, A) offers the opportunity to investigate viral infection, carcinogenesis, and vaccination against PV.

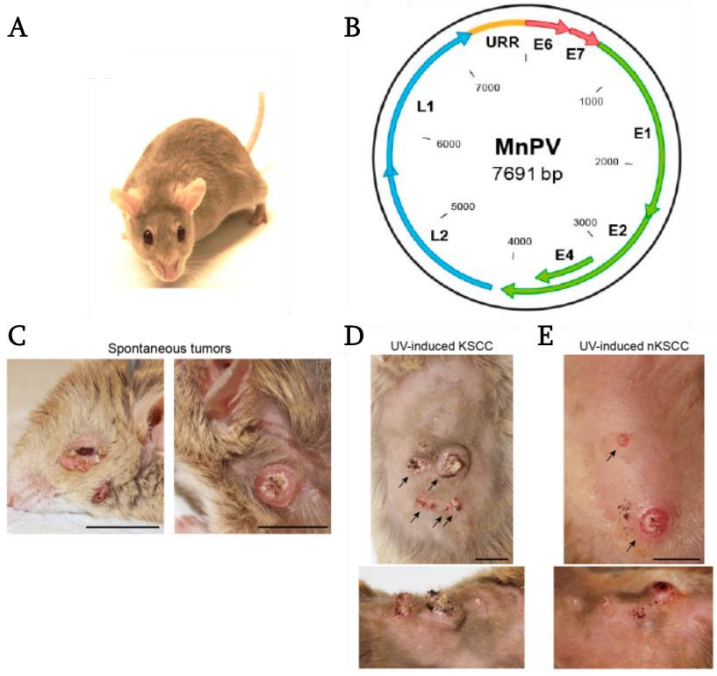


**Fig. 1.6.1 MnPV and development of skin cancer in the animal model *Mastomys coucha*.** *Mastomys coucha* (**A**) are naturally infected with the species-specific *Mastomys natalensis* papilloma virus (MnPV) (**B**). MnPV has a size of ca. 8 kb, harbouring an upstream regulatory region (URR) and encoding early genes (E1, E2, E4, E6 and E7) as well as the capsid proteins (L1, L2). Skin lesions can develop spontaneously (**C**). The animals serve as model for skin cancer since they develop UV-induced keratinizing squamous cell carcinomas (KSCCs) (**D**) as well as UV-induced non-keratinizing squamous cell carcinomas (nKSCCs) (**E**). The figure is adapted from [91].

The species *Mastomys* is phylogenetically related to rat and mouse [84]. Even though *Mastomys* have been used since 1939 as a model for plaque [85], the discrimination between *Mastomys coucha* and *Mastomys natalensis* was first made in 1977. In total, eight species were described so far. In 1978, a virus with structural characteristics of PVs was isolated from keratinizing keratoacanthomas as well as papillomas and keratinizing squamous cell carcinomas from *Mastomys natalensis* and therefore named *Mastomys natalensis* papillomavirus (MnPV) [86]. Years later, it was found that the virus was not detected in *Mastomys natalensis* but in *Mastomys coucha.* Both species are morphologically similar but differ on molecular levels [87-89].

MnPV has a size of ca. 8 kb (Fig. 1.6.1, B) and can be found in the nuclei of infected keratinocytes of the skin as well as in keratinized skin tumours [90]. As all PVs, it harbours an upstream regulatory region (URR). Furthermore, open reading frames coding for the early genes E1, E2 and E4 and the early oncogenes E6 and E7 as well as for the late genes L1 and L2, have been described. In contrast to α-HPV, MnPV is a ι-type, which does not contain an E5 open reading frame. The cutaneous MnPV is transferred from the parents to their offspring in early lifetime. Therefore, it mimics the infection process in humans and naturally infected *Mastomys coucha* can spontaneously develop skin lesions (Fig.1.6.1, C). As an immunocompetent animal model, *Mastomys coucha* allows investigating the immune response as well as changes in the immune system upon papillomavirus infection.

In previous work, the development of UV-induced SCCs was proven in the animal model *Mastomys coucha* [91]. MnPV-infeced animals irradiated with UVB developed tumours earlier and more often than virus-free or unirradiated animals. Here, two types of UV-induced SCCs were described: keratinizing SCCs (KSCCs) (Fig. 1.6.1, D) as well as non-keratinizing SCCs (nKSCCs) (Fig. 1.6.1, E). While well-differentiated KSCCs showed high viral loads and furthermore, expression of MnPV oncogenes could be detected, nKSCCs were poorly differentiated, had a low viral load and viral oncogenes did not show transcriptional activity.

In human skin cancer *TP53* is the most frequently mutated gene [92] with R273 and P278 in p53 being common mutated in the context of UVB exposure and SCCs [93, 94]. Therefore, the tumours were analysed regarding their *Trp53* status. Sequencing of the cDNA of the tumours revealed that nKSCCs showed significantly more mutations in *Trp53* than KSCCs. Similar to the hot-spot mutations in human skin cancer, two hot-spot mutations were detected in *Mastomys coucha Trp53*: R266 and P271, both located in the DNA-binding domain.

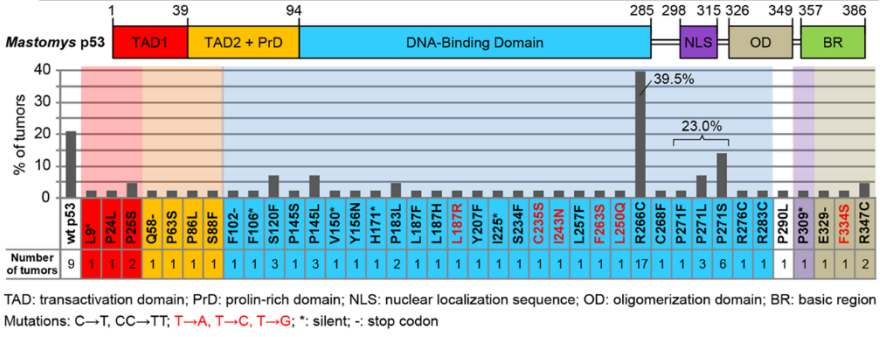


**Fig. 1.6.2 *Trp53* status in UV-induced SCCs in *Mastomys coucha*.** Mutations in *Trp53* identified in squamous cell carcinomas (SCCs). The number of tumours in which the mutation has been detected is indicated. The figure is adapted from [91].

Previously, spontaneously immortalized *Mastomys coucha* keratinocytes (Kera5) and two *Mastomys coucha* fibroblast cell lines (MaFi132 and MaFi191) were isolated from *Mastomys* skin and can be used for *in vitro* investigations [95]. Kera5 and MaFi132 harbour a point mutation in *Trp53,* which leads to an alternative splicing, resulting in the loss of p53. In contrast, MaFi191 express p53 wildtype. Based on those findings, Dr. M. Meister in our group induced a point mutation in MaFi191 usually harbouring p53 wildtype and developed the cell line MaFi191 R266C. Using this cell line, the aim was to investigate the role of mutant p53 in the formation of nKSCC. Those cells can be used as *in vitro* model to investigate the influence of the *Trp53* status on skin carcinogenesis and to investigate the influence of the *Trp53* mutation on invasiveness, which can also be favoured by defined physiological proteins such as heparin-binding epidermal growth factor-like factor (HB-EGF).

## 1.7. Heparin-binding epidermal growth factor-like factor (HB-EGF)

HB-EGF (heparin-binding epidermal growth factor-like factor) was first described 1991 as a component of the supernatant of macrophage-like U937 cells [96]. It was isolated using a heparin-affinity chromatography and described as a new member of the EGF (epidermal growth factor) family due to 40% sequence identity with human epidermal growth factor (EGF). By binding to the epidermal growth factor receptor (EGFR) and ErbB4/HER4, this protein contributes to the stimulation of different physiological processes such as proliferation, wound healing and adipogenesis [97]. HB-EGF is mitogenic for different cell types including keratinocytes and fibroblasts [98, 99]. Normally, low levels of HB-EGF are expressed in the skin but there is an increase in wound healing processes [100] stimulating keratinocytes to migration and invasiveness. Furthermore, it is upregulated in a number of cancer types, e.g., breast cancer and melanoma [101].

HB-EGF is synthesized as pro-peptide, which is then processed by various different ADAMs (a disintegrin and metalloproteinases) and MMPs (matrix metalloproteases) (ADAM 9, 10, 12 and 17, MMP -3 and -7) depending on the stimulus and treatment of the cells [102-105] (Fig. 1.7). In the HB-EGF precursor, the signal peptide, juxtamembrane and transmembrane domains have the highest degree of sequence conservation between different species, which indicates strong selective pressure on these regions [106, 107]. So far, human HB-EGF has been the best investigated. Its gene on chromosome 5 consists of 5 introns and 6 exons and the same has been reported for the murine HB-EGF gene on chromosome 18 [108, 109]. The human protein harbours two sites of O-linked glycosylation while only one site is conserved in rat and mouse forms [106]. Furthermore, for human HB-EGF different N-termini were identified (processed at 63, 72, 73 76 and 81 aa), but only 63, 73 and 74 aa have been shown to be biological active [96].

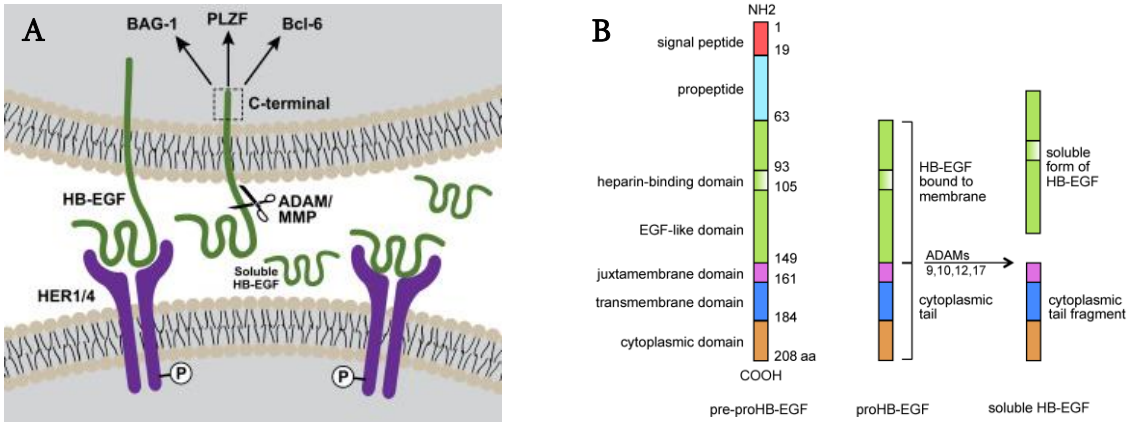


**Fig. 1.7 Location and structure of HB-EGF.** (**A**) The pro-form of HB-EGF is membrane bound and can act as diphtheria toxin receptor. After cleavage by different metalloproteases HB-EGF becomes soluble and binds to the EGFR (HER1) and HER4 leading to stimulation of e.g., proliferation (adapted from [105]). (**B**) HB-EGF is synthesized as pre-pro-peptide containing a signal peptide. Besides the heparin-binding domain, HB-EGF consists of an EGF-like, a juxtamembrane, a transmembrane and a cytoplasmic domain. proHB-EGF is a membrane bound protein which can be cleaved by different ADAMs (a disintegrin and metalloproteinase) and MMPs (matrix metalloproteases). Cleavage results in a cytoplasmatic fragment and soluble HB-EGF (here shown exemplary for human HB-EGF). The figure is adapted from [107].

Biologically active human HB-EGF has been shown to be cleaved at $Pro_{148}$-$Val_{149}$, at $Glu_{151}$-$Asn_{152}$ and at $Arg_{62}$-$Arg_{63}$ [103, 110, 111] and cleavage has also been reported for murine HB-EGF [110]. The intracellular domain is processed by a protease as well, which remains to be unidentified. The resulting carboxy-terminal domain can translocate to the nucleus where it induces the export of promyelocytic leukaemia zinc finger (PLZF), a transcriptional repressor [112], out of the nucleus. The repressor stimulates DNA replication by either induction of cyclin D transcription [112] or by induction of cyclin A expression [104].

However, HB-EGF cannot only be synthesised by epithelial cells, but also by immune cells stimulating nearby cells in a paracrine manner by binding to the EGF receptor [113-115].

### 1.7.1. HB-EGF and stimulation of EGFR

HB-EGF is one of seven EGFR ligands, and it can bind in an autocrine (binding of the membrane bound ligand to the receptor on the same cell), a paracrine (binding of the soluble product to a nearby cell) and a juxtacrine (binding of the membrane bound ligand to the receptor of a close cell) mode [116]. The pro-peptide of HB-EGF itself can function as a juxtacrine growth factor and additionally, in human cells, it can act as diphtheria toxin receptor [117]. The cleaved soluble product can stimulate the EGFR in an autocrine or paracrine manner.

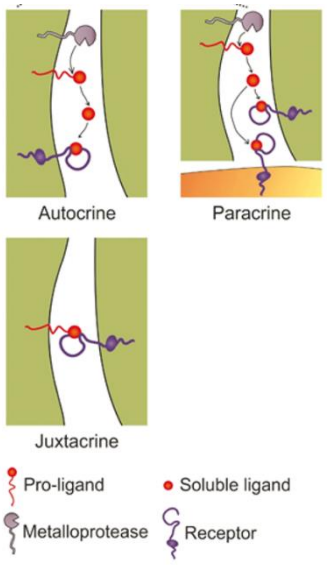


**Fig. 1.7.1.1 EGFR and its different kinds of stimulation.** Depending on environment and ligand the EGFR can be stimulated in different ways. When the ligand is released by a cell and binds to the receptor of the same cell, the cell is stimulated in an autocrine manner. Juxtacrine stimulation describes binding of a membrane bound ligand to the receptor on another cell. Cleavage of the ligand from the cell surface and stimulation of the receptor by the soluble product is described in the paracrine mechanism. The figure is adapted from [116].

The EGFR is a transmembrane glycoprotein, which has an extracellular domain as well as an intracellular domain. The extracellular domain serves as ligand binding domain, while the tyrosine kinase activity of the intracellular domain is stimulated upon ligand binding to the extracellular domain [118]. Stimulation of the EGFR results in dimerisation followed by its phosphorylation and activation of different pathway signalling mechanisms [119].

EGFR is overexpressed in different cancers e.g., head and neck cancer [120, 121], which results in resistance against radiotherapy or chemotherapy. Activation of pathways, such as the ERK/MAPK-pathway *via* the EGFR results in phosphorylation of the corresponding proteins involved in control of e.g., cell cycle progression, enhanced tissue invasion or proliferation [122, 123]. The activation of the ERK/MAPK-pathway through the EGFR receptor induces a signal cascade involving Ras, Raf as well as ERK1/2 (extracellular-signal-regulated kinase 1/2). This results in the translocation of phosphorylated ERK1/2 into the nucleus where it activates various transcription factors [124], which can bind to the EGFR to induce an autocrine activation loop. This in turn stimulates the EGFR-dependent PI3K/AKT signalling pathway [125].

Besides the stimulation of proliferation, the EGFR contributes to the regulation of DNA repair pathways [126]. E.g., EGF signalling contributes to the gene expression of the repair enzyme X-ray repair cross-complementing protein 1 (XRCC1) [127] and therefore influences DNA repair *via* non-homologous end-joining (NHEJ).

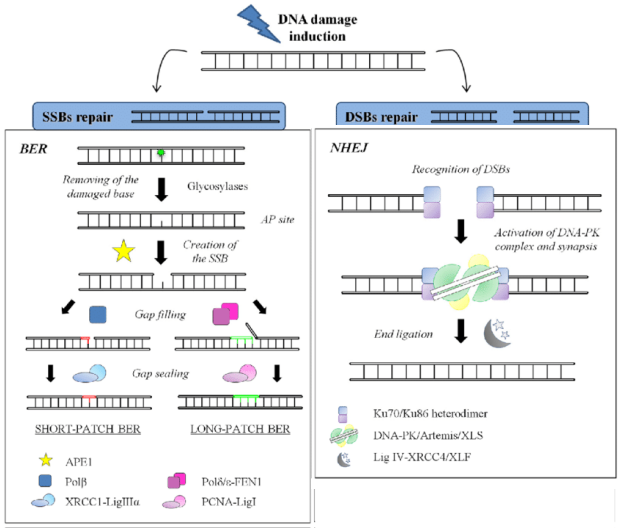


**Fig. 1.7.1.2 DNA repair mechanisms.** Depending on the induced cell damage and the cell cycle different DNA repair mechanisms are activated. Base excision repair (BER) mechanisms contribute to the repair of single strand breaks (SSBs), while non-homologous end-joining (NHEJ) is needed to repair DNA double strand breaks (DSBs) The figure is adapted from [129].

XRCC1 is not only involved in NHEJ, but also in the repair of single strand breaks (SSBs) via base excision repair (BER) [128, 129] (Fig. 1.7.1.2). To investigate the regulation of those pathways, techniques such as Western blot and ELISA can be performed. Those tools allow detecting defined proteins but are limited in defining their levels [130, 131]. For analysis of complete and complex protein mixtures with high sensitivity, the so-called "proteomics" approaches have been developed [132].

## 1.8. Proteomics

A powerful tool to study complex protein- and peptide mixtures in a qualitative and quantitative manner to gain a deeper understanding of the whole proteome in a cell provides proteomics using mass spectrometry (MS). Multiple different MS-based strategies and technologies exist and continuously contribute to the current understanding of all cellular processes. A widely used strategy for the analysis of a proteomes is called bottom-up proteomics, or shotgun proteomics [133]. In this approach, proteins are enzymatically digested into peptides before being separated by liquid chromatography and analysed by tandem-MS (MS/MS) (Fig. 1.8).

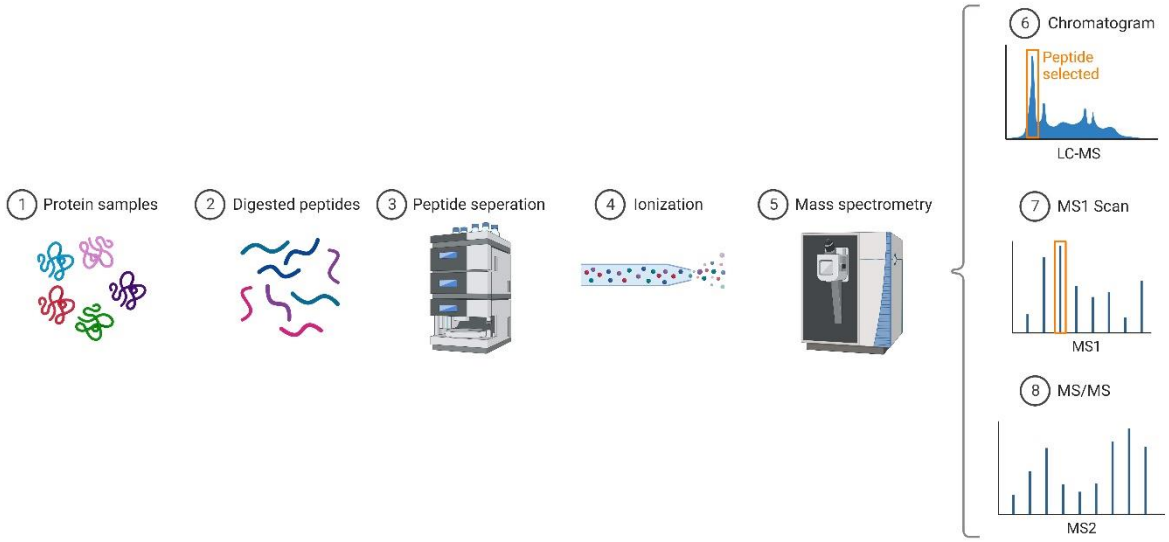


**Fig. 1.8 Schematic representation of the LC-MS/MS workflow.** Extracted proteins are separated and enzymatically digested. By liquid chromatography (LC) peptides are separated by their chemical properties before the ionized peptides are analysed by mass spectrometry (MS). The resulting spectra from MS are analysed in two scans (MS1 and MS2) allowing the identification of proteins. The figure was generated by using BioRendr.com.

Liquid chromatography can achieve chemical separation of peptide mixtures, which increases the rate of identification and quantification by reducing the sample complexity and increasing measurement time. In order to perform mass spectrometry, the molecules in the analyte need to be ionized and transferred into the gas phase. Biomolecules such as peptides and proteins are ionized usually through electrospray ionization (ESI) [134] to avoid excessive fragmentation. Mass analysers like linear ion traps, orbitraps and time of flight detectors [134, 135] measure the mass over charge ratio (m/z) of ions in the mass spectrometer.

The use of tandem mass spectrometry (MS/MS) allows for even more specific and sensitive analysis since masses of peptide ions are first scanned in an initial MS-round called MS1. Based on this MS1-analysis, peptide ions of specific masses, also called precursor ions, are subsequently selected and fragmented into smaller ions.

Peptide sequences fragments are analysed in a second MS (MS2) to enables the identification of the amino acid sequence of a peptide based on its fragmentation spectra. This allows for the determination of the exact structure and identity of the compounds in the mixture [136].

For the selection of precursor ions there is one main approach in proteomics: the data-dependent acquisition (DDA). DDA is the commonly used mode in proteomics that involves the acquisition of spectra from a sample in a sequential manner, with the selection of the next peptide to be fragmented based on the previous spectrum. In DDA mode peptide ions with the highest intensities are selected [137].

The inference of peptides and proteins from such spectral data requires complex bioinformatics tools. MaxQuant [138] is a common software tool for quantitative proteomics analysis, developed by the Max Planck Institute of Biochemistry. It allows identification and quantification of peptides and proteins in complex samples described by label free quantification (LFQ) [139]. This method relies on the comparison of the intensity of peptides across multiple samples to determine their relative abundance. After identification of the proteins, different programs, e.g., R, Perseus and ingenuity pathway analyses (IPA) can be used to perform statistical analyses and to identify predicted regulation of proteins comparing the proteome of different samples to each other. Furthermore, those programs enable assigning proteins to signalling pathways and to define their predicted regulation [140-142].

To compare the relative abundance of proteins between two conditions the log fold change (logFC) is used as a statistical measure. It is calculated by taking the logarithm (usually base 2) of the ratio of protein abundance in one condition compared to another. A positive logFC indicates that a protein is more abundant in the first condition, while a negative logFC indicates that it is more abundant in the second condition. The p-values further shows whether these different protein levels are statistically significant (typically less than 0.05) and indicates that the observed difference is unlikely to have occurred by chance alone [143]. Another statistical measure used to describe the regulation of proteins and predicted pathways is the z-score, which compares a value's relationship to the mean of a group of values. A z-score of 0 indicates that the data point's score is identical to the mean score, while a value of 1 indicates that a value is one standard deviation from the mean. Those z-scores can be positive or negative, indicating that the score is above or below the mean. Using the z-score, the significance of differently regulated e.g., proteins and pathways within different samples can be described [144].

In summary, proteomics is a powerful tool, which allows identifying the complex proteome of cells. This provides the opportunity in this work to investigate pathways stimulation upon DNA damage induction and HB-EGF treatment, based on a previous study from our collaboration partner.

## 1.9. HB-EGF and DNA damage repair

Previously, our collaborating lab in Israel (Prof. Dr. Rachmilewitz) detected a new mechanism: upon DNA damage induction by diethylnitrosamine (DEN) injection in murine liver, macrophages infiltrated to damaged sites and released the protein HB-EGF (Fig. 1.9) [114], resulting in lower levels of residual DSBs. Subsequently, the stimulation of EGFR signalling activity was identified as key player in enhanced DNA repair efficiency [145].

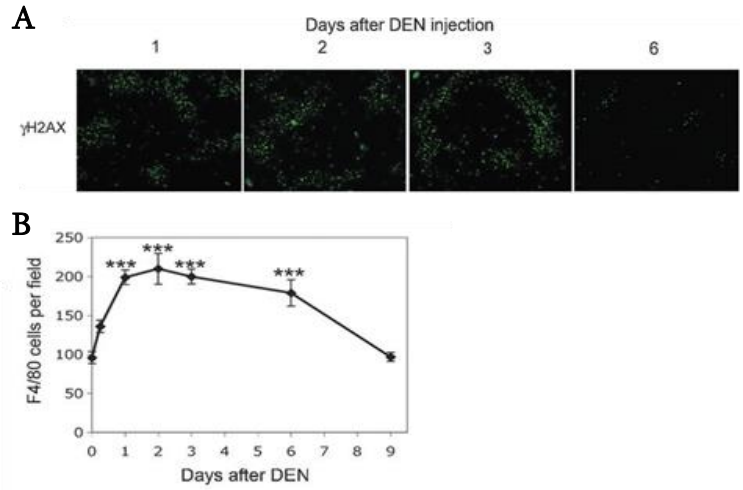


**Fig. 1.9 Recruitment of macrophages to damaged sites.** (**A**) The induction of DNA damage in murine lives was visualized by staining for γH2AX. (**B**) By staining for F4/80 the recruitment of macrophages could be shown (adapted from [114].

Those findings indicate that damaged cells send signals e.g., in form of cytokines, to induce an immune response and activate the immune system. Here, the unique role of immune cells in maintaining genome integrity and further the impact of the EGFR ligand HB-EGF on not only proliferation but also DNA repair has been identified.

In our animal model *Mastomys coucha*, the development of skin carcinogenesis induced by UV light and promoted by MnPV infection was observed. Furthermore, mutations in *Trp53* in tumour cells were detected. Here, we suggest that the UV-induced DNA damage is inefficiently repaired due to MnPV-infection, leading to changes in the immunological environment and therefore interference with HB-EGF function.

## 1.10. Aims of the thesis

My work focuses on investigations of the immune system in our animal model *Mastomys coucha*. Based on the division of the immune system into innate and adaptive immune response, this work is divided into two chapters:

### Chapter 1 – Innate immunity

Macrophage-derived HB-EGF was previously identified as a key player in DNA repair efficiency, connecting the innate immune response to DNA repair mechanisms. In my thesis, I aim to clarify whether the concept of macrophage-assisted DNA repair can be transferred to the animal model *Mastomys coucha* in the context of UVB and MnPV induced skin carcinogenesis. Therefore, the following conditions need to be adjusted (Fig. 1.10):

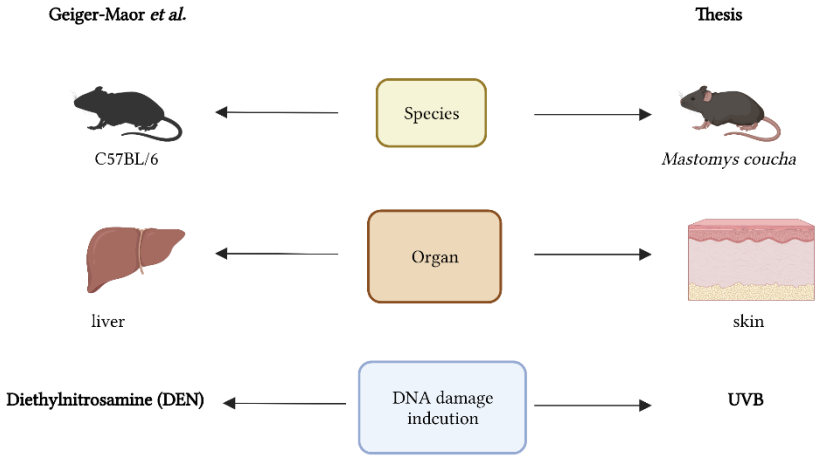


**Fig. 1.10 Transfer of the concept of macrophage-assisted DNA repair to the animal model *Mastomys coucha*.** Geiger-Maor *et al.* [114] investigated the concept of macrophage-assisted DNA repair in the liver of C57BL/6 mice upon DEN (diethylnitrosamine) injection. In the present work, this concept will be examined in the context of UVB irradiated *Mastomys* skin. The figure was generated by BioRendr.com.

The following tasks were addressed:

I. Developing tools to enable the detection of HB-EGF in *Mastomys* cells.

II. Investigation which cytokines are expressed in keratinocytes, responsible for the recruitment of immune cells to UV damaged areas and if the expression pattern changes upon irradiation and MnPV-infection.

III. Examination whether HB-EGF enhances DNA repair efficiency upon UVB irradiation in cells from animal model *Mastomys coucha*. Furthermore, the role *Trp53* in this scenario.

IV. Identification of HB-EGF stimulated pathways in *Mastomys* cells in relation to the *Trp53* status.

## Chapter 2 – Adaptive immunity

In this part of the thesis, priming the adaptive immune system for PV infection by vaccination is investigated. Here, examination of the cross-protective capacity of two L2-based vaccines in *Mastomys coucha* is performed. The vaccines were developed and provided by the lab of Prof. Dr. Martin Müller and Prof. Dr. R. Kirnbauer. This pilot study should clarify whether HPV L2-based vaccines can induce cross-reactivity against MnPV in *Mastomys coucha* as a model for other PV types and if protection against carcinogenesis is induced. Therefore, the following tasks were addressed:

I. Investigation of the development of neutralizing and protecting antibodies during immunisation.

II. Determination of the viral load and protection against MnPV infection to investigate whether vaccines can induce cross-protection in an infection model with its genuine PV.

# 2. Results

## Chapter I: Innate immunity

### 2.1. Tools to enable the detection of HB-EGF in the model system *Mastomys coucha*

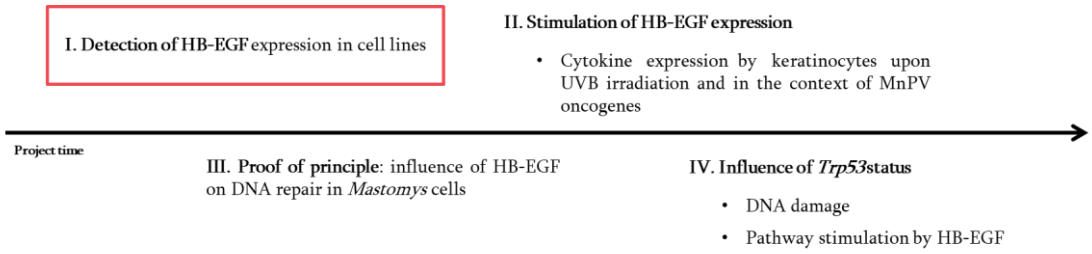


In the previous study from Geiger-Maor *et al.*, macrophage-derived HB-EGF was identified as a key player in enhancing DNA repair efficiency in murine liver cells as well as in damaged human fibroblasts [114].

The present study is aimed at analysing whether this concept can also be transferred to *Mastomys* skin. For this purpose, tools needed to be established for the detection of *Mastomys* HB-EGF. Therefore, commercial antibodies were tested for their cross-reactivity. In a first step, positive controls were designed and cloned to test the antibody reactivity.

#### Cloning of *Mastomys* HB-EGF

As antibodies against *Mastomys* HB-EGF are not established, the cross-reactivity of antibodies directed against other species had to be tested. Therefore, a sequence alignment [146] of rat, human, mouse and *Mastomys* HB-EGF was performed and revealed that the human and *Mastomys* sequences show 81% identity, while rat and *Mastomys* have 93% and *Mastomys* and mouse share 90% identity (Fig. 2.1.1., A). Even though rat and *Mastomys* HB-EGF share the highest identity, murine and *Mastomys* HB-EGF were cloned since working antibodies against murine HB-EGF were already established.

HB-EGF cDNA was isolated from *Mastomys* ear tissue and from murine 308kera cells and cloned into the pPK-CMV-E3 vector. A C-terminal HA-tag was included, which allows the detection of HB-EGF cleavage products independently from commercial HB-EGF antibodies. It has been reported that HB-EGF can be cleaved by different ADAM and matrix metalloproteinases, therefore different cleavage products were expected (Fig. 2.1.1, B).

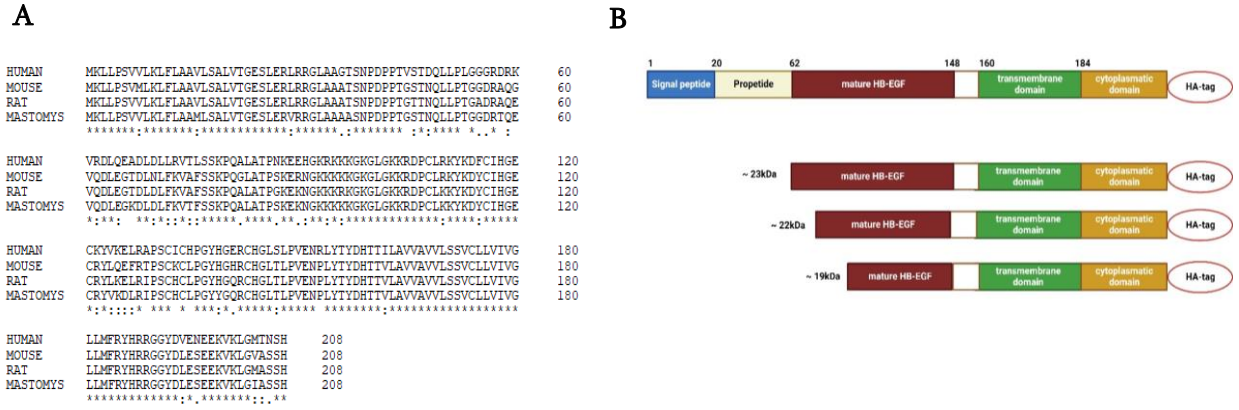


**Fig. 2.1.1 Protein sequence of HB-EGF and scheme of cloned HB-EGF** (**A**) Alignment of protein sequences from human, rat, mouse and *Mastomys* HB-EGF. Asterisks (*) indicate positions of fully conserved residues, while colons (:) mark the conservation between groups of strongly similar properties. Periods (.) indicate conservation between groups of weakly similar properties. Alignment was performed by using Clustal 1.2.4 [146]. (**B**) Schematic view of the HA-tagged HB-EGF. The pro-peptide, the expected cleavage products and their expected sizes (19 kDa, 22 kDa and 23 kDa) are shown. The different domains of HB-EGF are marked by different colours. The graphic was generated by using BioRender.com.

## Detection of HB-EGF via qPCR and Western blotting

In order to analyse the role of HB-EGF in *Mastomys*, tools for the detection of *Mastomys* HB-EGF had to be established. Therefore, the *Mastomys* fibroblast cell line MaFi132 was transfected with different amounts of the corresponding expression plasmids. Upon transfection, mRNA levels of *HB-EGF* increased depending on the amount of the transfected plasmid (Fig. 2.1.2, A), which proves successful transfection.

To test whether the HA-tagged HB-EGF protein is successfully synthesised in transfected MaFi132 cells, an anti-HA tag antibody was used. Western blot experiments with the HA-tag antibody showed three bands according to the known cleavage products of human HB-EGF at 19, 22 and 23 kDa (Fig. 2.1.2, B).

To establish a detection method for endogenous untagged HB-EGF an antibody against the murine protein was used (R&D, #AF8239), and tested for its sensitivity for *Mastomys* HB-EGF. The results reveal that murine and *Mastomys* HB-EGF can be directly detected by this antibody. However, endogenous HB-EGF was not detectable in untransfected MaFi132 (Fig. 2.1.2, B). Therefore, transfected MaFi132 were used as positive control in future experiments.

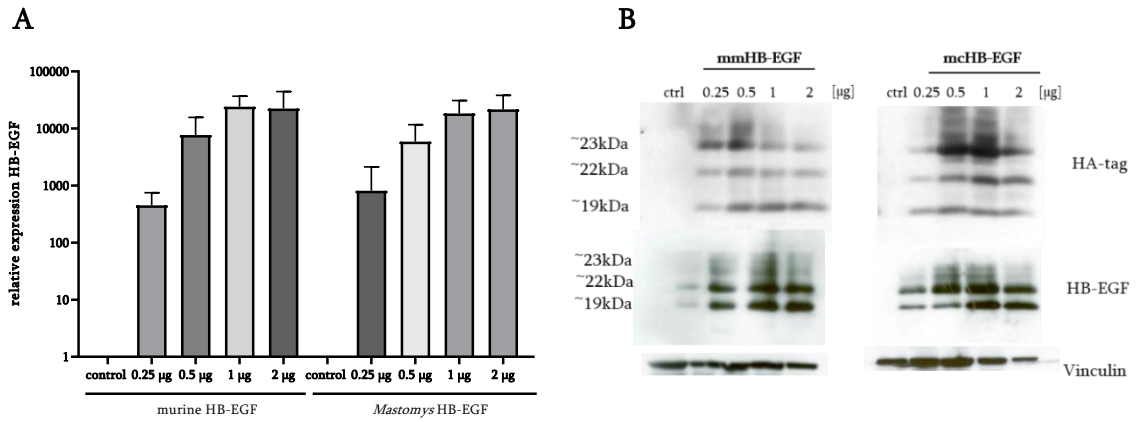


**Fig 2.1.2 Analyses of transfected MaFi132**. MaFi132 were transfected with either 0.25 µg, 0.5 µg, 1 µg or 2 µg of expression plasmid coding for murine or *Mastomys* HB-EGF and harvested 24 h post transfection. (**A**) qPCR analysis of transfected MaFi132. The expression of *Hbegf* in transfected cells is shown relative to control, which was arbitrarily set to 1 (n=3; mean ± SD) (y-axis scale: log10). *Hprt1* was chosen as reference gene. (**B**) Western blot to identify HB-EGF after transfection. 50 µg of each sample were loaded. Vinculin served as loading control.

In order to determine whether the lack of detection of endogenous HB-EGF in MaFi132 cells is due to absence of the protein in this particular cell line or low sensitivity of the Western blot, *HB-EGF* expression was compared to other cell lines by qPCR. These analyses revealed that *Hbegf* mRNA can be detected in HaCaT (human keratinocytes), THP-1 (human monocytes), 308kera (murine keratinocytes), and *Mastomys* fibroblasts (MaFi191) but not in J774A.1 (murine monocytes/macrophages) (Fig. 2.1.3, A). HaCaT showed the highest expression of *Hbegf*. Despite the high levels of *Hbegf* mRNA in HaCaT cells, the protein could not be detected by Western blotting (Fig. 2.1.3, B). Overall, the absence of HB-EGF detection could be due to a lack of translation from the *Hbegf* mRNA or to the low sensitivity of the Western blot analysis.

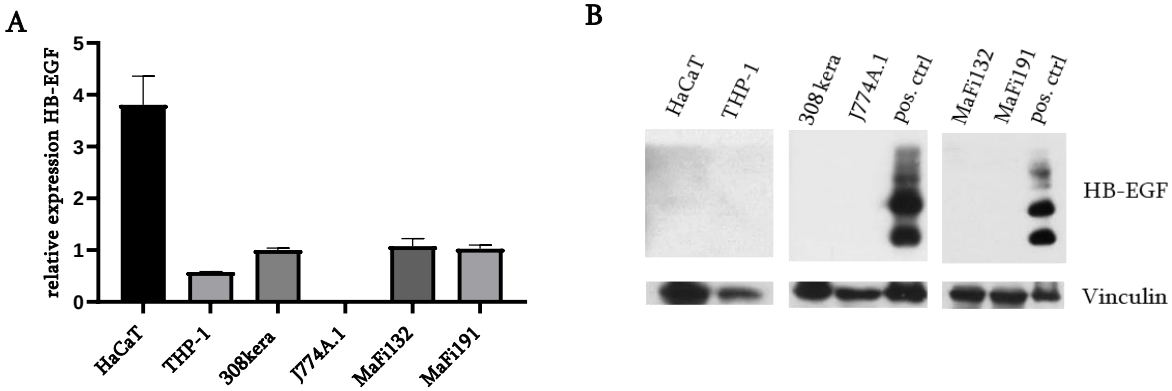


**Fig. 2.1.3 Analyses of HB-EGF levels in different cell lines.** (**A**) qPCR analyses were performed using specific primers for either human, murine or *Mastomys* HB-EGF depending on the cell line (n=3; mean ± SD). The expression of *Hbegf* was normalized to reference gene *Hprt1*. Here, the expression is arbitrarily set relative to 0. (**B**) Western blotting of the different cell lines. 50 µg of protein lysates per cell line or 25 µg of each positive control (pos. ctrl) (MaFi132 transfected with murine (line 5) or *Mastomys* HB-EGF (line 8)) were loaded on a 12% SDS gel. For the human cell lines, the membrane was incubated with anti-human HB-EGF antibody, while for the murine and *Mastomys* cells anti-mouse HB-EGF antibody was chosen. Vinculin was detected as loading control.

Since endogenous HB-EGF was not detectable in Western blot under normal conditions, different cell lines were exposed to UVB to investigate whether HB-EGF can be detected upon UVB exposure, as previously shown for murine keratinocytes [147]. qPCR analyses showed the tendency of upregulated mRNA levels of endogenous *Hbegf* upon UVB irradiation compared to the unirradiated control (Fig. 2.1.4, A). However, in Western blot, the endogenous protein was still not detectable after UVB irradiation (Fig. Fig. 2.1.4, B), which questions whether this method is sensitive enough to detect endogenous HB-EGF.

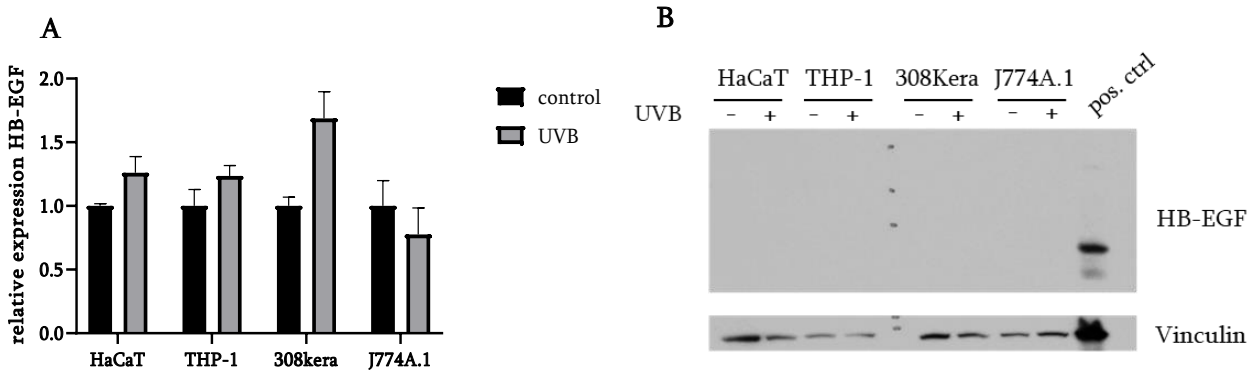


**Fig. 2.1.4 Analyses of HB-EGF levels in different cell lines upon UVB irradiation.** (**A**) The relative *Hbegf* expression of the cell lines upon UVB exposure was measured by qPCR. The expression in respective unirradiated controls were arbitrarily set to 1. *Hprt1* was chosen as reference gene. For the HaCaT and THP-1, primers for human *Hbegf* were used, for 308 keratinocytes and J774A.1) primers for murine *Hbegf* were used (n=3; mean ± SD). Keratinocytes were exposed to 50 mJ/cm² UVB, while monocytes/macrophages were treated with 20 mJ/cm². (**B**) 50 µg of each lysate of UVB treated and untreated cell lines were loaded on a 12% SDS gel. As positive control (pos. ctrl) 25 µg of MaFi132 transfected with murine HB-EGF were included. Vinculin was used as loading control.

Since HB-EGF levels were not directly influenced by UVB irradiation, I asked whether HB-EGF synthesis is stimulated by cytokines or other signal peptides released by UVB damaged cells in a paracrine manner. Therefore, co-cultivation was mimicked by incubation of murine J774A.1 cells with media collected from UVB irradiated murine 308kera. The results reveal that exposure to conditioned medium from UVB irradiated cells was not sufficient to induce detectable HB-EGF levels in J774A.1 cells (Fig. 2.1.5).

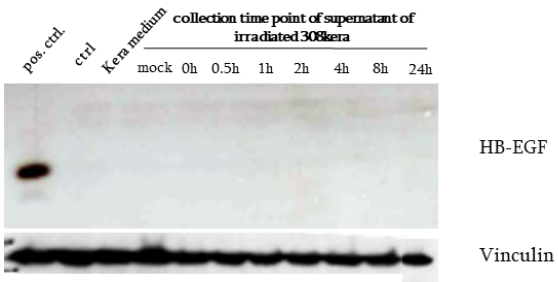


**Fig. 2.1.5 Western blotting of J774A.1 cells incubated with conditioned medium of 308kera.** 308kera cells were irradiated with 50 mJ/cm² and supernatant was collected at indicated time points. Afterwards, J774A.1 cells were incubated with the conditioned medium and harvested 24 h afterwards and 50 µg of the lysates investigated in Western blot analyses. As positive control (pos. ctrl.) transfected MaFi132 were included (line 1). As control, J774A.1 incubated with normal growth medium were included as well as J774A.1 incubated with 308kera growth medium only. The mock control represents J774A.1 incubated with supernatant from unirradiated 308kera. Vinculin was used as loading control.

In order to investigate whether primary cells respond differently, primary macrophages were isolated from *Mastomys coucha* and used in combination with *Mastomys* keratinocytes (Kera5). *Mastomys* macrophages were isolated from the bone marrow (bone marrow-derived macrophages = BMDMs) and from the peritoneum (peritoneal macrophages = PMs).

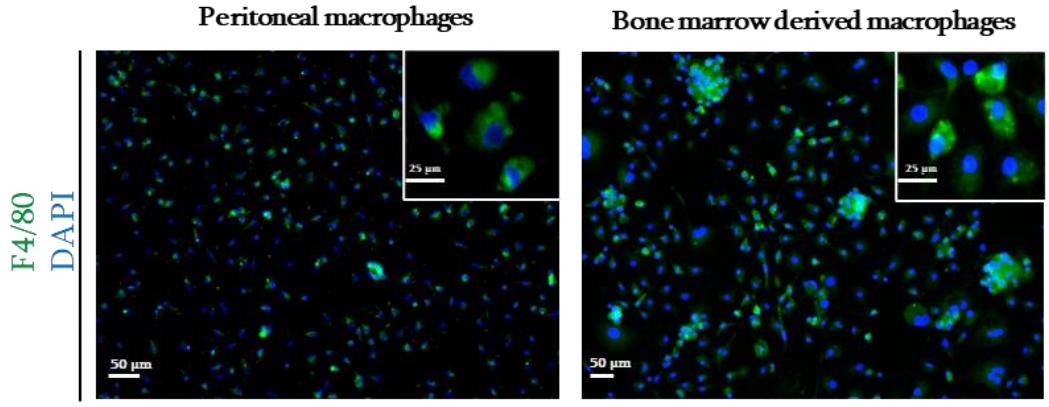


**Fig. 2.1.6 Immunofluorescence staining of isolated macrophages from *Mastomys coucha*.** Cells were isolated and seeded on glass slides. 2 days after isolation cells were fixed and stained for F4/80. For visualization of the nucleus DAPI was used.

PMs and BMDMs could be successfully isolated as shown by immunofluorescence staining against the macrophage-specific marker F4/80 (Fig. 2.1.6). While BMDMs appear in colonies, PMs occurred as single cells. This might be due to the addition of macrophage colony-stimulating factor (M-CSF) to the medium during isolation of BMDMs. M-CSF stimulates the differentiation of monocytes into macrophages [148, 149]. Since the number of isolated macrophages from bone marrow was higher and cells survived longer in cell culture, BMDMs were used for investigation of HB-EGF levels.

BMDMs were exposed to conditioned medium from UVB irradiated Kera5 cells. Subsequent qPCR analysis revealed that the mRNA levels of *Mastomys* keratinocytes increased upon UVB irradiation (Fig. 2.1.7, B). However, endogenous HB-EGF was not detected in Kera5 lysates in Western blot and exposure of BMDMs to conditioned medium from UVB irradiated Kera5 cells was not sufficient to induce detectable HB-EGF levels in BMDMs (Fig. 2.1.7).

Overall, the results reveal that *Hbegf* levels increase upon UVB exposure in *Mastomys* keratinocytes. Endogenous HB-EGF cannot be detected on protein level *via* Western blot. Neither direct UVB exposure of different cell lines nor stimulation of cells with conditioned medium from UVB irradiated cells could induce HB-EGF to a detectable level. However, *Mastomys* HB-EGF can be detected on Western blots when overexpressed in fibroblasts.

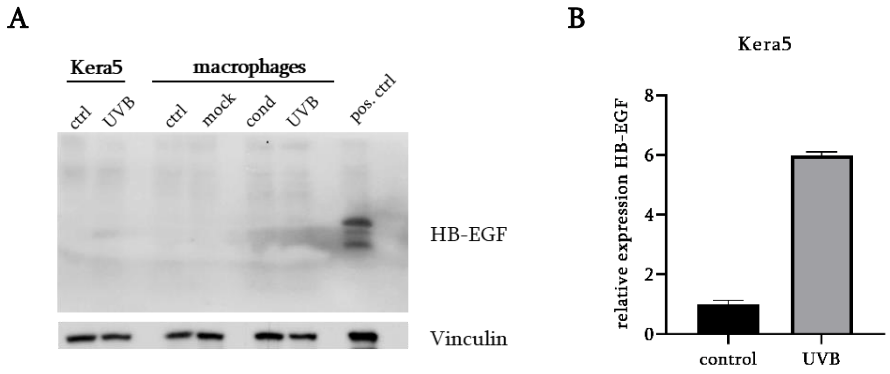


**Fig. 2.1.7 Analyses of HB-EGF levels in Kera5 and BMDM from *Mastomys coucha*.** (**A**) Western blotting of *Mastomys* cells. Vinculin was chosen as loading control. 50 µg of each sample and 25 µg of the positive control (pos. ctrl) (MaFi132 transfected with mcHB-EGF expression plasmid) were investigated. Kera5 were either untreated or exposed to 50 mJ/cm² UVB. 24 h afterwards, medium was collected and primary *Mastomys* macrophages were incubated with their normal growth medium (ctrl), medium from untreated Kera5 (mock) or medium from UVB irradiated Kera5 (cond.) for 24 h. Furthermore, macrophages exposed to 20 mJ/ cm² were harvested 24 h afterwards. (**B**) qPCR analysis of Kera5. Cells were unirradiated or irradiated with 50 mJ/cm² UVB and normalized to *Hprt1*. The UVB irradiated sample was set relative to control cells (control=1).

## Detection of HB-EGF in ELISA

For clarification whether the absence of the protein was due to low sensitivity of the Western blot analysis, the detection of HB-EGF in enzyme-linked immunosorbent assay (ELISA) was tested. Since ELISA is also used to detect proteins in supernatants of cultured cells, cleavage of the soluble HB-EGF from the cells surface can be investigated. Therefore, the commercially available mouse HB-EGF-specific ELISA from R&D was tested. The supernatants and lysates of murine cell lines (308kera and J774A.1) as well as from *Mastomys* cells (MaFi132, MaFi191, Kera5 and BMDMs) before and after UVB irradiation were analysed. Furthermore, samples from macrophages (murine and *Mastomys*) incubated with conditioned medium from keratinocytes (as described in Fig. 2.1.5 and Fig. 2.1.7) were included. Additionally, the lysates and supernatants of transfected MaFi132 were included as a positive control for *Mastomys* HB-EGF (Fig. 2.1.8).

In the ELISA, endogenous HB-EGF could not be detected in cell lysates or supernatants. Besides, for the positive control, signals could be detected in MaFi132 transfected with murine HB-EGF (Fig. 2.1.8, A). The detected concentration increased with the amount of the transfected plasmid. Furthermore, in the supernatant of cells transfected with murine HB-EGF, soluble HB-EGF could be detected. However, *Mastomys* HB-EGF could not be detected (Fig. 2.1.8, B).

Conclusively, ELISA cannot be used as a method for *Mastomys* HB-EGF protein detection, therefore qPCR is used in further experiments to investigate the *Hbegf* level in cells.

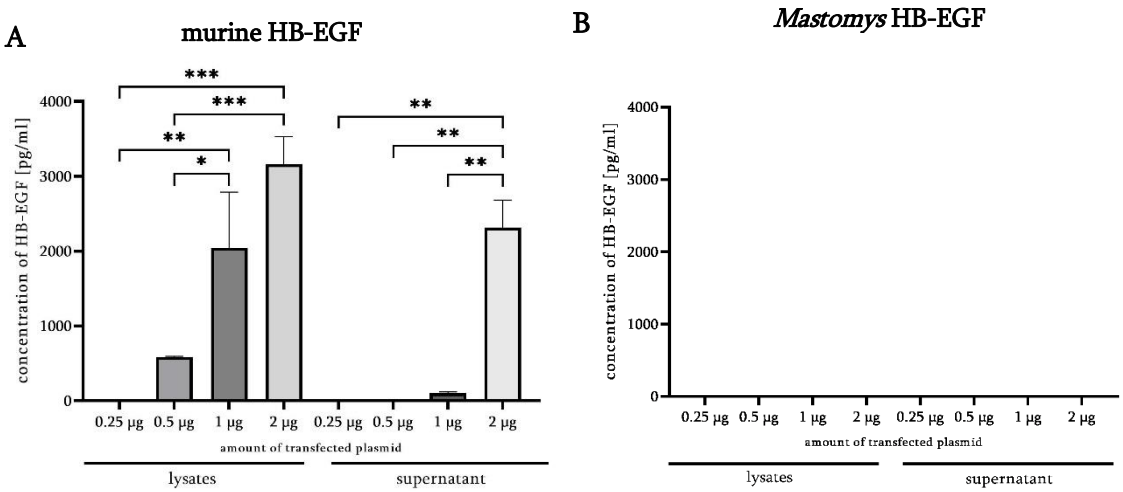


**Fig 2.1.8 Detection of HB-EGF in cell lysates and supernatants by using R&D ELISA kit.** 10 µg of lysates in 100 µl per sample per well were used. ELISA was performed in technical duplicates (mean ± SD). (**A**) The lysates and supernatants of MaFi132 transfected with murine HB-EGF were investigated as positive control. The concentration of HB-EGF is plotted against the amount of transfected plasmid. (**B**) MaFi132 were transfected with different amounts of plasmid coding for *Mastomys* HB-EGF (n=2; mean ± SD; Statistical calculations were done by GraphPad Prism9; One-way ANOVA; ***: $p < 0.001$, **: $p < 0.01$, *: $p < 0.05$)

## 2.2. Stimulation of the expression of HB-EGF in cells

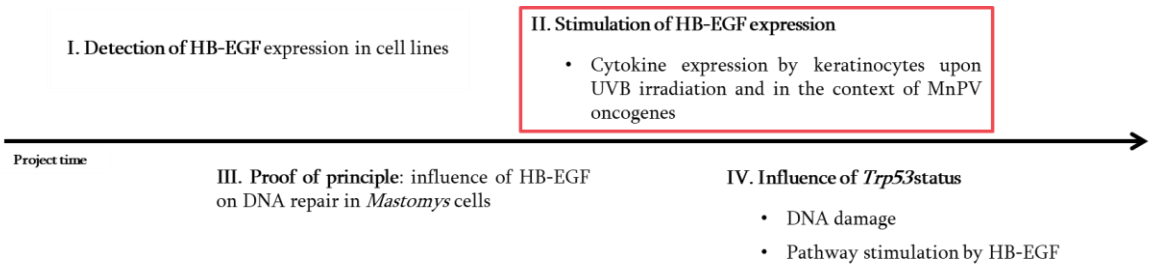


In the previous experiment, UVB irradiation showed no significant impact on HB-EGF levels in keratinocytes. In case of various cancer entities, HB-EGF has been shown to be upregulated [150]. Therefore, the question appeared whether MnPV infection, an important co-factor in skin carcinogenesis, affects *Hbegf* expression.

Our lab previously generated 308kera cell lines, which express the MnPV E6, E7 or E6/E7 oncogenes. These cell lines were used in the frame of this thesis to analyse the expression of *Hbegf* in the context of UVB irradiation and MnPV infection. Towards this aim, all cell lines were irradiated for defined time frames. When investigating the effect of UVB light on *Hbegf* mRNA expression in 308kera wildtype cells (Fig. 2.2.1, A), a peak after 8 h of irradiation could be detected (Fig. 2.1.5). MnPV E6 seemed not to influence this effect while MnPV E7 significantly enhanced the mRNA expression 24 h post irradiation (Fig. 2.2.1, B, C). Similar tendency could be detected in keratinocytes transduced with both oncogenes. Here, I could conclude that *Hbegf* expression changes in the presence of MnPV E7.

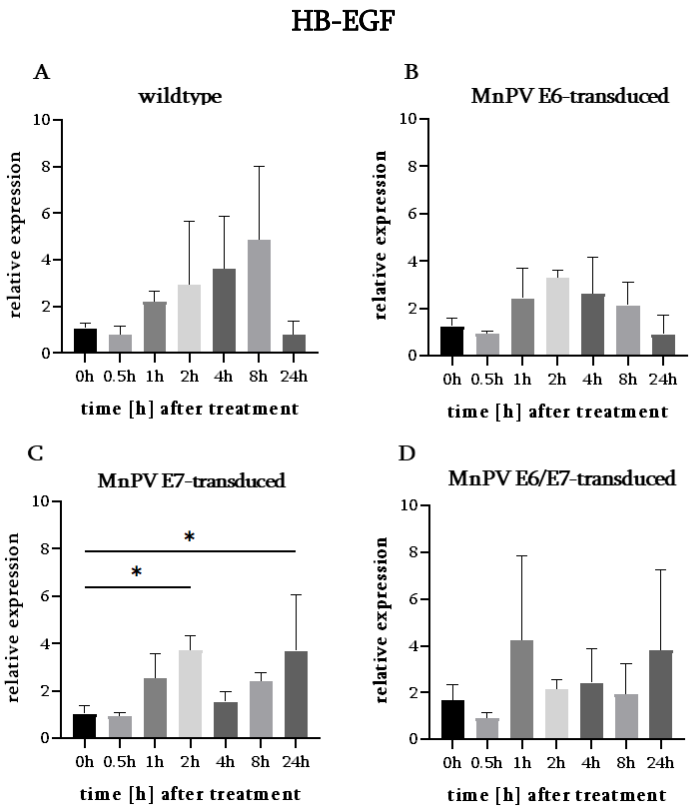


**Fig. 2.2.1 qPCR analyses of mRNA levels of *Hbegf* in 308kera.** Murine keratinocytes were irradiated with 50 mJ/cm² UVB and harvested at defined time points. For each time point an untreated control was harvested. qPCR was performed using specific primers for *Hbegf*. Samples were normalized to *Hprt1*. The treated samples were set relative to their untreated control from the same time point. Investigation of (**A**) 308kera wildtype cells, (**B**) cells stably expressing the oncogene MnPV E6, (**C**) MnPV E7 or (**D**) both oncogenes. (n=3; mean ± SD; Statistical calculations were done by GraphPad Prism9; ***: $p < 0.001$, **: $p < 0.01$, *: $p < 0.05$).

I could show that keratinocytes are able to express *Hbegf*. This might indicate an autocrine or juxtacrine mechanism upon DNA damage. Additionally, HB-EGF can be released by different immune cells, acting in a paracrine manner as previously described by our collaboration partner. Based on the previous observations, the next aim of my thesis was to study if the oncogenes influence the immunological environment upon UVB irradiation. Therefore, qPCRs were performed analysing the expression of different cytokines, which are potentially expressed by damaged cells to induce an immune response and to stimulate the infiltration of immune cells.

### Investigation of cytokine expression

Cytokines are small messenger molecules, involved in immune responses. Their functionality has been investigated in order to develop e.g., therapeutical treatments [151]. Induction of inflammatory immune responses in the skin by UVB, involves different cytokines [152]. Based on the literature, the pro-inflammatory cytokines TNFα, IL-6 and IL-1β were selected to be analysed. TNFα and IL-6 have been described to be up-regulated upon UVB irradiation in a dose and time dependent manner [153-156]. IL-1β was shown to be present in the supernatant of human keratinocytes [157] and its expression in epithelial cells can be stimulated by UVB exposure [158].

In Fig. 2.2.2, the expression of the selected cytokines is shown. In wildtype cells, *Tnfa* was significantly upregulated 8 h post UVB irradiation (Fig. 2.2.2, A), while the mRNA levels of *Il-6* and *Il-1beta* did not differ (Fig. 2.2.2, E and I). Upon UVB irradiation, MnPV E6 positive cells showed enhanced *Tnfa* and *Il-6* expression (Fig. 2.2.2, B and F). Investigating MnPV E7-transduced 308kera, a significant upregulation of the mRNA of all selected cytokines could be measured 24 h post UVB irradiation (Fig. 2.2.2, C, G and K). The same tendency could be observed in the keratinocytes transduced with both oncogenes (Fig. 2.2.2, D, H and L).

Overall, in line with previous results from the literature *Tnfa* expression is upregulated upon UVB exposure [159]. *Tnfa* expression was further enhanced in MnPV E7 positive cells, apparently an effect of the oncogene. The same effect was observed for the other pro-inflammatory cytokines, indicating that MnPV E7 enhances the pro-inflammatory immune response.

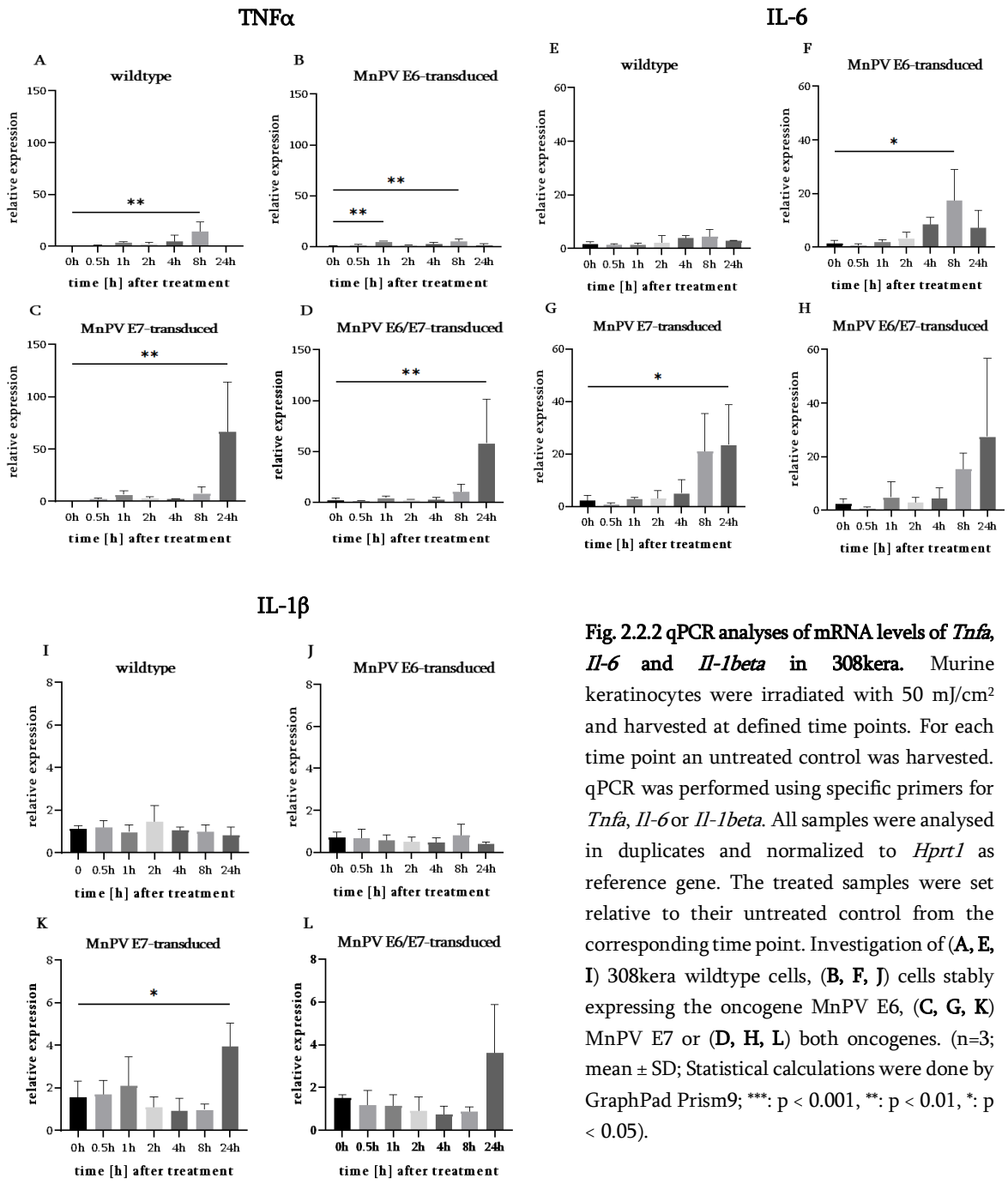


**Fig. 2.2.2 qPCR analyses of mRNA levels of *Tnfa*, *Il-6* and *Il-1beta* in 308kera.** Murine keratinocytes were irradiated with 50 mJ/cm² and harvested at defined time points. For each time point an untreated control was harvested. qPCR was performed using specific primers for *Tnfa*, *Il-6* or *Il-1beta*. All samples were analysed in duplicates and normalized to *Hprt1* as reference gene. The treated samples were set relative to their untreated control from the corresponding time point. Investigation of (**A, E, I**) 308kera wildtype cells, (**B, F, J**) cells stably expressing the oncogene MnPV E6, (**C, G, K**) MnPV E7 or (**D, H, L**) both oncogenes. (n=3; mean ± SD; Statistical calculations were done by GraphPad Prism9; ***: $p < 0.001$, **: $p < 0.01$, *: $p < 0.05$).

Since macrophages are of special interest in this work, the transduced keratinocytes were analysed regarding expression of cytokines, particularly known to stimulate monocytes and/or macrophages. One of those is monocyte chemoattractant protein-1 (MCP-1) also known as chemokine (CC-motif) ligand 2 (CCL2). MCP-1 contributes to enhanced expression of other cytokines and stimulates infiltration of macrophages to the site of inflammation [160, 161]. In the skin, expression of *Mcp1* is stimulated by UVB irradiation [154]. Furthermore, the expression of *Il-34* was investigated, which can be released by keratinocytes [162] to stimulate Langerhans cells that play an important role in the skin's immune system [163].

308kera wildtype cells showed no change in mRNA expression levels of *Mcp1* upon UVB irradiation (Fig. 2.2.3, A). In contrast, *Il-34* levels increased significantly (Fig. 2.2.3, E). The expression of cytokines did

not change in MnPV E6-transduced 308kera, while *Mcp1* and *Il-34* were both significantly upregulated in MnPV E7-transduced cells upon UVB irradiation (Fig. 2.2.3, C and G). The same tendency was observed in the 308kera stably expressing both oncogenes (Fig. 2.2.3, D and H). These observations show that MnPV E7 enhances the expression of the mRNA levels of both cytokines upon UVB irradiation, indicating that MnPV E7 enhanced the stimulation of monocytes/ macrophages and Langerhans cells.

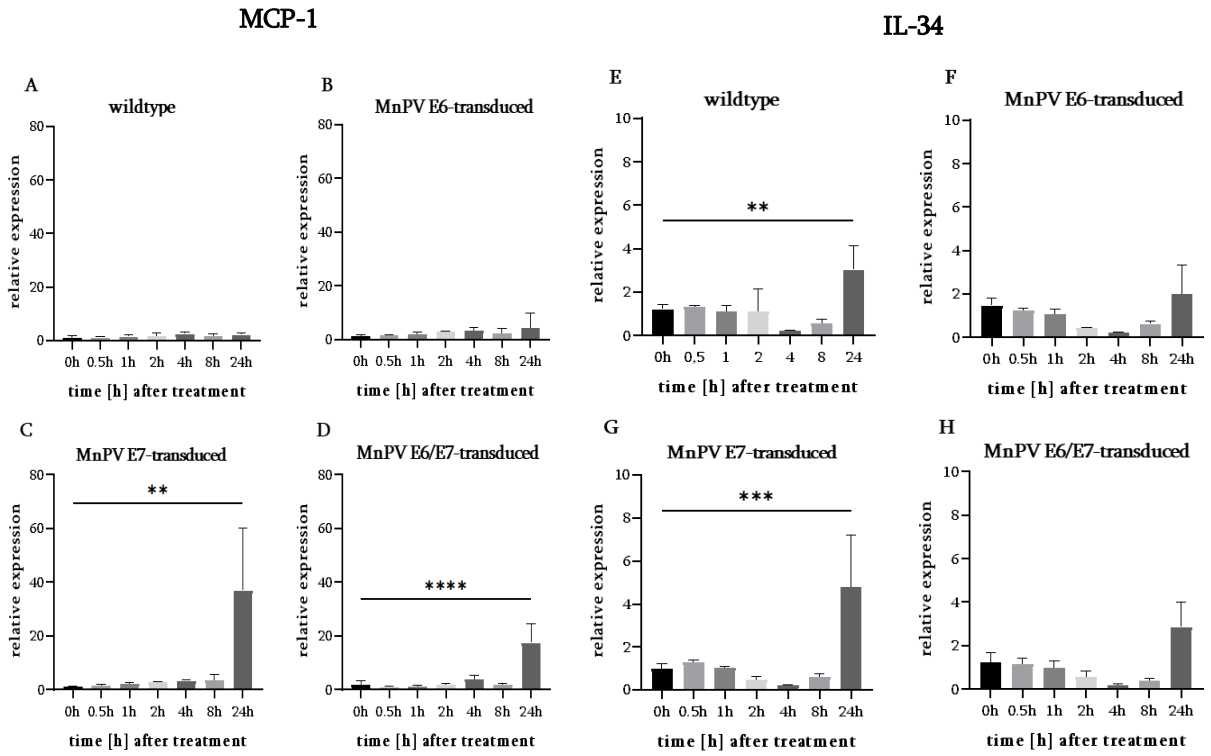


**Fig. 2.2.3 qPCR analyses of mRNA expression of *Mcp1* and *Il-34* in 308kera.** Murine keratinocytes were irradiated with 50 mJ/cm² and harvested at defined time points. For each time point an untreated control was harvested. After RNA extraction and reverse transcription, qPCR was performed using specific primers for *Mcp1* or *Il-34*. Samples were analysed in duplicates and normalized to *Hprt1*. The treated samples were set relative to their untreated control from the same time point. Investigation of (**A, E**) 308kera wildtype cells, (**B, F**) cells stably expressing the oncogene MnPV E6, (**C, G**) MnPV E7 or (**D, H**) both oncogenes. (n=3; mean ± SD; Statistical calculations were done by GraphPad Prism9; ***: $p < 0.001$, **: $p < 0.01$, *: $p < 0.05$).

In most of the qPCR analyses, a high SD is observed even though all experiments were performed following the same protocol and under the same conditions. To further investigate whether the selected cytokines play a role in the immune response and are influence by the presence of oncogenes, the protein levels in the supernatant of the cells need to be measured. Since the data regarding mRNA expression levels are not expressive and the number of samples, which should be measured is too high, the release of interleukins was not further investigated by e.g., interleukin ELISAs.

## 2.3. HB-EGF and DNA damage repair mechanisms

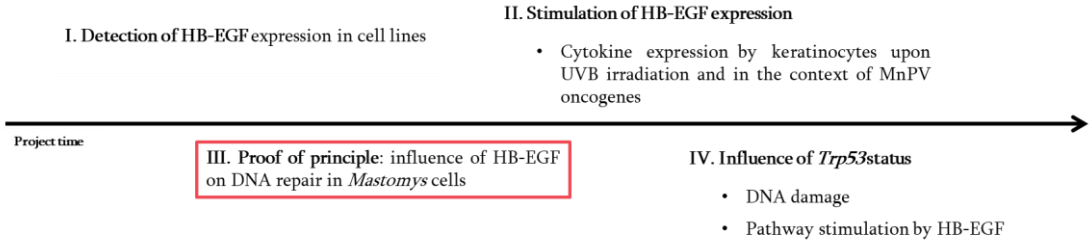


Geiger-Maor *et al.* showed in their studies that recombinant human HB-EGF enhances DNA repair efficiency upon DNA damage induction [114]. To investigate whether HB-EGF has an impact on *Mastomys* cells, *Mastomys* fibroblasts were irradiated with UVB light and afterwards incubated with media containing different concentrations of recombinant murine HB-EGF. To visualize DNA damage, γH2AX foci were detected and counted as a sensitive biomarker for DNA double-strand breaks (DSBs) [164].

As previously described, the *Trp53* status in *Mastomys* tumours differs. The most common mutation is R266C [91]. Therefore, the MaFi191 wildtype and MaFi191 R266C cell lines were included. In addition, MaFi132 cells were used, which contain a p53 splicing mutation causing the loss of the p53 protein. To analyse the effect of UVB exposure on cell lines with different p53 status, cells were exposed to different doses of UVB light and harvested at different time points (Fig. 2.3.1).

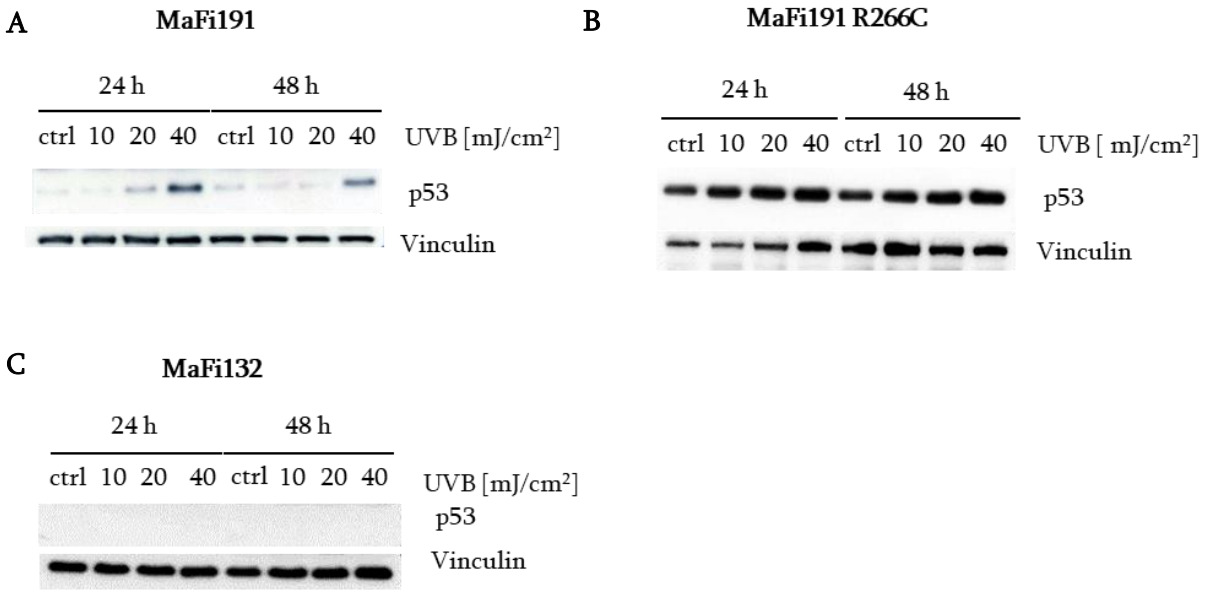


**Fig. 2.3.1 Western blotting of *Mastomys* fibroblasts.** Cells were exposed to either 10 mJ/cm², 20 mJ/cm² or 40 mJ/cm² UVB and harvested after 24 h or 48 h, respectively. (**A**) MaFi191 containing the p53 wildtype. (**B**) Analysis of MaFi191 R266C. (**C**) Western blot of MaFi132, which contain the splicing mutation of p53. As loading control, vinculin was detected.

In MaFi191, p53 accumulation increased with the UVB dose (Fig. 2.3.1, A). The cells harvested 24 h post treatment showed a detectable amount of p53 already after the exposure with a dose of 20 mJ/cm$^2$ while 48 h afterwards less p53 was detectable. A similar effect could be observed upon irradiation with 40 mJ/cm$^2$. In MaFi191 R266C cells, p53 levels were already stabilized in the control and only slightly increased upon UVB exposure (Fig. 2.3.1, B). In contrast to the MaFi191 wildtype cells, p53 was not downregulated after 48 h. This can be explained by the loss of p53 to function as a transcriptional factor for p21 [165, 166], a negative regulator of the stability of the p53 protein [167]. In accordance with the notion that the splicing variant in MaFi132 cells leads to a loss of p53, p53 was not detectable (Fig. 2.3.1, C).

After revealing that the p53 expression differed in the *Mastomys* fibroblast cell lines, the cells were irradiated and analysed regarding their DNA damage by staining for γH2AX foci (Fig. 2.3.2-2.3.4). In this experiment, recombinant murine HB-EGF was used. To verify the biological activity of HB-EGF, cells treated with fresh HB-EGF were compared to cells treated with HB-EGF denatured by heat-inactivation *prior to* use.

In the MaFi191, UVB irradiation induced up to 10 γH2AX foci/cell, the number of foci did not change after additional treatment with denatured HB-EGF (Fig. 2.3.2, B). In contrast, the number of γH2AX foci per cell decreased in a dose dependent manner when adding fresh HB-EGF (Fig. 2.3.2, C). Based on these results, HB-EGF has a positive effect on DNA repair efficiency in a dose-dependent manner in *Mastomys* fibroblasts harbouring p53 wildtype.

The same treatments were performed for MaFi191 R266C cells (Fig. 2.3.3) that showed the same effect regarding the γH2AX foci number. The number of foci decreased in a dose-dependent manner after adding fresh exogenous HB-EGF while denatured HB-EGF did not induce the same effect (Fig. 2.3.3, B and C). Interestingly, UVB irradiation induced up to 10 foci/cell in MaFi191 cells, while in the MaFi191 R266C cells a mean of 2.3 foci/cell was detected.

In the next step, MaFi132 cells were investigated regarding the effect of HB-EGF and UVB irradiation (Fig. 2.3.4). UVB light induced 5-10 foci/cell (Fig. 2.3.4, B, C) and further reacted more sensitively to HB-EGF treatment than the other cell lines. After adding the lowest concentration of HB-EGF, the number of foci per cell were not significantly different compared to mock cells.

Overall, these results demonstrate that the p53 status of a cell line alters the UVB-induced DNA damage response. In addition, the p53 status affects the reduction of DNA damage upon HB-EGF treatment. However, the mechanism by which HB-EGF stimulates DNA repair mechanisms remains elusive. To gain a more detailed understanding on the molecular alterations in *Mastomys* fibroblasts upon UVB exposure and HB-EGF treatment in dependence of the p53 status, proteome analyses were performed.

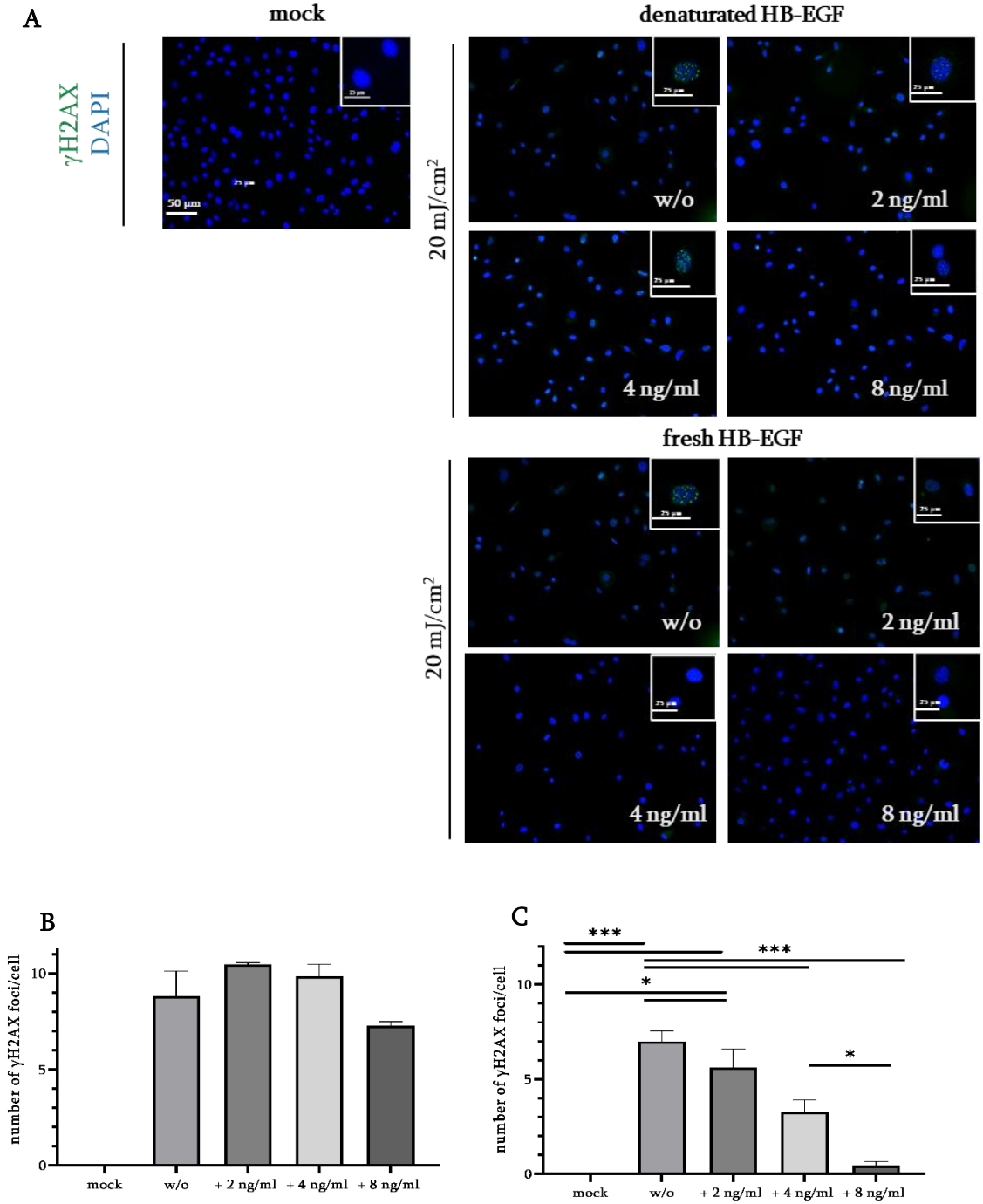


**Fig. 2.3.2 DNA damage detection in MaFi191 by staining for γH2AX foci.** MaFi191 cells were irradiated with 20 mJ/cm² UVB and afterwards incubated with different concentrations of denatured HB-EGF or fresh HB-EGF. As reference untreated cells (mock) were included. (**A**) Representative images of γH2AX foci in treated cells. DAPI was used to visualise the nuclei of the cells. The γH2AX foci (green) per cell were quantified for mock cells, (**B**) cells treated with denatured and (**C**) cells incubated with fresh HB-EGF. (n=3; mean ± SD; at least 100 cells were counted; ***: $p < 0.001$, **: $p < 0.01$, *: $p < 0.05$)

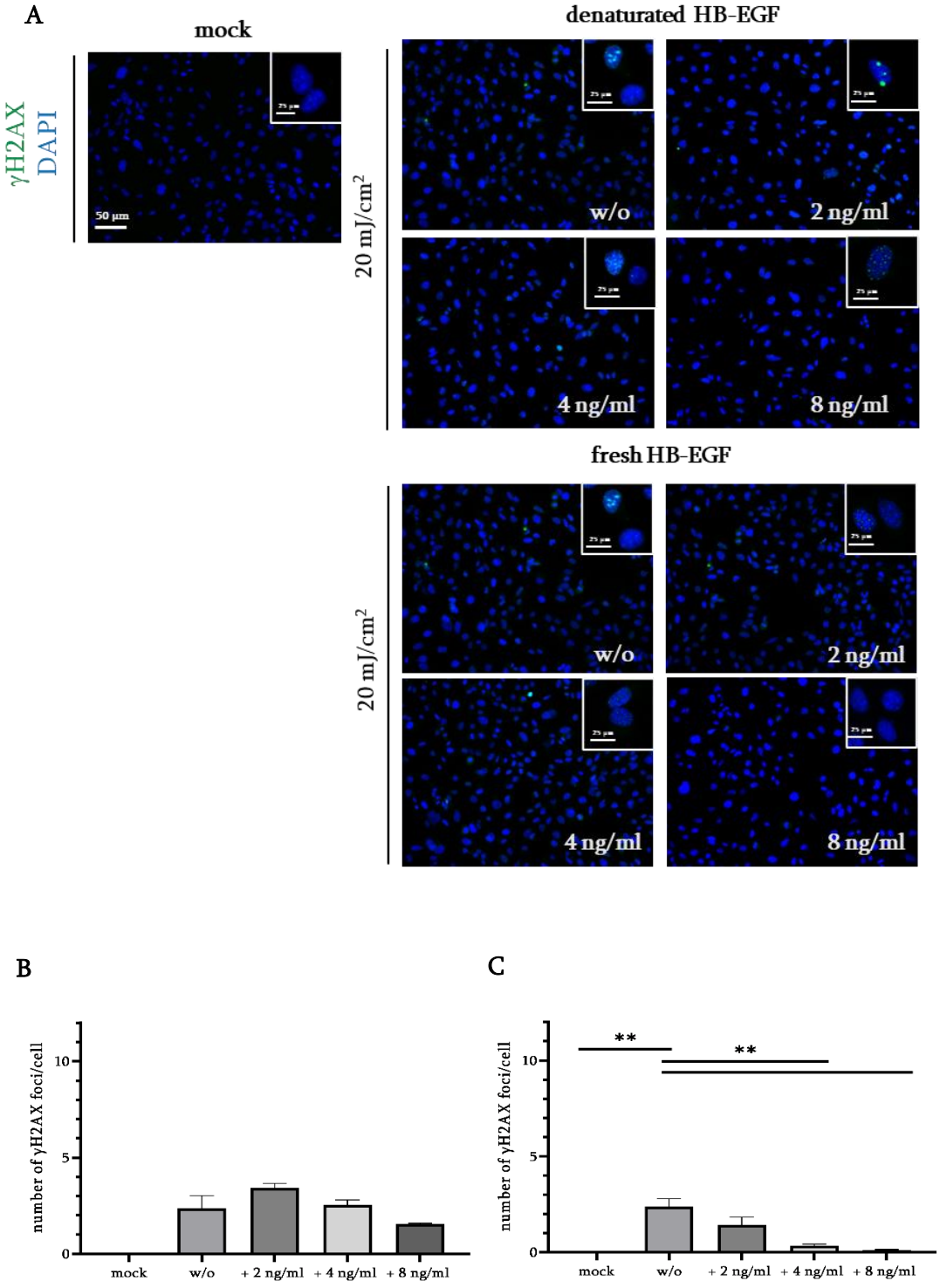


**Fig. 2.3.3 DNA damage detection in MaFi191 R266C by staining for γH2AX foci.** MaFi191 R266C cells were exposed to 20 mJ/cm² UVB and afterwards incubated with different concentrations of denatured HB-EGF or fresh exogenous HB-EGF. As reference untreated cells (mock) were included. (**A**) Representative images of γH2AX foci (green) in irradiated cells. DAPI was used to visualise the nuclei of the cells. The γH2AX foci per cell were quantified for mock cells, (**B**) cells treated with denatured and (**C**) cells incubated with fresh HB-EGF. (n=3; mean ± SD; at least 100 cells were counted; ***: $p < 0.001$, **: $p < 0.01$, *: $p < 0.05$)

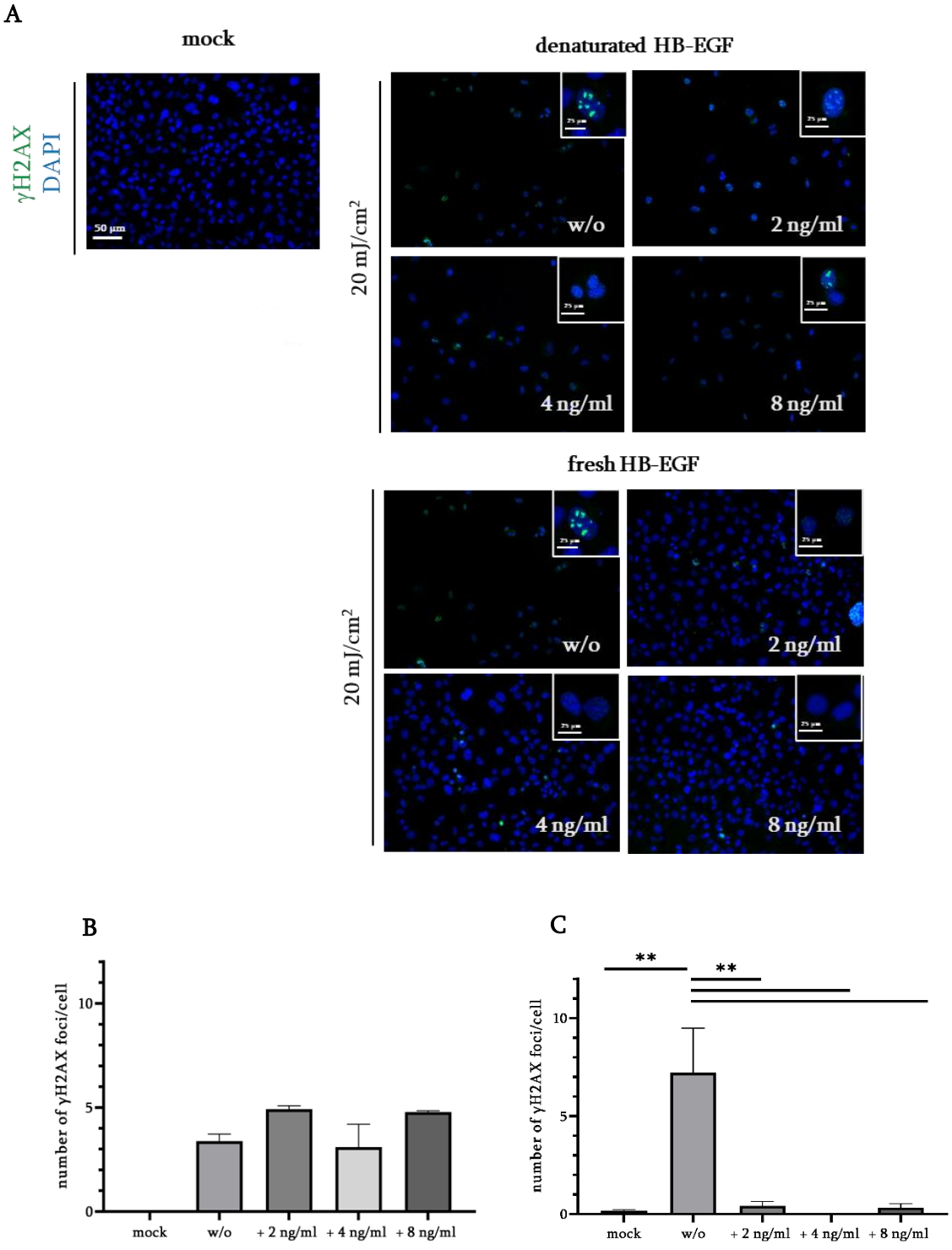


**Fig. 2.3.4 DNA damage detection in MaFi132 by staining for γH2AX foci.** MaFi132 cells were exposed to 20 mJ/cm² UVB and afterwards incubated with different concentrations of denatured HB-EGF or fresh HB-EGF. As reference untreated cells (mock) were included. (**A**) Representative images of γH2AX foci (green) in treated cells. DAPI was used to visualise the nuclei of the cells. The γH2AX foci per cell were quantified for mock cells, (**B**) cells treated with denatured and (**C**) cells incubated with fresh HB-EGF. (n=3; mean ±SD; at least 100 cells were counted; ***: $p < 0.001$, **: $p < 0.01$, *: $p < 0.05$)

## 2.4. Proteome analyses

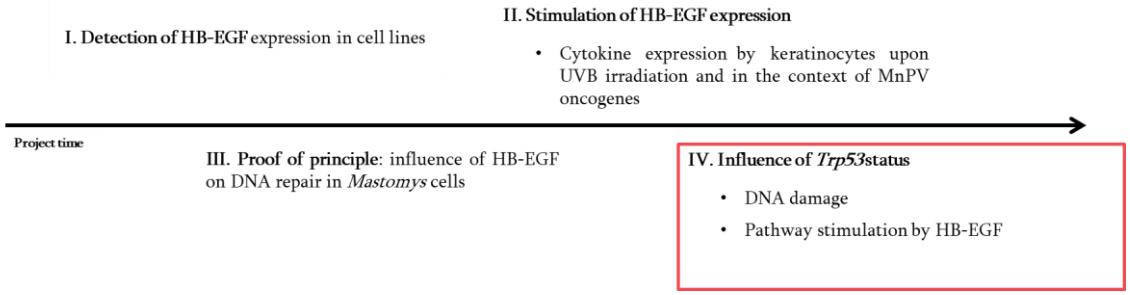


As shown above, HB-EGF enhanced the DNA repair efficiency upon UVB irradiation in a dose-dependent manner. This is consistent with the observations made in our collaboration partner's setup [114], where DSBs were induced by DEN. To clarify, which pathways are affected upon HB-EGF stimulation and if they differ compared to our collaboration partner's setup, the following questions were addressed:

1. Which pathways are stimulated upon UVB irradiation in contrast to γ-irradiation?

Multiple signalling pathways are involved in activating cellular DNA repair. Depending on the DNA damage induction as well as on the cell cycle, different pathways are stimulated. Here, I aim to compare, whether upon UVB irradiation similar pathways are activated as in our collaboration partner's setup. Therefore, γ-irradiation is included to induce the similar effects *in vitro* as DEN *in vivo*.

2. Which pathways are stimulated upon HB-EGF treatment?

Activation of the EGFR by HB-EGF can result in the stimulation of various pathways [97]. Here, I analysed the molecular changes upon HB-EGF treatment and studied whether responses differ after inducing DNA damage by UVB or γ -irradiation.

3. Does the p53 status change the cellular response upon DNA damage induction?

In human cancer, *TP53* has been shown to be frequently mutated in cancer cells leading to disfunction and enhanced cell proliferation [168], which has also been reported for our animal model *Mastomys coucha* [91]. Therefore, the effect of the *Trp53* status on DNA damage repair mechanisms is investigated. Towards this aim, three different *Mastomys* fibroblast cell lines with different *Trp53* status were included in this study.

There is an ample overlap of downstream pathways of EGFR and p53 signalling. Their analysis *via* immunoblotting studies is limited due to the availability of suitable antibodies. To overcome this limitation, proteome analyses were performed with the following conditions:

**Table 2.4.1 Treatments of *Mastomys* fibroblasts (MaFi132, MaFi191 and MaFi191R266C) for proteomic analyses.**

| name of treatment | 5 Gy | 20 mJ/cm² | 10 ng/ml HB-EGF |
|---|---|---|---|
| ctrl | - | - | - |
| ctrl HB-EGF | - | - | + |
| γ | + | - | - |
| γ HB-EGF | + | - | + |
| UVB | - | + | - |
| UVB HB-EGF | - | + | + |

To investigate the effect of HB-EGF on cellular pathways, cells were treated with 10 ng/ml recombinant mouse HB-EGF. Based on the abovementioned experiment where 8 ng/ml led to visible effects (see Fig. 2.3.2-2.3.4), I could ensure detectable effects in the cells by adding 10 ng/ml HB-EGF.

Mass spectrometry analyses were performed by the DKFZ core facility. Since no complete protein databases are available for *Mastomys*, the protein identification was based on the proteome of *Mus musculus*. In total, over 8000 proteins were identified in all samples. To define the up- or down-regulation of proteins, samples were compared to each other, and the log fold change (logFC) was calculated.

## Pathway stimulation upon DNA damage induction

UVB light primarily induces CPDs, which can further lead to DSBs [45] as detected in abovementioned experiments, (Fig. 2.3.2 – 2.3.4). While CPDs are repaired by nucleotide excision repair, DSBs are repaired in a cell-cycle dependent manner *via* non-homologous end joining (NHEJ) or homologous recombination (HR) [169]. To identify, which mechanisms are activated in our system, the proteome of irradiated cells was compared to the proteome of unirradiated cells. Mean differences of proteins belonging to different DNA repair mechanisms are shown in Fig 2.4.2.

For all cell lines, proteins involved in NER and NHEJ signalling pathways could be identified (Fig. 2.4.2). In MaFi191 p53 wildtype cells, proteins involved in NER are slightly upregulated upon UVB irradiation, while γ-irradiation did not induce this effect. Conclusively, in p53 wildtype cells NER signalling is more strongly affected by UVB irradiation than by γ-irradiation.

As shown before (Fig. 2.3.1), p53 is slightly upregulated upon UVB irradiation in MaFi191 R266C (logFC= 1.2, see suppl. table 7), since it is already stabilised *prior to* irradiation. However, this observation proves successful DNA damage induction. Furthermore, the protein MNAT1 (menage a trois 1) was detected to be upregulated in MaFi191 R266C upon UVB exposure (logFC= 1.0, see suppl. table 7). This effect could also be observed in p53 wildtype cells (logFC= 0.7; see suppl. table 2). MNAT1 is part of the Holo-TFIIH complex, which is involved in damage recognition *via* the global genome repair (GGR) representing one out of two NER signalling sub-pathways [170]. Interestingly, Polε (DNA polymerase epsilon), a polymerase

involved in the NER pathway [170] and frequently mutated in cancer [171, 172], is only significantly induced by UVB or γ- irradiation in MaFi132, which lack p53.

Furthermore, the activation of the NHEJ signalling pathway in irradiated cells was investigated, showing that MRE11 is slightly upregulated upon irradiation, indicating that the ends of DSBs are processed by the MRN-complex [173], which is part of the NHEJ pathway [174].

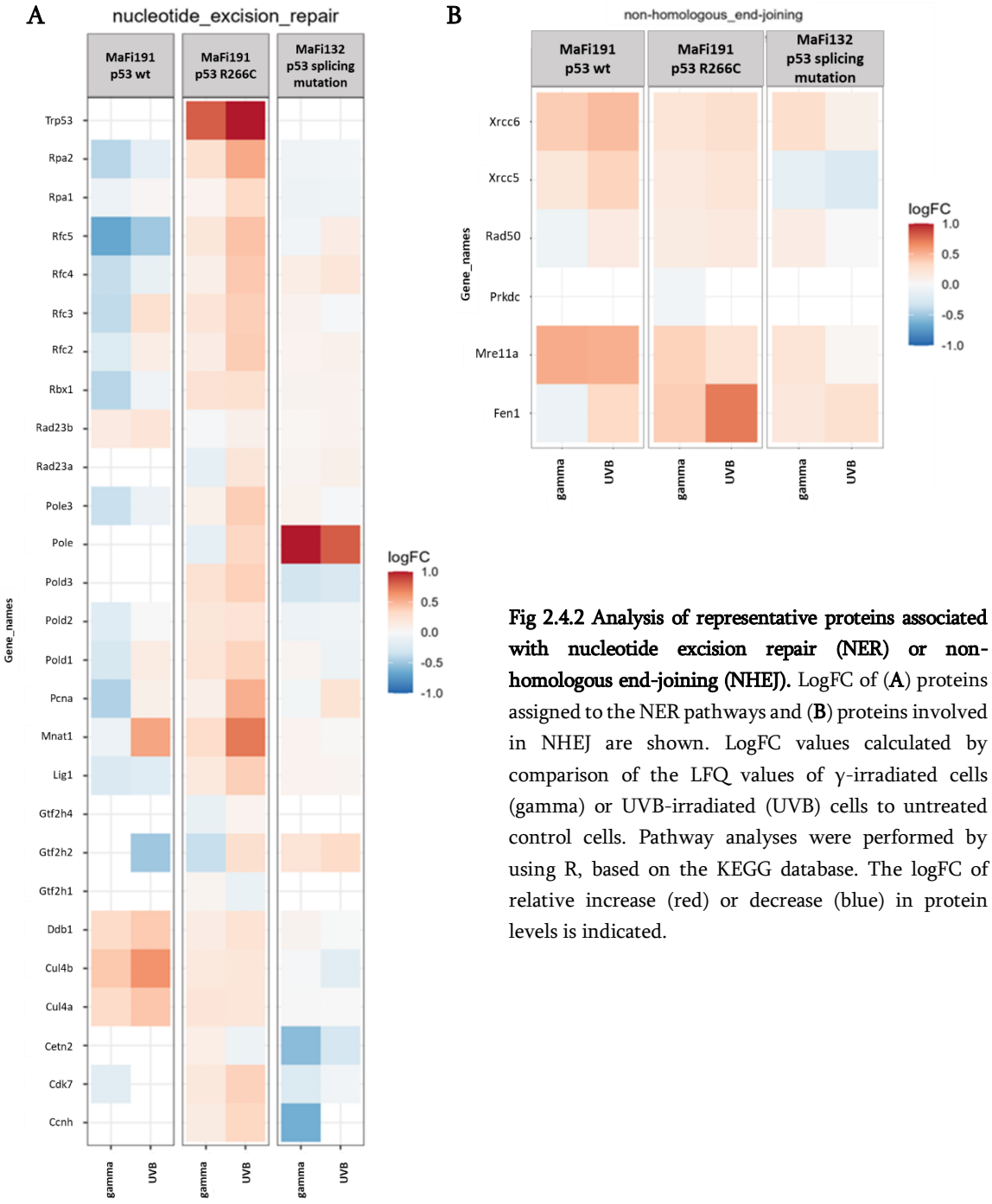


**Fig 2.4.2 Analysis of representative proteins associated with nucleotide excision repair (NER) or non-homologous end-joining (NHEJ).** LogFC of (**A**) proteins assigned to the NER pathways and (**B**) proteins involved in NHEJ are shown. LogFC values calculated by comparison of the LFQ values of γ-irradiated cells (gamma) or UVB-irradiated (UVB) cells to untreated control cells. Pathway analyses were performed by using R, based on the KEGG database. The logFC of relative increase (red) or decrease (blue) in protein levels is indicated.

As next, the regulation of proteins involved in the p53 signalling pathway was investigated (Fig. 2.4.3). Upon UVB irradiation, THBS1 (Thrombospondin 1), which mediates cell-cell-interaction, is significantly downregulated in all cell lines, which is consistent with the literature [175, 176]. Another interesting effect could be observed in UVB-irradiated MaFi191 R266C: In contrast to both other cell lines, CDK1, 2 and 4 were significantly upregulated. These cyclin-dependent kinases are cell cycle related and are inhibited by p21 [177, 178]. The transcription of p21 is downregulated due to the lack of transcriptional active p53 in this cell line resulting in malfunction of the regulation of the cyclin-dependent kinases.

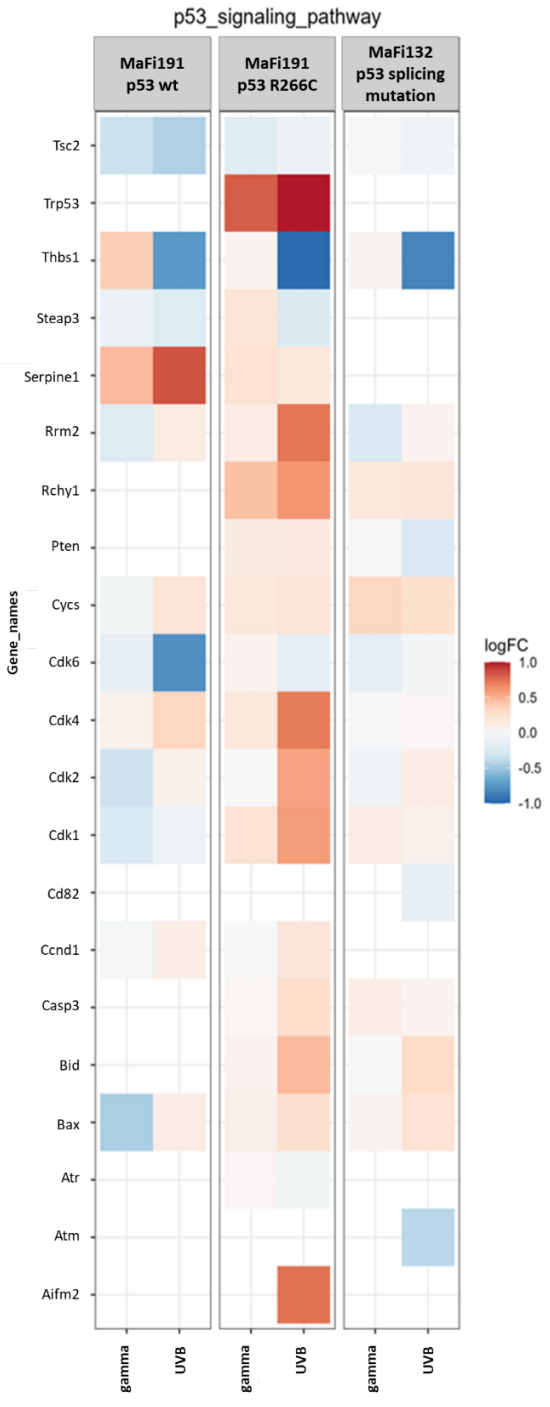


**Fig 2.4.3 Analysis of representative proteins associated with the p53 signalling pathway.** The logFC values calculated by comparison of LFQ values of γ-irradiated cells (gamma) or UVB-irradiated (UVB) cells to untreated control cells. Pathway analyses were performed using R, based on the KEGG database. The logFC of relative increase (red) or decrease (blue) in in protein levels is indicated.

Overall, these observations indicate that DNA damage repair mechanisms are stimulated in all fibroblast cell lines upon irradiation. Furthermore, disfunction of the cell cycle regulation due to mutated p53 could be detected upon UVB irradiation.

## Pathway regulation upon HB-EGF treatment

Upon HB-EGF treatment, the up-regulation of EGFR related pathways was expected. Therefore, ErbB signalling pathway as well as MAPK signalling pathway were investigated (Fig. 2.4.4). According to Fig 2.3.2 - 2.3.4 morphological changes could stably be seen after 24 h of irradiation treatment. Therefore, this timepoint was chosen for proteome analyses. Proteome analyses showed that the regulation of these pathways did not change significantly upon stimulation with HB-EGF 24 h post treatment.

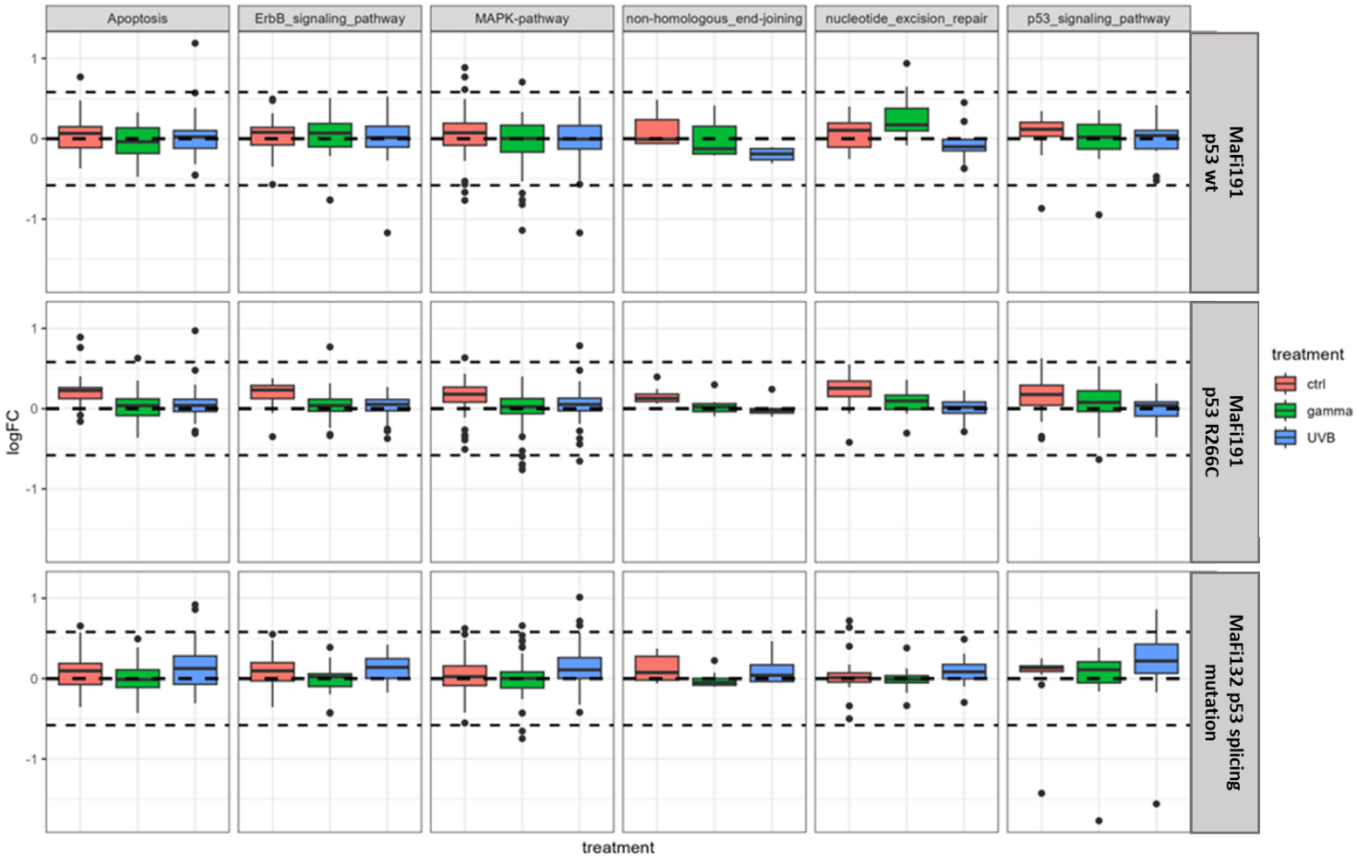


**Fig 2.4.4 Distribution of proteins upon HB-EGF treatment.** Proteins are shown allocated to the corresponding pathway based on the database KEGG. The proteome of HB-EGF treated cells was compared to the proteome of control cells (red), HB-EGF treated and γ-irradiated cells were compared to γ-irradiated cells (green), while UVB irradiated and HB-EGF treated cells were compared to UVB treated cells (blue). The logFC of all proteins belonging to a specific pathway are plotted. The dashed lines mark no change of expression (0) or differential expression of 0.5 and -0.5. The plot was generated by using R.

Next, the regulation of proteins involved in DNA repair mechanisms upon HB-EGF treatment was investigated. Here, DNA repair mechanisms of irradiated cells remained unchanged upon HB-EGF treatment (Fig. 2.4.5). Furthermore, the p53 levels did not change upon HB-EGF treatment in MaFi191 R266C (Fig. 2.4.4, B). Interestingly, Thrombospondin 1 (*Thbs1*) is downregulated upon HB-EGF treatment. Thrombospondin-1 can act in a context dependent and cell-specific manner as inhibitor or stimulator of cell

proliferation and adhesion [179]. Since HB-EGF is a growth factor, stimulation of cell proliferation was expected. Therefore, the assumption can be made that Thrombospondin 1 acts in an inhibitory manner regarding cell proliferation and is therefore downregulated upon stimulation with HB-EGF. However, further experiments are necessary to prove this hypothesis.

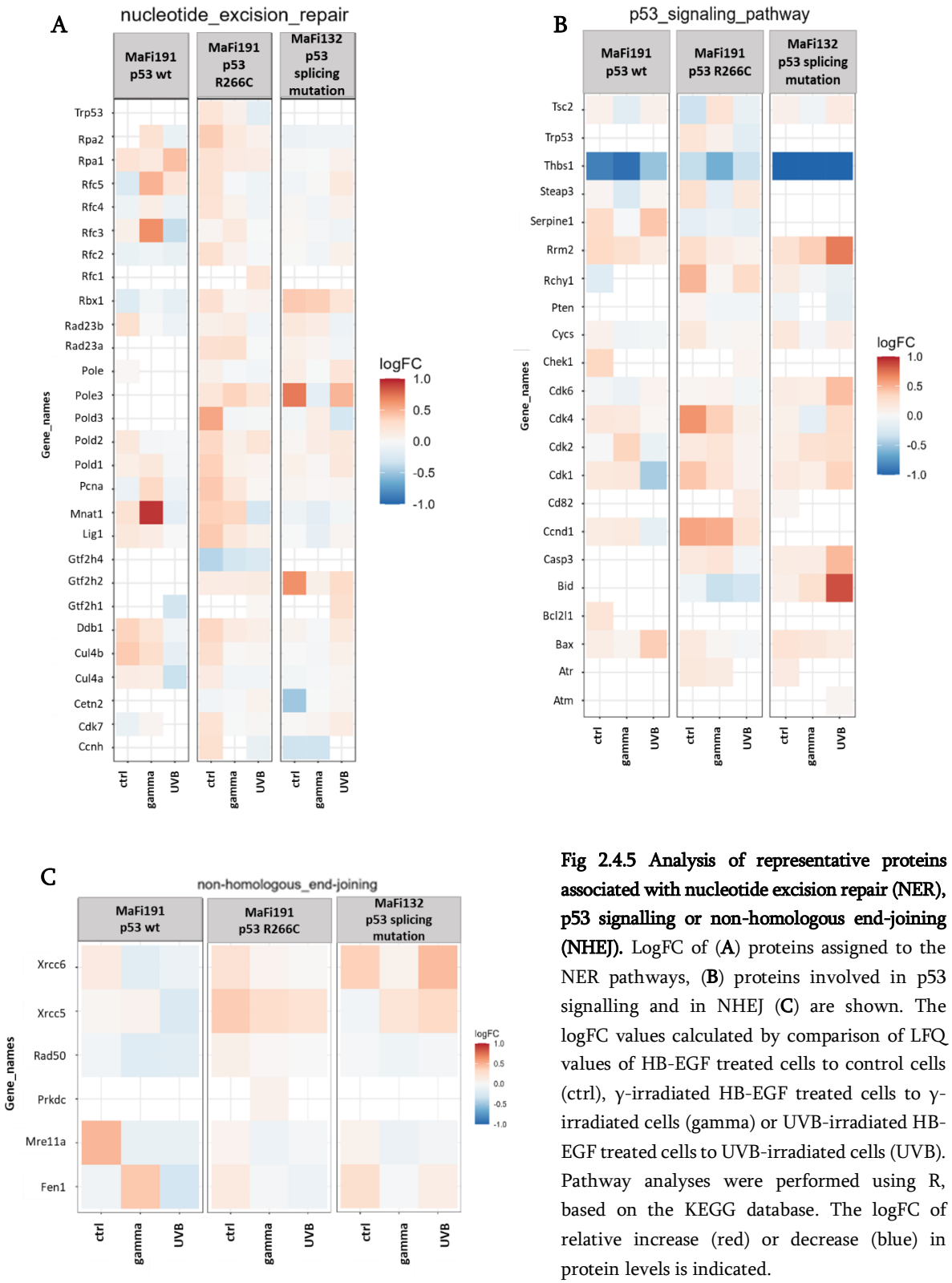


**Fig 2.4.5 Analysis of representative proteins associated with nucleotide excision repair (NER), p53 signalling or non-homologous end-joining (NHEJ).** LogFC of (**A**) proteins assigned to the NER pathways, (**B**) proteins involved in p53 signalling and in NHEJ (**C**) are shown. The logFC values calculated by comparison of LFQ values of HB-EGF treated cells to control cells (ctrl), γ-irradiated HB-EGF treated cells to γ-irradiated cells (gamma) or UVB-irradiated HB-EGF treated cells to UVB-irradiated cells (UVB). Pathway analyses were performed using R, based on the KEGG database. The logFC of relative increase (red) or decrease (blue) in protein levels is indicated.

## Pathway regulation in the absence of p53

P53 is commonly mutated in cancer and loss of p53 causes genomic instability in a variety of cancer types [93]. In order to analyse the cellular response to HB-EGF and UVB irradiation in the absence of p53, differentially regulated proteins were analysed in MaFi132 cells.

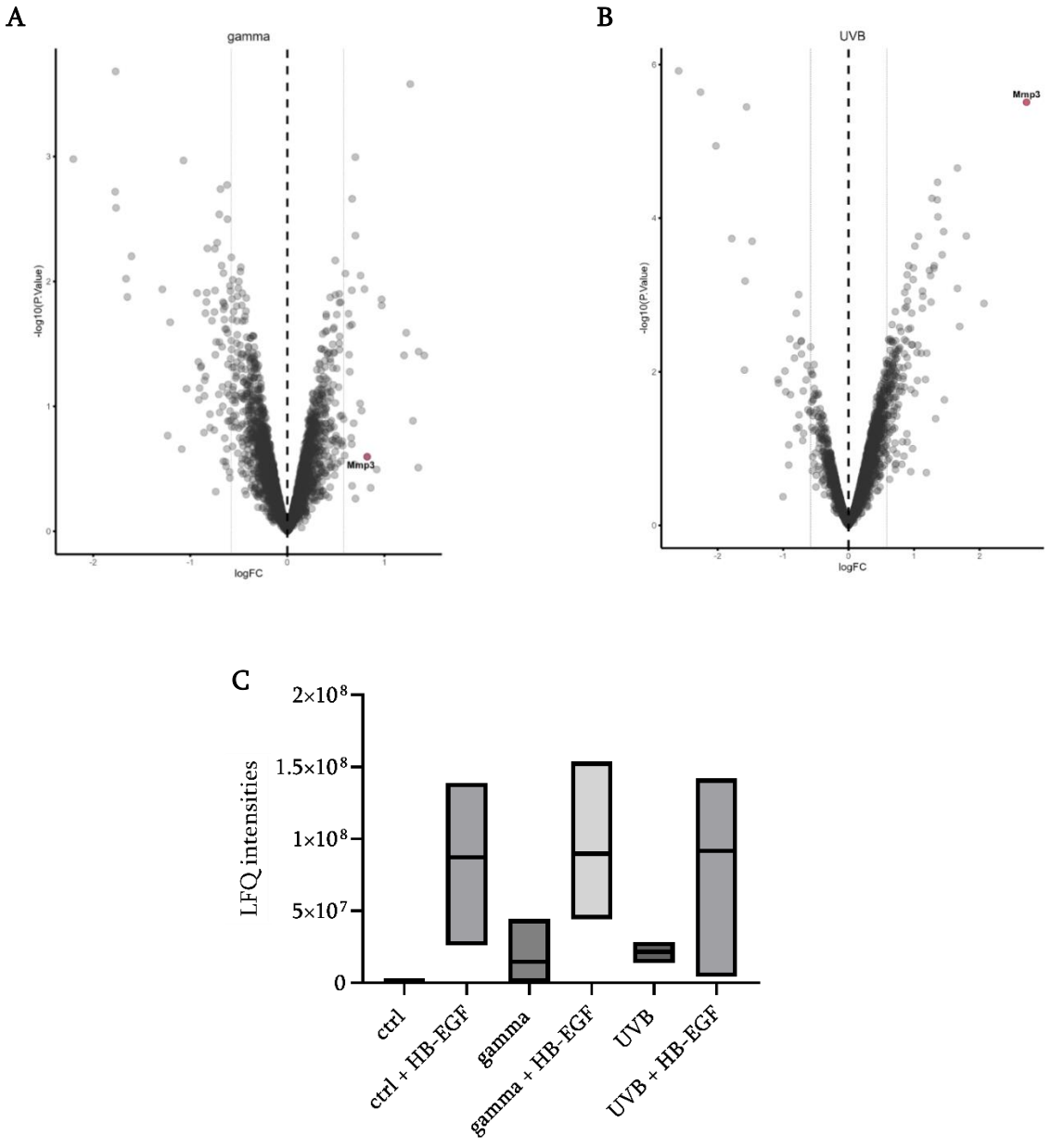


**Fig 2.4.6 Regulation of MMP-3 in MaFi132.** Statistical analyses were performed comparing different conditions regarding the regulation of the proteins. The resulting $\log_2$ fold change is plotted against the according $-\log_{10}$ p-value in Volcano plots (**A, B**). In (**A**) MaFi132 γ-irradiated cells treated with HB-EGF were compared to γ-irradiated cells while in (**B**) the UVB irradiated HB-EGF treated cells were compared to UVB irradiated cells. The figures were generated with R. (**C**) Boxplot of the LFQ intensities. The mean of LFQ intensity of MMP-3 of the replicates from each condition are shown. The graph was generated using GraphPad Prism 9.4.1.

One significantly upregulated protein is matrix metalloproteinase-3 (MMP-3, also known as Stromelysin-1) that cleaves HB-EGF from the cell surface [180] and has been shown to exist as inactive pro-form and as active MMP-3 [181].

MMP-3 was significantly upregulated upon stimulation by HB-EGF in UVB-irradiated MaFi132 (Fig. 2.4.6, B; see Suppl. table 15). Furthermore, it was detected to be slightly upregulated in HB-EGF-treated and γ-irradiated MaFi132 cells, which, however, was not significant (logFC=0.8; p=0.43) (Fig. 2.4.6, A). By analysing the LFQ intensities, MMP-3 could be detected in HB-EGF treated unirradiated cells as well, but since the control cells lacked MMP-3, no logFC could be calculated (Fig. 2.4.6, C). MMP-3 is enhanced upon HB-EGF treatment independently from irradiation.

These findings could be verified by Western blotting (Fig. 2.4.7). Here, MaFi132 cells showed detectable levels of MMP-3 upon incubation with recombinant murine HB-EGF. Furthermore, two bands could be detected, indicating the presence of the inactive pro-form and the active form of MMP-3.

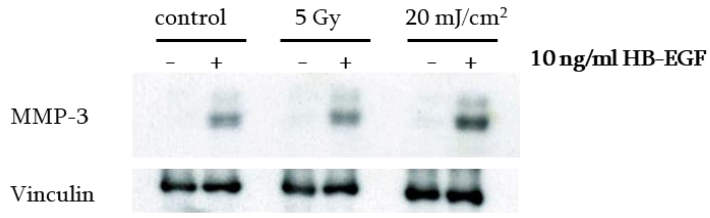


**Fig 2.4.7 Western blot of MaFi132 detecting MMP-3.** MaFi132 were irradiated using either 5 Gy or 20 mJ/cm². Afterwards, cells were incubated with normal growth medium or medium supplemented with 10 ng/ml recombinant murine HB-EGF. Cells were harvested 24 h after treatment. Vinculin was detected as loading control.

To verify, that MMP-3 was upregulated due to the stimulation with recombinant murine HB-EGF, the MAPK/ERK-pathway was investigated. Different inhibitors, targeting proteins involved in the cascade of the MAPK/ERK-pathway, were used (Fig. 2.4.8). Afatinib inhibits the EGF-receptor directly, while Sorafenib targets the Raf kinase and SCH772984 targets ERK1/2.

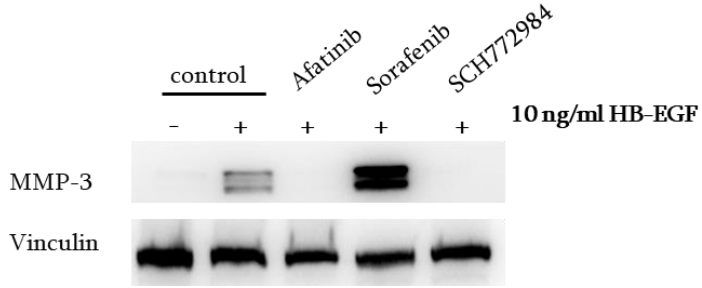


**Fig 2.4.8 Western blot of MaFi132 detecting MMP-3 in HB-EGF stimulated cells.** MaFi132 were stimulated with 10 ng/ml of recombinant mouse HB-EGF. To inhibit stimulation via ERK/MAPK pathway, 1 µM of either Afatinib, Sorafenib or SCH772984 were added. Cell lysates were compared to lysates of untreated control cells and control cells treated only with HB-EGF. 50 µg per sample were loaded on 10% SDS gel. Vinculin was detected as loading control.

Stimulation with HB-EGF induced upregulation of MMP-3, while additional treatment with Afatinib resulted in the loss of MMP-3. The same effect could be observed after treatment with the ERK1/2 inhibitor SCH772984. Interestingly, MMP-3 was even more upregulated when cells were treated with Sorafenib compared to cells treated with HB-EGF only, indicating a mutation in the Raf kinase. Here, the upregulation of MMP-3 can be observed *via* the stimulation of the EGF receptor in p53 deficient cells.

Overall, these analyses showed that upon UVB irradiation, NER pathway mechanisms are stimulated *via* GGR. Furthermore, the NHEJ repair mechanisms, involving the MRN-complex, are activated upon γ- and UVB irradiation.

The HB-EGF treatment did not result in clearly differently regulated pathways. The *Trp53* status showed no obvious influence on the cellular mechanisms investigated after HB-EGF treatment. As cells were harvested 24 h post treatment, proteins which induce morphological changes of the cells might be back to their normal levels. Therefore, in order to capture molecular responses upon irradiation and HB-EGF treatment, cells need to be analysed at an earlier time point.

# 3. Results

## Chapter II: Adaptive Immunity

**Please note that the data is part of the publication Ahmels et al, 2022.*

To prevent carcinogenesis, vaccines have been developed priming the adaptive immune system against HPV infection [65, 66]. Those vaccines based on the L1 protein induce high antibody titers but show low cross-protection against other HPV types [182]. Papillomavirus minor capsid L2 based vaccines represent an alternative strategy based on their highly conserved sequence among different PV types [79]. In this part, the cross-protection of two L2-based vaccines is examined in the immunocompetent preclinical model *Mastomys coucha*: the HPV16 RG1-VLPs (obtained from Prof. Dr. R. Kirnbauer) and the CUT-PANHPVAX (obtained from Prof. Dr. M. Müller) [183].

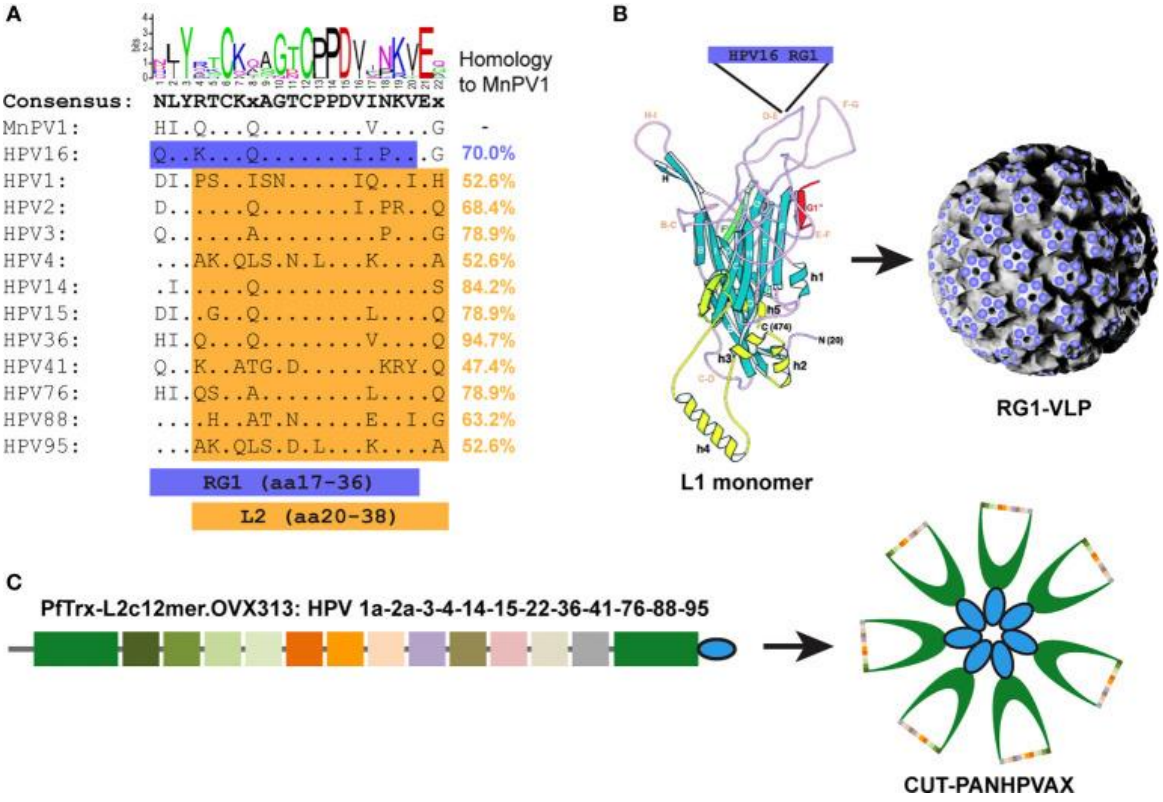


**Fig. 3.1 Structure and homology of the L2 based vaccines.** In (**A**) the homology of the L2 peptides is shown (blue: peptide from HPV16 RG1 vaccine; orange: peptides from the CUT-PANHPVAX vaccine). The percentage on the site describes the homology between each peptide to MnPV1. For alignment of the sequences Clustal 2.0.12 was used. For the determination of the consensus sequence EMBOSS Cons was used [146]. Visualisation was performed using WebLogo. (**B**) The HPV16 RG1-VLP consists of L1 monomers containing a DE surface loop in which the RG1 epitope (aa17-36 from HPV16 L2) is inserted. Monomers assemble to VLPs presenting the L2 epitope on the surface. In (**C**) the construction of the CUT-PANHPVAX is shown, which consists of a protein including L2 peptides (aa20-36) from twelve HPV types (HPV types 1a, 2a, 3, 4, 14, 15, 22, 36, 41, 76, 88 and 95). Insertion of the fusion protein into the thioredoxin scaffold (PfTrx, green) and fusion to the OVX313 domains (blue) lead to peptides assembling to heptamers. This figure is adapted from [183].

The HPV-RG1 VLP vaccine contains modified HPV16-L1 VLPs with the HPV16-RG1 epitope entrapped in the immunogenic DE-surface loop of L1. Based on this construction, assembled VLPs present the HPV16-RG1 epitope on their surfaces in a repetitive and highly immunogenic manner (Fig. 3.1, B) [72, 75, 77]. In contrast, the CUT-PANHPVAX vaccine contains L2 epitopes (aa 20-38) of twelve different HPV types (HPV types 1a, 2a, 3, 4, 14, 15, 22, 36, 41, 76, 88 and 95) (Fig. 3.1, C), which are grouped into multimeric polytopes. Those are inserted into the N-terminus of the thioredoxin (Trx) protein of the archaea *Pyrococcus furiosus* (Pf), which is protease-resistant, highly thermostable and has further a strong polypeptide solubilisation capacity [184]. C-terminal fusion of the PfTrx-Lc12mer construct to OVX313 (a hybrid derivative of the complement C4-binding protein) [185] allows the assembling of the peptides to heptamers. Alignment of the sequence of the 12 different epitopes shows a range between 47.4% and 94.7% identity between MnPV L2 and the oligomerized L2 epitopes, while the HPV16 RG1 and MnPV L2 share 70% identity (Fig. 3.1, A).

However, to assess the cross-protective capacity of the two L2-based vaccines in *Mastomys coucha* the following experimental procedure was performed.

Virus-free animals were vaccinated every second week with either HPV16 RG1-VLPs or CUT-PANHPVAX. As positive control, one animal group was vaccinated with MnPV-L1 VLPs and as negative control, PBS was injected in one animal group. Experimental infection with MnPV virions was performed 10 weeks after the first immunisation.

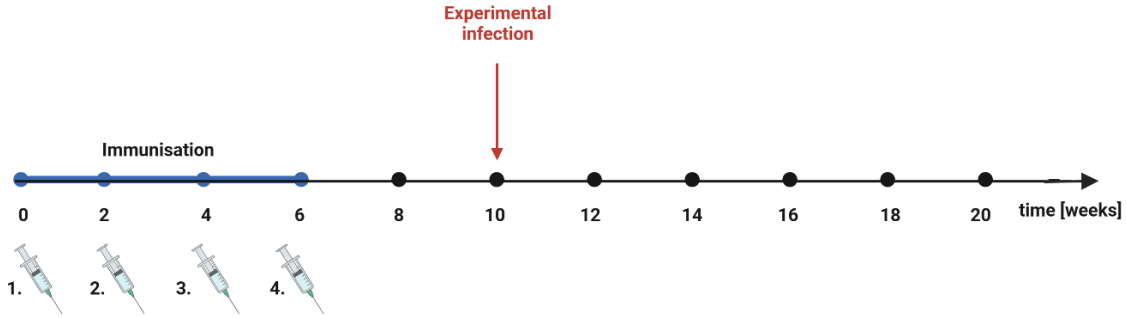


**Fig. 3.2 Experimental setup for vaccination study.** 8 weeks-old virus-free animals were immunized every second week, starting at week 0 (blue marked time) for four times. Per group, 6 animals were vaccinated subcutaneously (half male, half female). The animals were experimentally infected on their shaved backs 10 weeks after the first immunisation. Blood samples were taken every second week, starting at week 0 pre immunisation. The figure was created using BioRender.com.

### Reactivity during immunisation

To investigate the development of reactive antibodies against MnPV, the reactivity during immunisation was monitored (Fig. 3.3, A). Animals immunised with PBS or MnPV VLPs did not react in a GST-MnPV L2-ELISA (week 0 vs week 10, $^{ns}p>0.999$, Two-Way-ANOVA). In contrast, animals vaccinated with HPV16 RG1-VLPs or CUT-PANHPVAX showed increasing reactivity. Interestingly, the HPV16 RG1-vaccinated animals (week 0 vs. week 10, $^{**}p=0.0065$, Two-Way-ANOVA) reacted slightly lower than animals vaccinated with CUT-PANHPVAX (week 0 vs. week 10, $^{***}p<0.0001$, Two-Way-ANOVA). This effect can be explained by the higher homology of the HPV L2 peptides of the CUT-PANHPVAX to MnPV L2. Moreover, CUT-PANHPVAX contains epitopes from 12 different HPV types, whereas HPV16 RG1-VLPs only present an epitope of one HPV type. This may enhance the chance of inducing cross-reactivity.

In the MnPV VLP-ELISA, PBS-vaccinated animals showed no reactivity, whereas in the positive control group the reactivity increased after the first immunisation (week 0 vs. week 10, $^{***}p<0.0001$, Two-Way-ANOVA) (Fig. 3.3, B). The sera from CUT-PANHPVAX-vaccinated animals did not react in MnPV VLP-ELISA while the HPV16 RG1-epitope induced a strong cross-reactivity against MnPV VLPs.

Additionally, the (cross-)neutralisation was tested by PBNA using MnPV pseudovirions (Fig. 3.3, C). After four weeks, high L1-mediated neutralising antibody titers were measured in the sera of MnPV VLP-vaccinated animals as before in the MnPV VLP-ELISA. In contrast, animals vaccinated with HPV16 RG1-VLPs or CUT-PANHPVAX showed low cross-neutralisation (week 0 vs. week 10, $^{ns}p>0.9999$, Two-Way-ANOVA, for both groups) even though both L2-based vaccines induced high antibody titers against L2 (Fig. 3.3., A). These contradictory observations might be explained be the low sensitivity of the L1-based PBNA to detect L2-mediated neutralisation [186]. To increase the sensitivity for L2-based neutralisation, PsVs were pre-treated with furin to expose L2, which usually happens after binding of L1 to HPSGs during infection [187]. In the FC-PBNA, cross-neutralizing antibodies could be detected in the sera of HPV16 RG1-vaccinated animals (3 out of 6) and in the sera of CUT-PANHPVAX-vaccinated animals (4 out of 6) (Fig. 3.3, D).

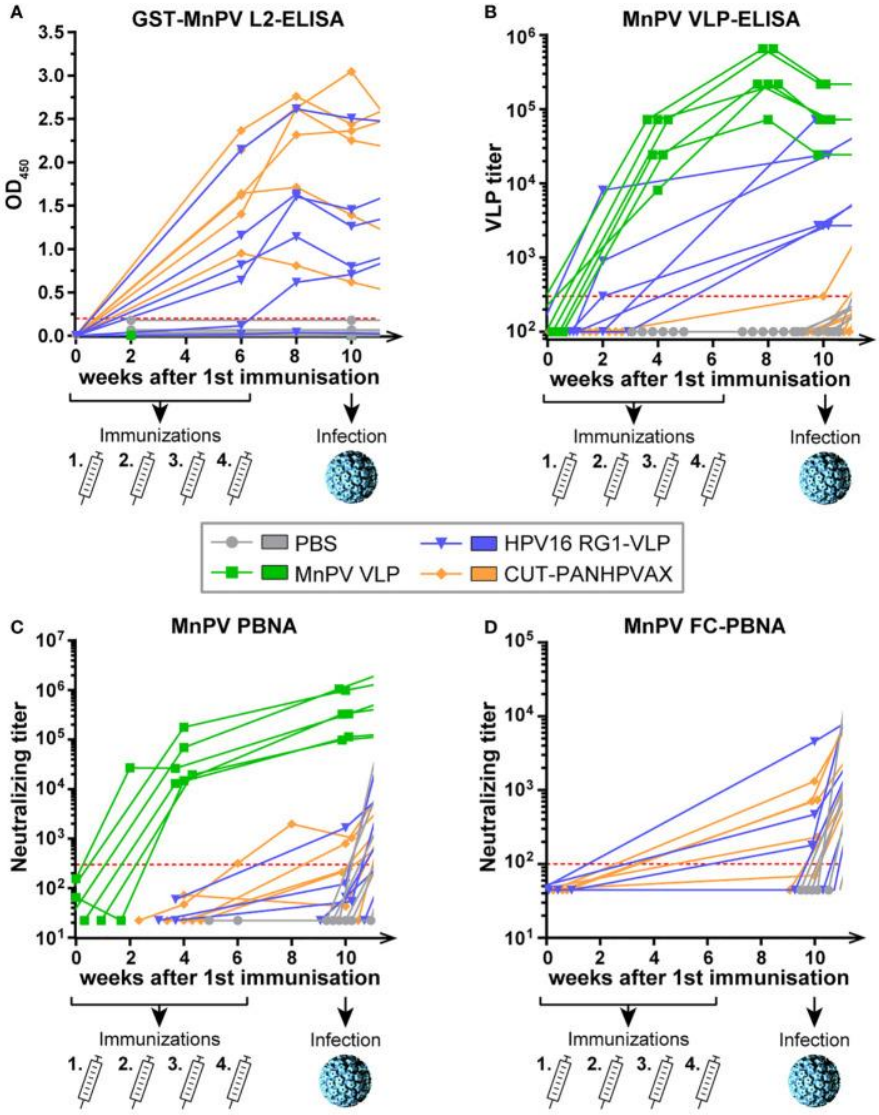


**Fig. 3.3 Seroconversion during vaccination.** (**A**) GST-MnPV L2-ELISA, (**B**) MnPV VLP-ELISA, (**C**) MnPV PBNA and (**D**) MnPV FC-PBNA. Animals were injected with PBS (grey), MnPV VLP (green), HPV16 RG1-VLP (blue) or CUT-PANHPVAX (orange) every second week for four times. The methods' cut off is marked by the dash line (for GST-MnPV L2-ELISA: $OD_{450}$=0.2; for MnPV VLP-ELISA: titer of 300; for MnPV PBNA: titer of 300; for MnPV FC-PBNA: titer of 100). The dashed lines present the methods' cut off. The figures are adapted from [183]. (In the GST-MnPV L2-ELISA and the MnPV FC-PBNA, VLP sera were not measured due to limited quantity of sera)

### Reactivity after viral infection

Subsequently, the protection against viral infection was examined. Hence, four weeks after immunisation, experimental infection was performed by applying infectious MnPV virions previously obtained from papilloma extract at the shaved backs of the animals.

Except for the MnPV VLP-vaccinated group, the reactivity against MnPV VLP increased in all animals after the experimental infection (Fig. 3.4, B), while the reactivity against L2 did not change in most animals (Fig. 3.4, A). This can be explained by the L2 protein being hidden in the capsids of infectious virions.

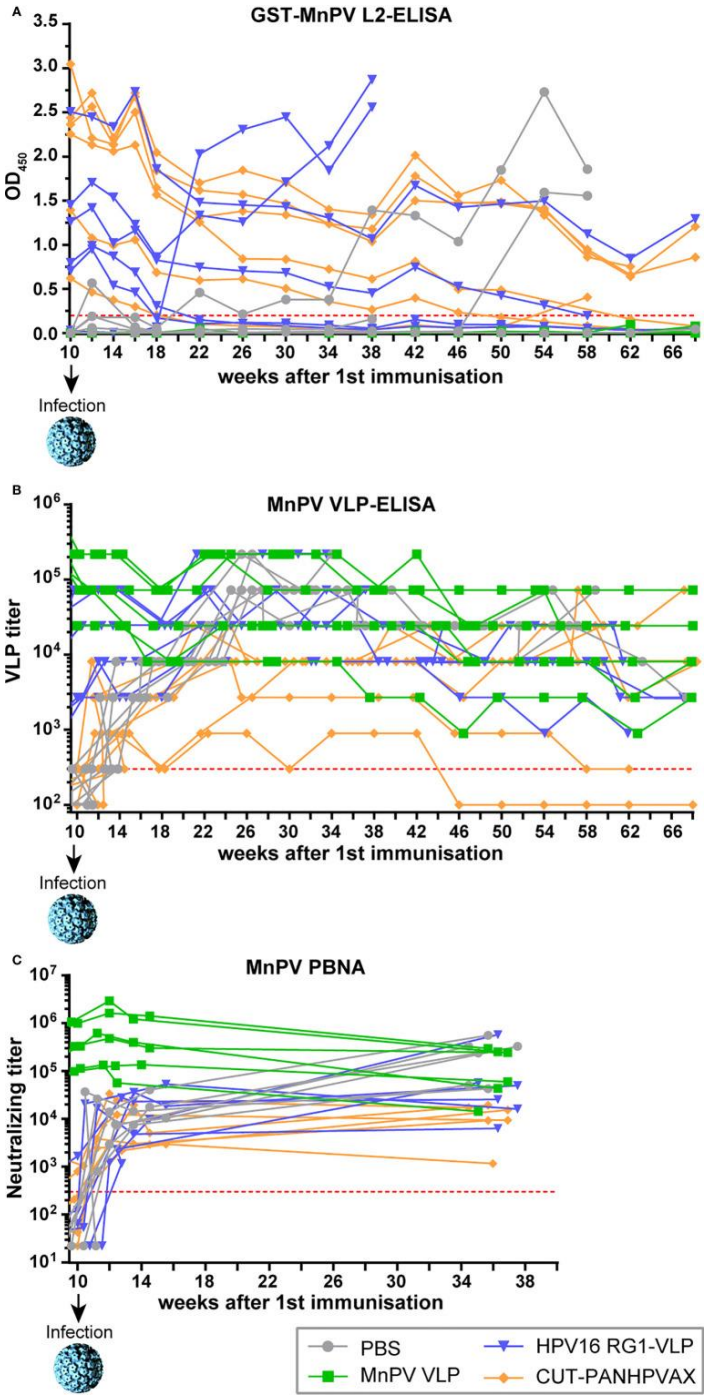


**Fig. 3.4 Serological responses of vaccinated animals after MnPV infection.** At indicated time points, sera were obtained from vaccinated animals and measured in (**A**) GST-MnPV L2-ELISA, (**B**) MnPV VLP-ELISA and (**C**) MnPV PBNA. Four weeks after final immunisation with PBS (grey), MnPV VLP (green), HPV16 RG1-VLP (blue) and CUT-PANHPVAX (orange), animals were experimentally locally infected on their shaved backs. In all groups n=6 animals were included. The methods' cut-off is marked by dashed lines (GST-ELISA: OD450=0.2; MnPV VLP-ELISA and MnPV PBNA: titer of 300). The figure is adapted from [183].

After infection, titres of neutralizing antibodies above the cut-off were detected for all animals (Fig. 3.4, C). Since the MnPV VLP-vaccinated animals developed high antibody titres before infection, no boost of their seroreactivity in VLP-ELISA and MnPV PBNA could be observed (Fig. 3.4, B, C).

In the GST-MnPV L2 ELISA, two HPV16 RG1 VLP-vaccinated animals showed increased reactivity after week 18 (Fig. 3.4, A), but no cross-reactivity could be detected in the MnPV L1-PBNA *prior to* infection (Fig. 3.3, C). Those two animals developed skin tumours and were consequently considered as non-responders. Similar effects could be monitored for two PBS- vaccinated animals, which developed tumours after showing an increased reactivity after week 34 and 46.

### Viral load and tumour development

Furthermore, viral load in plucked hair bulbs and tumour development were observed over time to investigate whether the HPV-L2-based vaccines can cross-protect against MnPV infection.

In Fig. 3.5, A, successful experimental infection for all animals is indicated due to viral loads above the method's cut-off. PBS-vaccinated animals showed a strongly increased median viral load after viral infection (100-100,000 copies/cell), while the median viral load of VLP-vaccinated animals was slightly above the cut-off with 1-10 copies/cell (Fig. 3.5, B). This proves an effective protection by MnPV VLP-vaccination. Excluding the two non-responder animals, which showed similar viral loads as the PBS control group, the viral load of HPV16 RG1- and CUT-PANHPVAX- vaccinated animals fluctuated between 1-100 copies/cell, similar to the median viral load of MnPV VLP-vaccinated animals.

In Fig. 3.5, C, the tumour development in the infected animals is monitored. Five out of six PBS-vaccinated animals started to develop visible skin tumours 12 weeks after infection, while no tumours were detected in MnPV VLP-vaccinated animals. In the HPV16 RG1 VLP-vaccinated animal group, two out of six developed a skin tumour at week 30, which were the two previously identified non-responders. At week 48, one animal from the CUT-PANHPVAX-vaccinated group developed a skin tumour.

Comparing the protection efficiency of the two group L2-based vaccines to the fully protective MnPV VLP-vaccine, no significant differences could be defined.

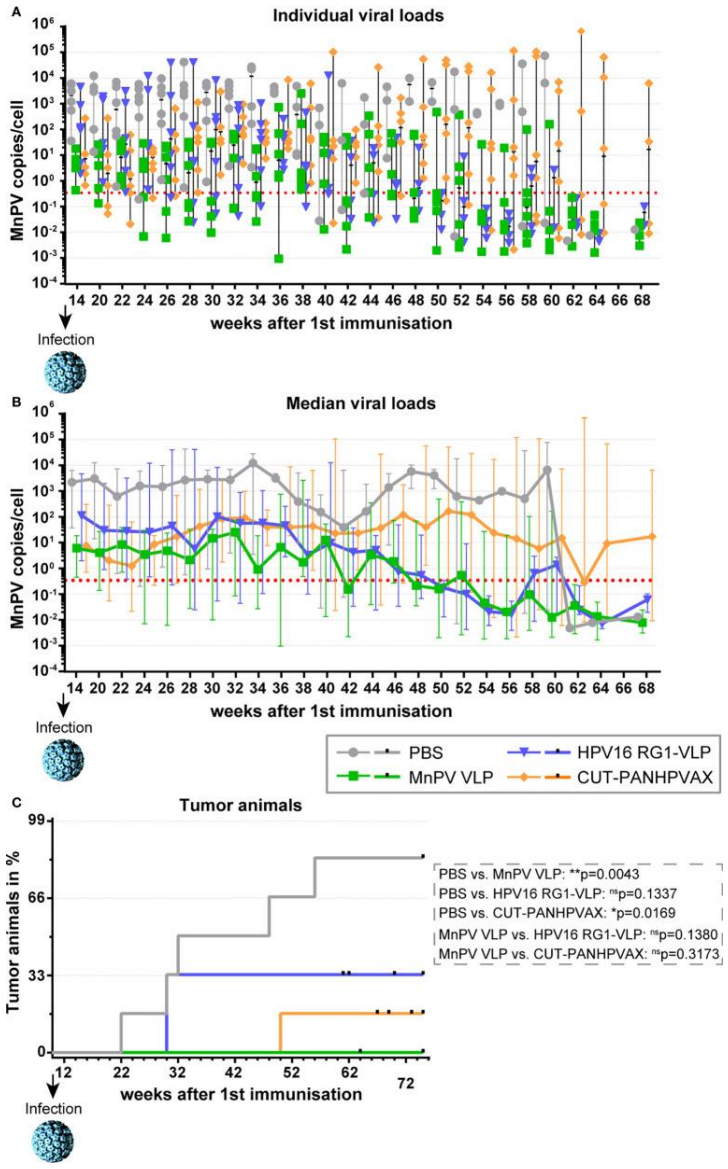


**Fig. 3.5 Viral load and tumour development after viral infection.** To measure the viral load, plugged hair was collected over time and analysed *via* qPCR. Analyses shown for (**A**) individual animals or (**B**) for the respective vaccination group (median ± range). The methods' cut-off is marked by dashed lines based on hair extracted *prior to* experimental infection (0.946 copies/cell). Animals were observed over time for the development of tumours (**C**). The small vertical bars represent excluded animals which died for unknown reasons before tumour development. To describe the differences between the vaccination groups the log-Rank test was included. The figure is adapted from [183].

Further investigations of the epithelial tumours showed the expression of early (E4; Fig. 3.6, C) as well as late (L1 (green) Fig. 3.6, D; L2 (red) Fig. 3.6, E) proteins, which results from persistent MnPV infection. Positive Ki67 (red, Fig. 3.6, D) and E-cadherin (green, Fig. 3.6, E) staining in benign tumours revealed hyperproliferation of infected epithelial cells. Additionally, high viral numbers could be detected in those tumours (Fig. 3.6, B, insert). Histological characterisation of infected skin showed detectable signs of infection, which were not observed in the skin of animals that developed cross-neutralising antibodies due to vaccination (Fig. 3.6, F).

In summary, this pilot study indicates that the L2-based vaccines have the potential to induce cross-neutralisation against PV-infection.

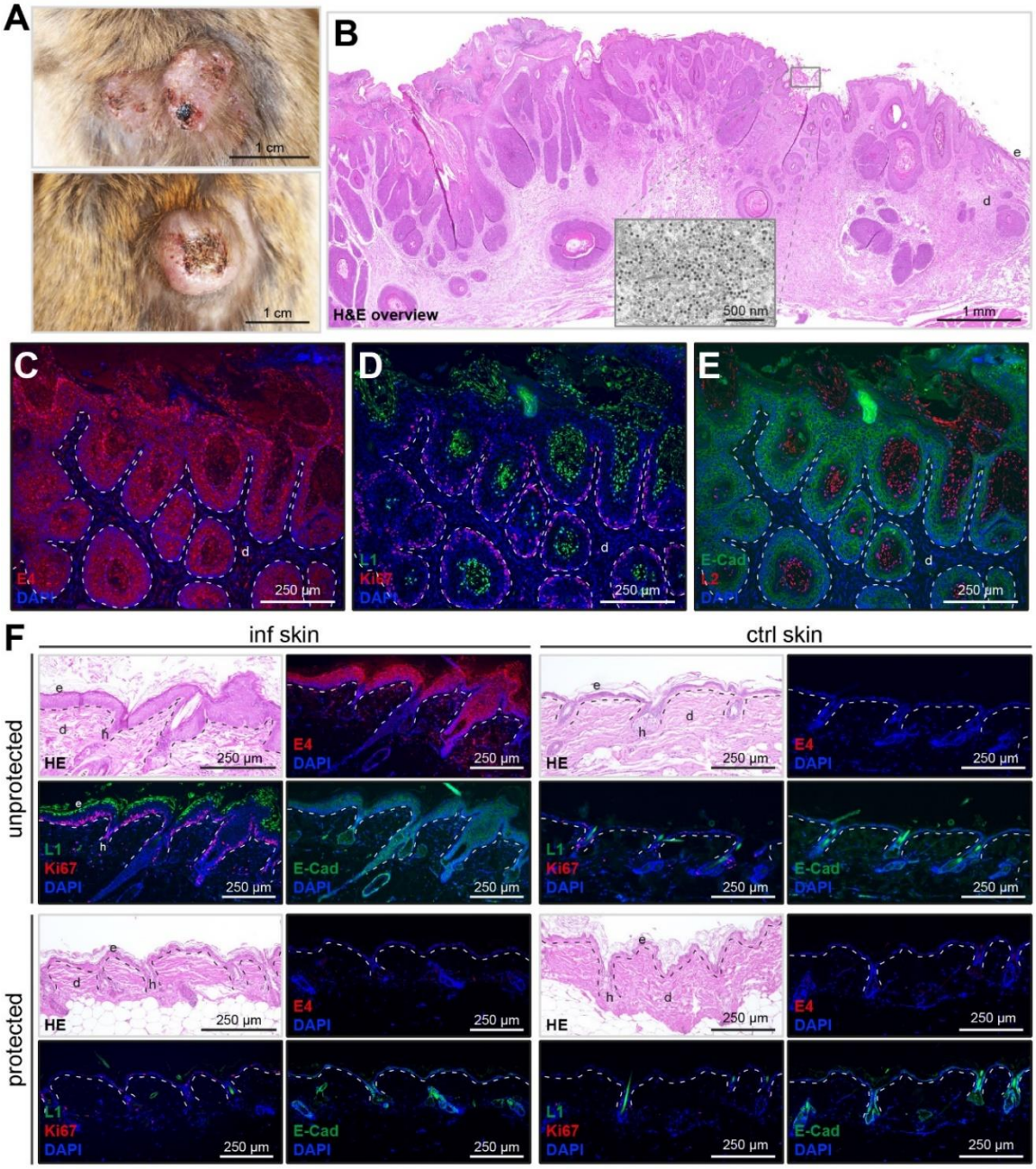


**Fig. 3.6 Histological analyses of MnPV-induced skin changes and tumour development.** (**A**) Representative benign MnPV-induced skin tumours after experimental infection of animals from the mock control group are shown. The HE-staining of papilloma from infected control animals were performed (**B**). Transmission electron microscopy identified viral replication in the keratinized outermost layer by (TEM; inset). Early gene expression was detected by staining for E4 (red) (**C**). In (**D**), the proliferation in corresponding areas is proofed by Ki67 staining (red) and co-staining for L1 (green) revealed the expression of late genes as well as in (**E**) by staining for L2. To reveal the origin of infected cells, E-cadherin (green). (**F**) Representative tissue stainings of unprotected and protected vaccinated animals. From the same animal, experimentally infected ("inf") and uninfected control skin ("ctrl") was HE-stained. Furthermore, immunofluorescence staining for MnPV E4 or Ki67 (red), L1 or E-cadherin (green) were performed. Visualisation of the nuclei were achieved by DAPI staining (blue). The figure is adapted from [183].

# 4. Discussion

## Chapter I: Innate Immunity

Our collaboration partners previously study showed that macrophages play a critical role in DNA repair efficiency in mouse liver, thereby connecting the innate immune system to DNA repair mechanisms [114]. However, it was unclear whether this concept could be transferred to of UVB/ PV-induced skin carcinogenesis. Therefore, the first part of this work focused on the innate immune system and analysed whether a macrophage-assisted DNA repair can be exists in the skin of to the animal model *Mastomys coucha.*

### The animal model *Mastomys coucha* and its limitations

Although *Mastomys* is one of the best models to mimic natural infection and tumour formation, it has the drawback that antibodies and analytical kits are not commercially available [188]. Therefore, antibodies and methods needed to be laboriously established before starting final experiments [189]. Since the model is phylogenetically related to mice and rat, tools and protocols designed for these species could at least be taken as a reference.

The protein HB-EGF has been described to be present in human, mice and rats. Alignment of the protein sequences revealed that mouse and *Mastomys* HB-EGF protein sequences share a high similarity of 90% (Fig. 2.1.1). Therefore, the cross-reactivity of anti-mouse HB-EGF antibodies against *Mastomys* EB-EGF was tested. Generally, only a few antibodies were available against HB-EGF, and only one of them successfully detected HB-EGF in Western blotting after ectopic overexpression in fibroblasts. Restricting further experiments, endogenous HB-EGF could not be detected by Western blotting independently from cell type and treatment (Fig. 2.1.4, 2.1.5 and 2.1.7). Using an ELISA kit, murine HB-EGF, but not *Mastomys* HB-EGF, was detectable in cell lysates after overexpression in fibroblasts. Furthermore, it could be shown that the supernatant of transduced fibroblasts contained murine soluble HB-EGF. However, endogenous murine HB-EGF and *Mastomys* HB-EGF could not be detected (Fig. 2.1.8). The observation that overexpressed *Mastomys* HB-EGF was detected by Western blot and not detectable in ELISA can potentially be explained by the fact that the ELISA kit includes monoclonal antibodies. Monoclonal antibodies against murine HB-EGF provided by R&D bind to the region between $Asp_{63}$ and $Leu_{148}$. This region shares 83% identity with the *Mastomys* sequence. Possibly these slight differences in the sequence lead to a slightly different folding in the protein [190-192], which prevents the mouse-specific antibody from binding to *Mastomys* HB-EGF in the ELISA. For Western blotting, a polyclonal antibody was used, which enhances the chance to detect multiple epitopes.

The inability to detect endogenous HB-EGF could be explained by low levels of HB-EGF or low sensitivity of Western blotting. Harlow and Lane [193] reported, that in Western blotting 10 – 100 fmol of a protein can be detected. Transferring this to the protein HB-EGF (size ~23 kDa) would mean that at least 11.5 ng of the protein need to be in a total of 20 µg protein to be detected in Western blot, while in the R&D ELISA 0.03 ng/ml of the protein can already be detected. Furthermore, the Western blot method includes series of independent steps, enhancing the susceptibility to errors [194-198], while the ELISA is performed within a few incubation steps. However, to further investigate, whether HB-EGF plays a crucial role in our system alternative approaches to detect HB-EGF need to be established.

Another limitation of studying infection and tumour development in *Mastomys* is the low availability of *Mastomys* cell lines. In previous works, several fibroblast cell lines as well as one keratinocyte cell line could be isolated and expanded from *Mastomys* skin [95]. In the context of PV-infection, keratinocytes are the targeted cell type, but the isolated keratinocytes could not be successfully expanded and transfected for experiments. Alternatively, murine keratinocytes (308kera) were considered, which have been successfully transduced with the MnPV oncogenes and were therefore used to investigate the influence of MnPV E6 and E7 on the immune response (Chapter 2.2). However, this cell line contains a *H-ras* mutation at codon 61 [199] leading to activation of the Ras protein, which is involved in MAPK signalling. This pathway is activated upon ligand binding to the EGFR [200]. Effects by HB-EGF as upstream activator of EGFR signalling may be masked by the constitutive activation of downstream regulator Ras that already mediates signalling. Therefore, *Mastomys* fibroblasts were used to investigate the effect of recombinant murine HB-EGF on *Mastomys* cells.

Furthermore, macrophages were successfully isolated from *Mastomys* bone marrow as well as peritoneal (Fig. 2.1.6) to investigate whether the expression of HB-EGF is stimulated upon UVB irradiation or by mimicking co-cultivation (Fig. 2.1.7). However, since the detection of HB-EGF did not function as expected as well for murine macrophages, the investigation of HB-EGF in the context of UVB irradiation and MnPV infection could not be performed as planned.

### MnPV oncogenes and the immunological environment

Cytokines are a group of signalling molecules that play a crucial role in the functioning of the immune system [52]. They can enhance or reduce the inflammatory immune response and are therefore referred to as pro- or anti-inflammatory cytokines [201-203]. Previous studies showed that the cytokine expression can be influenced by HPV infection in HPV-positive women [57, 204-206]. Furthermore, the cytokine pattern differs in persistently infected cells [207]. Additionally, the expression of pro-inflammatory cytokines such as TNFα, IL-1β and IL-6 upon UVB irradiation has been reported [153, 154, 158, 159] and were therefore analysed besides the mRNA levels of HB-EGF.

In the current study, *Hbegf* expression as well as the mRNA levels of the pro-inflammatory cytokines TNFα, IL-6 and IL-1β [153] was significantly upregulated upon UVB irradiation in MnPV E7-transduced keratinocytes. This indicates that MnPV E7 supports the proliferation of damaged cells and apparently also shifts the immunological environment towards chronic inflammation, which was previously described for persistent infection with cutaneous HPVs [208-212]. Even though PVs try to escape the inflammatory immune response to avoid clearance of infected cells, they also use pro-inflammatory cytokines to favour their own replication [213, 214].

Furthermore, MCP-1 and IL-34, which were reported to stimulate monocytes and Langerhans cells [161, 162] were analyzed. Monocytes as well as Langerhans cells play a crucial role in the immune system's defense against pathogens [163, 215, 216]. While Langerhans cells serve as APCs (antigen presenting cells) by presenting antigens of captured pathogens on their surface to stimulate other immune cells to action [163, 217], monocytes can differentiate into macrophages [218, 219]. In the skin, macrophages can release cytokines as well as growth factors contributing to the stimulation of the immune response and tissue repair [220-223]. In the present experiment, *Il-34* mRNA is upregulated upon UVB irradiation independently from

the presence of oncogenes (Fig. 2.2.3, B), this was not the case for *Mcp1*, which is upregulated in MnPV E7-transduced cells upon UVB irradiation. IL-34 specifically stimulates Langerhans cells (LCs) in the skin. Upon UVB irradiation, depletion of the LCs niche has been observed [224]. If one transfers this *in vitro* observation to the skin, this could indicate that the increase of IL-34 after 24 h lead to the recruitment of newly developed LCs to the skin site after preceding depletion due to UVB irradiation. The mRNA level of *Mcp1* is upregulated in the presence of MnPV E7, indicating that the stimulation of the monocytes and macrophages in this system is favoured. In the case of chronic inflammation upon infection with cutaneous HPVs, macrophage infiltration was reported [225], which seemed to be stimulated also in our setup. Overall, this *in vitro*-system seemed to mimic the effect of persistent HPV infection.

However, high standard deviations could be observed throughout the qPCR analyses even though experimental replicates were performed under the same conditions. Here, the cell cycle might play a crucial role, as many proteins and signaling pathways are cell cycle-dependent and can interfere with the expression of interleukins [226, 227]. In these experiments, cytokine expression was mainly enhanced at later time points. Upon DNA damage induction, cells undergo cell cycle arrest, in which transcription of genes is repressed [228]. This could explain the enhanced mRNA expression at late time points.

To draw a clear conclusion regarding cytokines and the change in the expression pattern in the context of MnPV infection and UVB irradiation, cells would need to be synchronized or the current state of the cell cycle needs to be defined. Additionally, identification of the immune cells in UVB irradiated infected skin will allow to draw a final conclusion about the immunological environment in the presence of the MnPV E7 oncogene.

### DNA damage detection and pathway analyses

UVB light induces cyclobutane pyrimidine dimers (CPDs) in exposed DNA, which can result in γH2AX foci due to the collision of replication forks [229]. Detection of these foci has been shown to be the most reliable method to visualize DSBs upon DNA damage induction [164] and has also been used here. γH2AX has been shown to be correlated to DNA damage induction detecting DNA double strand breaks (DSBs) [164, 229]

Since enhanced DNA repair efficiency could be detected upon HB-EGF treatment of UVB irradiated cells, proteomic analyses were performed to define, which pathways are regulated. Since our collaboration partner used DEN to induce DNA damage [114], γ-irradiation was included to mimic similar effects [230] and to compare their findings to DNA damage upon UVB-irradiation and HB-EGF treatment.

DNA repair mechanisms are regulated in a cell cycle and damage-dependent manner [169, 229]: While CPDs are repaired by nucleotide excision repair (NER), DSBs can be repaired by homologous recombination (HR) or non-homologous end-joining (NHEJ) [154, 170]. NER as well as NHEJ can further be divided into sub-pathways, which differ in the complexes recognising DNA breaks [231, 232]. In my study, proteins involved in DNA damage repair pathways had a logFC varying between -1 and 1 (meaning a doubling of the levels) Upon DNA damage induction protein regulation can occur in different ways: Besides the phosphorylation of proteins e.g, ATM and ATR [145, 229, 233-236], the degradation and stabilisation of protein, e.g., p53, are altered [237]. upon DNA damage induction [238]. In this proteome analyses, the stabilisation and degradation of proteins is detected, while the phosphorylation of proteins, a fast induced

process, is not considered. However, the protein Thrombospondin 1, which has been reported to influence cell proliferation [179], is downregulated upon UVB irradiation (Fig. 2.4.2), which is consistent with previous studies [175] and proves that the experimental setup was carried out correctly.

In general, the NER pathway apparently plays a more important role after UVB irradiation than after γ-irradiation, which is in line with previous studies [239-244]. This effect is most obvious in MaFi191 R266C cells. In contrast, the NHEJ signalling pathway is similarly regulated in γ- and UVB irradiated cells (Fig. 2.4.2). Furthermore, the results of the proteome analysis allow conclusions on the kind of induced DNA damage. For example, the protein MNAT1 is upregulated upon UVB irradiation, which is part of the Holo-TFIIH complex (Fig. 4, B) [170]. This complex contributes to the global genome repair (GGR), a sub pathway of NER, in which lesions are removed throughout the genome regardless of whether any specific sequence is transcribed or not [245]. Additionally, MRE11 is upregulated, a protein, which is part of the MRN complex (Fig. 4, A) [173]. This complex binds to open ends of DNA strands [246] and can contribute to both the HR as well as the NHEJ pathway [247]. Even though no significant differences in pathway regulation between the different cell lines could be observed, the data indicate that the same DNA repair pathways are stimulated with different methods of DNA damage induction.

For further investigations, the phosphorylation status of the proteome needs to be analysed in a time dependent manner. Due to time limitations this could not be performed in this work.

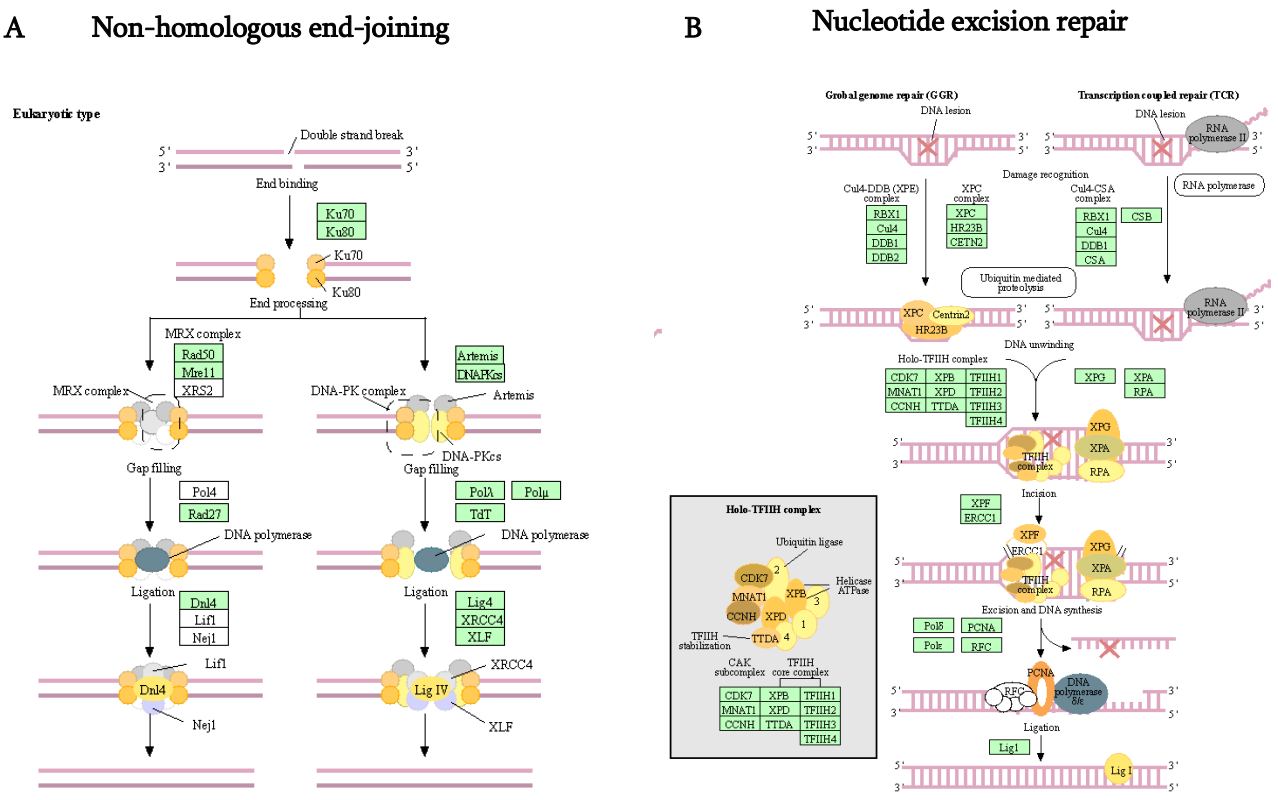


**Fig. 4 Schematic overview of DNA damage repair mechanisms.** The elimination of DSBs is performed *via* **(A)** nonhomologous end joining (NHEJ). NHEJ involves binding of the KU heterodimer binds to double-stranded DNA ends, recruitment of DNA-PKcs or MRX complex (or: MRN complex), processing of ends, and recruitment of the DNA ligase IV (LIG4)-XRCC4 complex, which brings about ligation. Nucleotide excision repair (NER) is a mechanism to repair bulky DNA damage caused by e.g., exposure to UV-light **(B)**. Two different sub-pathways of NER known as transcription-coupled repair (TCR-NER) and global genome repair (GGR-NER). Damage recognition in GGR-NER involves XPC-hHR23B complex together with XPE complex. The figures were adapted from KEGG database [272-274].

### Pathway regulation upon HB-EGF stimulation

HB-EGF is one of several EGFR ligands that can stimulate proliferation and cell growth [248, 249] and has been shown to enhance DNA damage repair efficiency [114]. Comparing the proteome of control cells to HB-EGF treated cells and HB-EGF treated irradiated cells to irradiated cells, no clear difference in the protein regulation could be observed. However, Thrombospondin 1 is downregulated after UVB irradiation and followed HB-EGF treatment in all cell lines (Fig. 2.4.4, B). Thrombospondin 1 has been reported to act as a stimulator or inhibitor for cell proliferation and cell adhesion in a context-dependent and cell specific manner [179]. Since HB-EGF acts as a stimulator for cell proliferation, Thrombospondin 1 might act as an inhibitor, which is downregulated upon HB-EGF treatment to support proliferation of the cells. In contrast, proliferation has been reported to be inhibited after UVB irradiation [176]. This would indicate that Thrombospondin 1 acts as a stimulator of cellular proliferation mechanisms (Fig. 2.4.2). To clarify the function of Thrombospondin 1 in the different scenarios, further analyses, including targeting e.g., HB-EGF-activated ERK/MAPK signalling are necessary.

In this study, only slight differences in the proteome of HB-EGF treated cells compared to untreated cells could be observed, which indicates that the proteins, which are responsible for the morphological effects (Fig. 2.3.2-2.3.4), are already back to their normal state after 24 h. Eichelbaum *et al.* [250] developed a method to enrich newly synthesized proteins allowing more precise conclusion about the protein regulation in cells. Furthermore, EGFR related pathways such as MAPK-signalling function *via* phosphorylation and dephosphorylation of proteins. Therefore, the identification of the phospho-status of proteins over the time will allow to conclude if EGFR- related pathways are differently regulated in the context of DNA damage induction and HB-EGF treatment.

### MMP-3 expression is stimulated by HB-EGF

MMP-3 can cleave the HB-EGF [180]. Here, I could show that in MaFi132 cells, MMP-3 is upregulated via the ERK/MAPK-pathway upon activation of the EGFR by HB-EGF (Fig. 2.4.5). In the proteomics data, MMP-3 was predicted to be upregulated upon HB-EGF treatment (Fig. 2.4.5, C). This effect could further be detected in Western blotting (Fig. 2.4.6). Interestingly, the inhibition of the MAPK pathway targeting the RAF kinase was not successful (Fig. 2.4.7). MaFi132 is a spontaneously immortalized cell line isolated from *Mastomys* skin [95] that contains a *Trp53* mutation that leads to a loss of p53 due to alternative splicing. However, that does not exclude the presence of mutations in other genes, such as *RAF1*, which has been described to be frequently mutated in tumours, supporting uncontrolled proliferation [251]. The MaFi132 cell line might contain a mutation in *RAF1,* leading to the inability of inhibitor binding and its downregulation. Due to time limitations, DNA sequencing could not be performed in this thesis, which is needed to confirm these observations. Furthermore, DNA polymerase epsilon was upregulated upon DNA damage induction by UVB or γ-irradiation (Fig. 2.4.2, A). In the literature, no direct interaction between p53 and the polymerase is described so far, but polymerase epsilon has been shown to be frequently mutated in different cancer types, supporting proliferation of mutated cells [172].

However, HB-EGF upregulates a matrix metalloproteinase (Fig. 2.4.7), which is able to cleave the protein itself, indicating that a feedback loop is induced. In M2 macrophages, a mechanism, in which a intracellular feedback loop is induced upon the presence of MMP-9, was previously reported [249]. To proof this theory in our system, the development of a tool able to detect HB-EGF (soluble and membrane bound) is necessary.

# Chapter II: Adaptive Immunity

**Please note that this discussion is part of Ahmels et al. 2022*

## Cross-protective vaccination

Vaccinations have been developed in order to prevent diseases induced by infectious agents [252]. Multivalent L1-based vaccines against several mucosal HPV types have been licensed [68], but their cross-protection against other HPV types is limited [182]. Therefore, alternative vaccine strategies have been developed based on the highly conserved L2 protein, leading to cross-protection and cross-neutralisation [253].

In the current study, the animal model *Mastomys coucha* served as a pre-clinical model to investigate the cross-protection of two L2-based vaccines: The HPV16 RG1-VLPs present the RG1 epitope of HPV16 L2 on their surface [77, 254], while the CUT-PANHPVAX contains L2 sequences of twelve different cutaneous HPV types, which are oligomerized and entrapped into a thioredoxin scaffold (Fig. 3.1) [255]. As positive control, one group was vaccinated with MnPV VLPs, since their protective effect against MnPV-infection has been previously proven [256]. virus-free animals were vaccinated *prior to* experimental infection with MnPV. Examination of the cross-protection was performed by monitoring viral-load, seroconversion and tumour development during the duration of the experiment.

Both vaccines induced strong cross-reactivity against MnPV L2 (Fig. 3.3, A) mediated by the highly conserved peptide between aa17-38 of the L2 protein [257]. Furthermore, cross-neutralizing antibodies were detected by FC-PBNA (Fig. 3.3, D), a more sensitive method for the detection of L2-mediated neutralising antibodies as compared to the conventional PBNA [217]. Even though the HPV16 RG-1 vaccine showed cross-reactive potential, it seemed to be slightly lower compared to the CUT-PANHPVAX vaccination (Fig. 3.3). While the RG1 epitope of HPV16 shares only 70% identity with the RG1 peptide of MnPV L2, the CUT-PANHPVAX vaccine contains epitopes of L2 of twelve cutaneous HPVs reaching up to 94.7% sequence identity to MnPV L2 (Fig. 3.1).

In contrast to the CUT-PANHPVAX vaccine, HPV16 RG1 VLPs could theoretically induce additional cross-reactive antibodies against the L1 protein [77], but even though all animals of the HPV16 RG1-VLP vaccinated group showed reactivity against MnPV VLPs (Fig. 3.3, A), only one animal showed cross-neutralisation in PBNA (Fig. 3.3, C). This implies that internal HPV16 VLP epitopes mainly induce cross-reactive antibodies against MnPV VLP. But those epitopes are only presented upon disruption of a minor fraction of the RG1-VLPs, which can accidently happen, when antigens are prepared or during injection. Such linear epitopes have been reported to be targets of cross-reactive antibodies [258]. On the contrary,

neutralising antibodies have been found to be often directed against surface epitopes, which consist of different loops [258, 259].

The different constructions of the L2-based vaccines affect their reactivity against L2, as all six CUT-PANHPVAX vaccinated animals developed cross-reactive antibodies against MnPV L2 and five of them also cross-neutralised furin-cleaved MnPV pseudovirions (Fig. 3.3). Furthermore, five out of six HPV16 RG1-vaccinated animals showed cross-reaction against MnPV L2, but only three developed cross-neutralising antibodies (Fig. 3.3). Similar effects were observed for the licensed vaccine Gardasil®9, where complete protection against some HPV types could not be achieved in a heterologous rabbit skin model [260]. Therefore, in addition to appropriate *in vitro* criteria, natural immunocompetent infection models are necessary to predict the protective effect of vaccines [186, 261].

To monitor the viral load and the effect of vaccination in animals after experimental infection, collected hair bulbs were used to quantify MnPV (Fig. 3.5). While MnPV VLP-vaccinated animals showed low viral loads (1-10 copies/ cell), the viral load was up to ten times higher in HPV16 RG1- and CUT-PANHPVAX-vaccinated animals. However, the load was still lower compared to mock-vaccinated animals (Fig. 3.5, B). This fits with the high neutralising antibody titres after to vaccination with VLPs that can prevent reinfection of the skin and the spread of the virus.

L1 and L2 antibodies have different modes of action, which can affect the mean viral load. While neutralisation by L1-induced antibodies already occurs when the virus reaches the epithelium, anti-L2 antibodies can only bind to the virion in the basement membrane when they are further processed by furin convertase [22]. This could allow a shorter time window for binding of the antibodies. Therefore, L2-based immunisation could elicit a non-sterilising humoral response, unlike VLP-based immunisation [182]. Antibodies can also stimulate cells of the innate immune system, e.g., neutrophils and macrophages, and recruit them to antiviral activities [217]. These antibody-induced responses may contribute to the overall effect of immunisation but were not the focus of this study.

However, it is important to note that the statistical power of the analyses was limited, since only 6 animals per group were analysed. While a statistically significant protective effect was observed for the CUT-PANHPVAX vaccine compared to the mock vaccinated group, two non-responders were present in the HPV16 RG1-VLP group, showing no neutralisation in MnPV L1-PBNA (both animals) and no reactivity in MnPV L2 ELISA (one animal). A larger vaccination study would therefore be required to be able to make a concrete statement.

However, the correlation between viral load and skin carcinogenesis could be clearly observed: while unprotected animals had a high viral load and developed skin tumours, MnPV VLP-vaccinated animals remained tumour-free. This scenario has already been shown in several studies in which the amount of HPV DNA could be correlated with the development of skin tumours [262, 263]. These observations were also made in the animals vaccinated with the L2-based immunogens, which correlates with the success of vaccination (Fig. 3.5).

In contrast to mock vaccination and non-responders, histological analyses of the skin of protected animals did not showed thickened, hyperproliferative epidermis. This epidermis can develop into skin tumours (Fig. 3.6), regardless of the type of neutralising antibody induction. In humans, actinic keratoses (AK) are a precursor of SCC and were also associated with cutaneous HPV types [264, 265].

Since a viral load was measurable despite vaccination, the induced immunity does not appear to be sterilising, but may prevent the development of tumours after infection. In addition, visualisation by L1 and

L2 staining (Fig. 3.6, E and F) and in EM (Fig. 3.6, C) demonstrated that MnPV can pass through its entire cycle, which is not the case in vaccinated animals.

This study serves as a starting experiment for statistically validated studies. In addition, based on these results, studies can be conducted to investigate the influence of UV irradiation and/or immunosuppression in a naturally, preclinical and immunocompetent model. This would allow to get closer to the situation of patients.

However, this study demonstrated the protective efficacy of L2-based vaccines against MnPV infection and skin tumour development by induction of cross-neutralising antibodies. In summary, L2-based vaccination strategies can induce cross-protective immunity against cutaneous PVs.

# 5. Material

## 5.1. Chemicals

| | |
|---|---|
| 2-Propanol | Merck Calbiochem, Darmstadt |
| 6 × DNA Loading Dye | Fermentas, St. Leon-Rot |
| Acetic acid | Merck Calbiochem, Darmstadt |
| Acrylamide-Bis (29:1), 30% w/v | Serva Feinbiochemica, Heidelberg |
| AddaVax™ | Invitrogen™, Karlsruhe |
| Agarose | Sigma-Aldrich, Steinheim |
| Ammonium persulfate | Sigma-Aldrich, Steinheim |
| Ammonium sulfate | Carl Roth GmbH, Karlsruhe |
| Aqua ad injectable | Braun, Melsungen |
| Bradford Reagent | Bio-Rad Laboratories, München |
| Bromophenol blue | Serva Feinbiochemica, Heidelberg |
| BSA Molecular Biology Grade (20 mg/ml) | New England BioLabs, Frankfurt |
| complete mini EDTA free protease inhibitors | Roche, Darmstadt |
| Coomassie Brilliant Blue G-250 | AppliChem, Darmstadt |
| DAPI | Sigma-Aldrich, Steinheim |
| Dithiothreitol (DTT) | Biomol, Hamburg |
| DMSO (dimethylsulfoxide) | Carl Roth GmbH, Karlsruhe |
| dNTPs Set PCR Grade | Invitrogen™, Karlsruhe |
| EB buffer | Qiagen, Hilden |
| EDTA | Carl Roth GmbH, Karlsruhe |
| ECL SuperSignal | West Femto Thermo Fisher Scientific, USA |
| Enhanced Chemiluminescence Substrate (ECL) | PerkinElmer, USA |
| Ethidium bromide, 1% solution | Sigma-Aldrich, Steinheim |
| Formaldehyde (37%) | Sigma-Aldrich, Steinheim |
| Glucose | Carl Roth GmbH, Karlsruhe |
| Goat serum Thermo Fisher Scientific | Darmstadt |
| $H_2O_2$ | Merck Calbiochem, Darmstadt |
| $H_3PO_4$ | Sigma-Aldrich, Steinheim |
| HEPES | Carl Roth GmbH, Karlsruhe |
| HCl | Carl Roth GmbH, Karlsruhe |
| IsoFlo 100% v/v inhalation gas, liquid | Toetis Österreich GmbH, Wien |
| Glycine | Gerbu, Gaibach |
| Ethanol, absolute | Merck Calbiochem, Darmstadt |
| Methanol | Sigma-Aldrich, Steinheim |
| $MgCl_2$ | Merck Calbiochem, Darmstadt |
| $MgSO_4$ | Serva Feinbiochemica, Heidelberg |
| Milk powder, blotting grade | Carl Roth GmbH, Karlsruhe |
| MTT | Sigma-Aldrich, Steinheim |
| NaCl | Carl Roth GmbH, Karlsruhe |
| $Na_2CO_3$ | Carl Roth GmbH, Karlsruhe |
| $NaHCO_3$ | Sigma-Aldrich, Steinheim |
| $Na_2HPO_4$ | Carl Roth GmbH, Karlsruhe |
| NaOH | Carl Roth GmbH, Karlsruhe |
| phosphoSTOP phosphatases inhibitors | Roche, Darmstadt |

| | |
|---|---|
| RiboLock RNase inhibitor | Thermo Scientific, St. Leon-Rot |
| Sodium deoxycholate | Merck Calbiochem, Darmstadt |
| Sodium dodecyl sulfate (SDS), ultra-pure | Carl Roth GmbH, Karlsruhe |
| sodium orthovanadate | Sigma-Aldrich, Steinheim |
| Tetramethylethylenediamine (TEMED) | Sigma-Aldrich, Steinheim |
| Triton® X-100 | Serva Feinbiochemica, Heidelberg |
| Trizma®base (Tris) | Sigma-Aldrich, Steinheim |
| Tween® 20 | Gerbu, Gaibach |
| 3,3',5,5'-Tetramethylbenzidine (TMB) | Sigma-Aldrich, Steinheim |
| Phenylmethylsulfonyl fluoride (PMSF) | Roche Diagnostics, Mannheim |
| Urea | Fluka, Schwerte |
| β-Mercaptoethanol | Sigma-Aldrich, Steinheim |

## 5.2. Buffers and solutions

| | |
|---|---|
| Ammonium persulfate (APS) | 10% (w/v) in water |
| Blocking Buffer (Immunofluorescence) | 1 x PBS<br>1% (v/v) FCS |
| Cryo Medium | 10% DMSO<br>30% FBS<br>60% Medium |
| Casein Blocking Buffer | 0.2% (w/v) casein in PBST |
| Coating Buffer (ELISA) | 50 mM Carbonate buffer, pH 9.6<br>1 part 50 mM $Na_2CO_3$<br>4 parts 50 mM $NaHCO_3$ |
| Colloidal Coomassie G-250 Staining Solution (1 L) | 100 ml $ddH_2O$<br>100 ml $H_3PO_4$<br>100 g Ammonium sulfate<br>1.2 g Coomassie Blue G-250<br>Fill to 800 ml ddH2O<br>200 ml Methanol (100%) |
| DTT | 1 M |
| Kanamycin | 50 mg/ml |
| LB Agar Plates | 1.5% (w/v) Bacto Agar in LB medium supplemented with antibiotics |
| PBS (10 x) | 1.24 M NaCl<br>0.22 M $Na_2HPO_4$<br>0.1 M $KH_2PO_4$<br>Adjust the pH exactly to 7.2 |
| PBST (1 x) | 1 x PBS, pH 7.2<br>0.1% (v/v) Tween 20 |
| Permeabilization Buffer | 1 x PBS |

| | |
|---|---|
| | 0.5% (v/v) TritonX-100 |
| Phosphoproteom lysis buffer | 100 mM Tris-HCl pH 8.5<br>7 M Urea<br>1% Triton-X 100<br>10 U/ml DNase I<br>1 mM magnesium chloride<br>1% Benzonase (add 1 µl to 1000 µl buffer)<br>1 mM sodium orthovanadate<br>phosphoSTOP phosphatases inhibitors<br>complete mini EDTA free protease inhibitors |
| RIPA lysis buffer | 10 mM Tris-HCl pH 8.0<br>150 mM NaCl<br>1 mM EDTA<br>1% NP 40<br>0.1% SDS |
| SDS Loading Dye (5 x) | 1% (w/v) SDS<br>0.03% (w/v) Bromophenol blue<br>12.5% (v/v) β-mercaptoethanol<br>5 mM EDTA, pH 8.0<br>47.3% (v/v) Glycerol<br>0.3 M Tris, pH 6.8<br>2.5 mM NaF |
| SDS Running Buffer (10 x) | 1% SDS<br>0.25 M Tris<br>1.9 M Glycine |
| SOC Medium [**266**] | 2% (w/v) Bacto-Trypton<br>0.5% (w/v) Yeast extract<br>10 mM NaCl<br>2.5 mM KCl<br>10 mM $MgCl_2$<br>10 mM $MgSO_4$<br>20 mM Glucose |
| Substrate Buffer (ELISA) | 100 mM Sodium acetate<br>pH 6.0 (with acetic acid) |
| TAE Buffer (50 x) | 2 M Tris<br>0.25 M NaAc<br>0.05 M EDTA, pH 8.0<br>Adjust to pH 7.8 with acetic acid |
| TBS (10 x) | Tris 0.5 M<br>NaCl 1.5 M<br>pH 7.5 |
| TBST (1 x) | 1 x TBS, pH 7.5<br>0.1% (v/v) Tween 20 |
| TMB Stock Solution | 10 mg/ml TMB in DMSO |
| Trypan Blue Solution | 0.25% Trypan blue in 1 x PBS |

| | |
|---|---|
| 10 x Towbin Transfer Buffer [**267**] | 0.25 M Tris<br>1.9 M Glycine |
| 4 x Minimal Essential Medium (524 ml) | 40 ml HBSS 10 x<br>345 ml dd$H_2O$<br>Autoclave<br>6 ml MEM vitamin solution 100 x<br>32 ml MEM amino acids 50 x<br>16 ml non-essential amino acids (NEA) 100 x<br>4 ml L-glutamine (200 mM)<br>16 ml $NaHCO_3$, 7,5% (w/v)<br>5 ml Penicillin/Streptomycin<br>50 ml FBS<br>Adjust to pH 7.3 with 4 M HCl |

## 5.3. Consumables

| | |
|---|---|
| Alhydrogel adjuvant 2% | InvivoGen, San Diego, USA |
| Amersham™ Hybond™ P 0.45 PVDF | Th. Geyer, Renningen |
| Bradford Reagenz | PerkinElmer, USA |
| Cell culture dishes (6, 10 cm) | TPP, Trasadingen, Switzerland |
| Cell culture flasks (25, 75 $cm^2$) | TPP, Trasadingen, Switzerland |
| Cell culture flasks 175 $cm^2$ | Greiner, Frickenhausen |
| Cell culture plates (6, 12, 24, 96 well) | Greiner, Frickenhausen |
| Cell scraper | Corning Sigma, München |
| Chelex resin | Bio-Rad, USA |
| Cover slides Menzel-Gläser | Thermo Fisher Scientific, Darmstadt |
| Dako Faramount Aqueous Mounting Medium | Agilent, Karlsruhe |
| Fixogum Rubber Cement | Marabuwerke GmbH & Co KG, Tamm |
| *Gaussia* glow juice | PJK Biotech, Kleinblittersdorf, Germany |
| Gloves (Microflex® XCEED) | MICRFLEX, USA |
| Incidin® Foam | Ecolab Deutschland, Monheim am Rhein |
| MultiplateTM PCR Plates 96-well, clear | Bio-Rad, München |
| Needles, sterile (20G, 25G, 27G) | Braun, Melsungen |
| Nunc® Cryo Tubes | Sigma-Aldrich, Steinheim |
| Nunc™ F96 MicroWell TM White Polystyrene Plate | ThermoFisher Scientific, Darmstadt |
| Objektträger Superfrost® | Plus Carl Roth GmbH, Karlsruhe |
| Optical Adhesive Covers MicroAmp | ABiosystems, Foster City, USA |
| PCR Single Cap 8er Soft Strips | Biozym, Hessisch Oldendorf |
| PCR-plate, 96x 0,2ml, full skirted, low profile, highly transparent | Nerbe plus, Winsen/ Luhe |
| Polysorb Nunc-Immuno plates | ThermoFisher Scientific, Darmstadt |
| Precellsy keramik-kit 1.4 mm | VWR International, Bruchsal |
| Precision Wipes | Kimberly-Clark Professional, Reigate, UK |
| Protein LowBind Tube 1.5 ml | Eppendorf, Hamburg |

| | |
|---|---|
| Reaction Tubes (0.5, 1.5 and 2.0 ml) | Eppendorf, Hamburg |
| Reaction Tubes (15 and 50 ml) | Greiner, Frickenhausen |
| Scalpels, disposable | Feather Safety Razor, Osaka, Japan |
| Sigma Adjuvant System (SAS) | Sigma-Aldrich, St. Louis, USA |
| Special autoclavable bags | Nerbe plus GmbH, Winsen/Luhe |
| Syringes, single use 1 ml | Th. Geyer GmbH, Renningen |
| TipOne sterile pipette filter tips (10 µl, 20 µl, 100 µl, 200 µl, 1000 µl) | Starlab, Ahrensburg |
| Whatman 3 mm filter paper | GE Healthcare, Munich |
| X-ray films Super RX | RX Fuji, Japan |

## 5.4. Laboratory equipment

| | |
|---|---|
| Analytical scale ABJ-120-4NM | Kern & Sohn GmbH, Balingen |
| Autoradiography Cassettes | Kodak, Stuttgart |
| Bacterial shaker G25 | Infors, Bottmingen, Switzerland |
| Precellys 24 tissue homogenizer | Bertin Technologies, France |
| Cell Observer | Carl Zeiss, Oberkochen |
| Centrifuge Heraeus Fresco 17 | ThermoFisher Scientific, Darmstadt |
| Centrifuge Megafuge 1.0R | Heraeus, Hanau |
| Centrifuge Rotina 380R M | M&S Laborgeräte, Wiesloch |
| Centrifuge Sprout Oldendorf | Biozym, Hessisch Oldendorf |
| CoolCell® SV2 BioCision | San Rafael, USA |
| CFX96 Touch Real-Time PCR detection system | Bio-Rad, München |
| Confocal Olympus FluoView FV1000 | Olympus, Hamburg |
| Developing machine CURIX 60 | AGFA, Cologne |
| Duomax 2030 rocking platform | Heidolph Instruments, Schwabach |
| Freezer profi line | Liebherr, Ludwigshafen |
| Freezer VIPTM Series -80 °C | Sanyo, USA |
| Fridge Premium | Liebherr, Ludwigshafen |

| | |
|---|---|
| Gel documentation system GELSTICK INTAS | Science Imaging Instruments |
| Incubator C200 | LaBoTect, Göttingen |
| Kern EMB 1200-1 Tischwaage 1200 g | KERN & SOHN GmbH, Balingen |
| Liquid nitrogen tank | CHRONOS Biosafe Messer, Griesheim |
| Magnetic stirrer MR3000 | Heidolph Instruments, Schwabach |
| Microscope Dialux 22 | Ernst Leitz GmBH, Wetzlar |
| Microscope Olympus CK2 | Olympus, Hamburg |
| Microwave | DeLonghi GmbH, Seligenstadt |
| Mini Trans-Blot® Cell | Bio-Rad, München |
| Mini-PROTEAN® 3 Cell | Bio-Rad, München |
| Moser ChroMini Pro Trimmer | Wahl GmbH, Unterkirnach |
| Multichannel Pipette RAININ (50-200 µl) | Eppendorf, Hamburg |
| MyCycler thermal cycler | Bio-Rad, München |
| Neubauer hemocytometer | Bender&Hobein, Bruchsal |
| Peltier Thermal Cycler PTC-200 | MJ Research, St. Bruno, Canada |
| pH-meter 761 | Calimatic Knick, Berlin |
| Pipette Boy Integra | Biosciences GmbH, Fernwald |
| Pipettes Research (2, 10, 20, 100, 200, 1000 µl) | Eppendorf, Hamburg |
| Plate reader Synergy 2 | BioTek®, Bad Friedrichshall |
| Plate Reader SPECTROstar Nano BMG | LABTECH, Ortenberg |
| Power supply PowerPacTM HC/basic | Bio-Rad, München |
| Precellys 24 homogenizer | Peqlab, Erlangen |
| Roller Mixer SRT9D | Stuart, USA |
| Spectrophotometer NanoDropâ ND-1000 | NanoDrop, USA |
| STERI-CULT 200 Incubator | Forma Scientifc, Marietta, USA |

| | |
|---|---|
| SterilGARD Hood | Baker Company, Sanford, USA |
| Thermal Cycler C1000TM | Bio-Rad, München |
| Thermomixer compact/pico | Eppendorf, Hamburg |
| UV irradiation box & lid for animals | DKFZ fine mechanics workshop, Vilber Lourmat Deutschland |
| UV irradiator Bio-Spectra | Vilber Lourmat Deutschland Eberhardzell |
| UV detector Variocontrol | Waldmann Medizintechnik, Schwenningen |
| UV table UV 181 BL | Waldmann Medizintechnik, Schwenningen |
| UV table N90 | Benda Konrad, Wiesloch |
| Vortexer Reax top | Heidolph Instruments, Schwabach |
| Water bath | GFL - Gesellschaft für Labortechnik GmbH, Burgwedel |

## 5.5. DNA and Protein Size Markers

| | |
|---|---|
| GeneRuler™ 1 kb DNA Ladder | ThermoFisher Scientific, Darmstadt |
| PageRuler™ Prestained Protein Ladder | ThermoFisher Scientific, Darmstadt |

## 5.6. Kits

| | |
|---|---|
| Axygen™ AxyPrep™ Plasmid Miniprep Kit | Fisher Scientific GmbH, Schwerte |
| CloneJET PCR Cloning Kit | ThermoFisher Scientific, Darmstadt |
| QIAquick® Gel Extraction Kit | Qiagen, Hilden |
| QIAprep® Spin Miniprep Kit | Qiagen, Hilden |
| QIAGEN® Plasmid Midi Kit | Qiagen, Hilden |
| RNeasy® Mini Kit | Qiagen, Hilden |
| TURBO DNA-free™ Kit | ThermoFisher Scientific, Darmstadt |

## 5.7. Universal enzymes

| | |
|---|---|
| Benzonase | Merck Calbiochem, Darmstadt |
| DreamTaqTM Green DNA Polymerase | ThermoFisher Scientific, Darmstadt |
| DreamTaqTM Green PCR Master Mix (2 ×) | ThermoFisher Scientific, Darmstadt |
| FastAP Thermosensitive Alkaline Phosphatase | Thermo Scientific, St. Leon-Rot |
| iTaqTM Universal SYBR® Green Supermix (2 ×) | Bio-Rad, München |
| Phusionâ High-Fidelity DNA Polymerase | New England BioLabs, Frankfurt |
| Phusionâ High-Fidelity PCR Master Mix (2 ×) | New England Biolabs |
| RevertAid Reverse Transcriptase | Thermo Fisher Scientific, Darmstadt |
| T4 DNA Ligase | New England BioLabs, Frankfurt |

## 5.8. Restriction enzymes

| | |
|---|---|
| FastDigest EcoRI | ThermoFisher Scientific, Darmstadt |
| FastDigest HindIII | ThermoFisher Scientific, Darmstadt |
| FastDigest XhoI | ThermoFisher Scientific, Darmstadt |

## 5.9. Reagents for Cell Culture

| | |
|---|---|
| 0.25% Trypsin/EDTA | Invitrogen™, Karlsruhe |
| ACK lysing buffer | Gibco™, Schwerte |
| Afatinib | Sigma-Aldrich, Steinheim |
| Dulbecco's Modified Eagle's Medium (DMEM) | Sigma-Aldrich, Steinheim |
| Dulbecco's Phosphate Buffered Saline (DPBS) | Invitrogen™, Karlsruhe |
| Dimethylsulfoxid (DMSO) | Carl Roth GmbH, Karlsruhe |
| Fetal Bovine Serum (FBS) | Linaris GmbH, Wertheim |
| Hank's Balanced Salt Solution (HBSS) (10 ×, - $CaCl_2$, -$MgCl_2$, -phenol red) | ThermoFisher Scientific, Darmstadt |
| L-glutamine (200 mM) | ThermoFisher Scientific, Darmstadt |
| Recombinant mouse M-CSF protein | Abcam, Berlin |
| MEM Amino Acids 50 × (-L-glutamine) | Sigma-Aldrich, Steinheim |
| MEM Vitamin Solution 100 × | Sigma-Aldrich, Steinheim |
| $NaHCO_3$, 7.5% (w/v) | Biochrom, Berlin |
| Non-essential amino acids (NEA) 100 × | Biochrom, Berlin |

| | |
|---|---|
| Opti-MEM serum-free medium | Invitrogen™, Karlsruhe |
| Penicillin/Streptomycin (10,000 U/ml) | ThermoFisher Scientific, Darmstadt |
| RPMI 1640 | Sigma-Aldrich, Steinheim |
| SCH772984 | Sigma-Aldrich, Steinheim |
| Sorafenib | Sigma-Aldrich, Steinheim |
| Trypan blue | Biochrom, Berlin |
| Turbofect *in vitro* Transfection Reagent | ThermoFisher Scientific, Darmstadt |
| Recombinant Mouse HB-EGF Protein, NBP2-35069 | Novus Biologicals, Wiesbaden |

## 5.10. Cell lines

**Table 5.10 Cell lines used in this study.** In the table below the cell lines, their properties and references are listed and described.

| Cell line | Properties | Reference |
|---|---|---|
| 308 murine keratinocytes | Murine immortalized keratinocytes | Kindly provided by Prof. Dr. P. Krieg, DKFZ, [268] |
| MnPV E6-transduced 308 keratinocytes | Murine immortalized keratinocytes transduced with MnPV E6 | Prof. Dr. P. Krieg, DKFZ, [268], modified by M. Schäfer |
| MnPV E7-transduced 308 keratinocytes | Murine immortalized keratinocytes transduced with MnPV E7 | Prof. Dr. P. Krieg, DKFZ, [268], modified by M. Schäfer |
| MnPV E6/E7-transduced 308 keratinocytes | Murine immortalized keratinocytes transduced with MnPV E6 | Prof. Dr. P. Krieg, DKFZ, [268], modified by M. Schäfer |

**Table 5.10 Cell lines used in this study.** In the table below the cell lines, their properties and references are listed and described.

| | | |
|---|---|---|
| Kera5 | *Mastomys*-derived keratinocytes | **[95]** |
| HeLaT (HeLaT clone-4) | HPV18 human cervical carcinoma cell line stably expressing one copy of SV40 T-antigen under control of a CMV promotor | Kindly provided by Prof. Dr. M. Müller, DKFZ [269] |
| J774A.1 | Murine monocytes/ macrophages | CLS, Cat.: #400220 |
| MaFi132 | Spontaneously immortalized *Mastomys*-derived fibroblasts | [95] |
| MaFi191 | *Mastomys*-derived fibroblasts harbouring *Trp53* wt | Dr. D. Hasche, DKFZ |
| MaFi191 R266C | Mastomys-derived fibroblasts (MaFi191) containing the mutation R266C in *Trp53* | Dr. D. Hasche, DKFZ modified by Dr. M. Meister |
| THP-1 | Human leukemia monocytic | Kindly provided by Prof. Dr. J. Rachmilewitz, Weizmann Institute Israel |

## 5.11. Oligonucleotides

All oligonucleotides were synthesized and provided by Sigma-Aldrich, Germany.

### 5.11.1. Primers for semi-quantitative polymerase chain reaction (qPCR)

**Table 5.11.1 Primers for qPCR.** The table below describes the exon spanning primers designed and used in this study. The primer sequences are given including the length of their respective product.

| Primer name | Sequence 5' to 3' | Application | Product length [bp] |
|---|---|---|---|
| mmIL-18 forw | TCAGACAACTTTGGCCGACT | qPCR | 133 |
| mmIL-18 rev | GGGGTTCACTGGCACTTTGA | | |
| mmTNFα forw | TAGCCCACGTCGTAGCAAAC | qPCR | 136 |
| mmTNFα rev | ACAAGGTACAACCCATCGGC | | |
| mmIL-6 forw | CCCAATTTCCAATGCTCTCCT | qPCR | 140 |
| mmIL-6 rev | CGCACTAGGTTTGCCGAGTA | | |
| mmIL-7 forw | CTAAATCGTGCTGCTCGCAA | qPCR | 107 |
| mmIL-7 rev | TTCACCAGTGTTTGTGTGCC | | |
| mmIL-10 forw | AGCCGCTTCATCCCTGAAAA | qPCR | 139 |
| mmIL-10 rev | TGCTGCTACAAAGGCAGACA | | |
| mmIL-1β forw | ATGCCACCTTTTGACAGTGATG | qPCR | 115 |
| mmIL-1β rev | GCTGGATGCTCTCATCTGGA | | |
| mmMCP-1 forw | TGACCCCAAGAAGGAATGGG | qPCR | 104 |
| mmMCP-1 rev | ACCTTAGGGCAGATGCAGTT | | |
| mmIL-34 forw | CCAAAGCCTTGCTGGACAAC | qPCR | 140 |
| mmIL-34 rev | ACATTGCATCAAGGACCCCG | | |
| mmHB-EGF forw | CTCTTGCAAATGCCTCCCTG | qPCR | 140 |
| mmHB-EGF rev | CAAGAAGACAGACGGACGACA | | |
| huHB-EGF forw | GGTGGTGCTGAAGCTCTTTC | qPCR | 140 |
| huHB-EGF rev | GCTGGTCCGTGGATACAGTG | | |
| mcHB-EGF forw | AGCTCTTTCTAGCCGCAATGT | qPCR | 131 |
| mcHB-EGF rev | ATCTCCTCCTGTGGGTAGCA | | |
| HPRT1 forw | GAAGGAGATGGGAGGCCATC | qPCR | 185 |
| HPRT1 rev | CTTTTATGTCCCCCGTTGACTG | | |
| MnPV L1 forw | ACGGCAACTCATGCTTCTTC | qPCR | 133 |
| MnPV L1 rev | CTCTGTGCCTGTCCATCCTT | | |
| β-globin forw | ACCATGGTGCACCTTACTGAC | qPCR | 146 |
| β-globin rev | TCCAGGCACCCAACTTCTAC | | |

### 5.11.2. Primers for the construction of expression plasmids

**Table 5.11.2 Primers for the construction of expression plasmids.** The sequences of the primers are given including the restriction site (green), the Kozak consensus sequence (grey) and the start codon (red).

| Primer name | Sequence 5' to 3' | Restriction sites |
|---|---|---|
| SL01 | ATGAAGCTGCTGCCGTCG | - |
| SL02 | TCAGTGGGAGCTAGCCACGCC | - |
| SL03 | TATACTCGAGGCCATGAAGCTGCTGCCGTCG | XhoI |
| SL04 | TATAGAATTCATGTGGGAGCTAGCCACGCC | EcoRI |
| SL08 | TATAAAGCTTGCCATGAAGCTGCTGCCGTCG | HindIII |
| SL09 | TATAGAATTCTTGGTGGGAACTAGCTATGCCC | EcoRI |

### 5.11.3. Plasmids

**Table 5.11.3 Plasmids used in this thesis.** Commercially available and cloned expression plasmids are listed. As tag HA (hemagglutinin) was used.

| Plasmid name | Cloning primers | Properties | tag |
|---|---|---|---|
| pPK-CMV-E3 | - | Empty cloning vector<br>CMV promoter and enhancer<br>PromoKine, Heidelberg | - |
| mmHB-EGF pPK-CMV-E3 | SL03<br>SL04 | Murine HB-EGF | HA |
| mcHB-EGF pPK-CMV-E3 | SL08<br>SL09 | *Mastomys* HB-EGF | HA |

## 5.12. Antibody List

**Table 5.12 Antibodies used in this study.** The application and dilution of the antibodies used in this study are shown below. Furthermore, the company producing the antibody is given.

| Antibody | Source | Application | Dilution solution |
|---|---|---|---|
| Anti-E-Cadherin, mouse ploYclonal | BD Transduction; Cat. #: 610181 | IHC: 1:500 | 5% goat serum in PBS |
| Anti-F4/80 (D2S9R) XP, rabbit | Cell Signaling; Cat. #: 70076T | IF: 1:500 | 1% BSA in PBS |
| Anti-HA (3F10), rat monoclonal | Roche; Cat. #: 11867423001 | WB: 1:1,000 | 5% milk in TBS-T |
| Anti-mouse HB-EGF, polyclonal sheep IgG | R&D systems; Cat. #: AF8239 | WB: 1:500 | 5% milk in TBS-T |
| Anti-human HB-EGF, polyclonal goat IgG | R&D systems; Cat. #: AF259 | WB: 1:500 | 5% milk in TBS-T |

**Table 5.12 Antibodies used in this study.** The application and dilution of the antibodies used in this study are shown below. Furthermore, the company producing the antibody is given.

| | | | |
|---|---|---|---|
| Anti-Ki67, rabbit polyclonal | Bethyl Lab; Cat. #: IHC-00375-T | IHC: 1:200 | 5% goat serum in PBS |
| Anti-MnPV E4, mouse monoclonal | Self-made | IHC | 5% goat serum in PBS |
| anti-MnPV-L1, *Mastomys* monoclonal | Self-made | IHC | 5% goat serum in PBS |
| Anti-K18L2, mouse monoclonal | Provided by Prof. Dr. M. Müller [257] | IHC: 1:200 | 5% goat serum in PBS |
| Anti-phosHistone H2AX (Ser139) clone JBW301 | Merck Millipore; Cat. #: 05-636-25 | IF: 1:650 | 1% BSA in PBS |
| Anti-MMP3, goat polyclonal | R&D systems; Cat. #: AF548 | WB: 1:1,000 | 5% milk in TBS-T |
| Anti-p53 (1C12), mouse mono | Cell Signaling; Cat. #: 2524 | WB: 1:1,000 | 5% BSA in TBS-T |
| Anti-Vinculin (7F9), mouse monoclonal | Santa Cruz; Cat. #: sc-73614 | IF: 1:1,000,<br>WB: 1:4,000 | 1% BSA in PBS<br>5% BSA or 5% milk in TBS-T |
| AlexaFluor488 Goat-anti mouse IgG (H+L) | Invitrogen™; Cat. #: A11029 | IF: 1:1,000<br>IHC: 1:1,000 | 1% BSA in PBS<br>5% goat serum in PBS |
| Alexa594 Goat-anti mouse IgG (H+L) | Invitrogen™; Cat. #: A11032 | IHC: 1,1000 | 5% goat serum in PBS |
| Alexa594 goat anti-rabbit IgG (H+L) | Invitrogen™; Cat. #: A11072 | IHC: 1,1000 | 5% goat serum in PBS |
| Anti-Mouse IgG HRP Conjugate | Promega; Cat. #: W4021 | WB: 1:10,000 | 5% BSA or 5% milk in TBS-T |
| Anti-Rabbit IgG (H&L) HRP Conjugate | Promega; Cat. #: W4011 | WB: 1:10,000 | 5% BSA or 5% milk in TBS-T |
| Goat anti-Rat IgG (H+L) HRP | JacksonImmunoResearch; Cat. #: 112-035-143 | WB: 1:10,000 | 5% BSA or 5% milk in TBS-T |
| Donkey anti-Goat IgG (H+L) HRP conjugate | Invitrogen™; Cat. #: A15999 | WB: 1:5,000 | 5% BSA or 5% milk in TBS-T |

# 6. Methods

## 6.1. Isolation and analysis of proteins

### 6.1.1. Extraction and quantification of proteins

Cells were harvested by scratching in 1x DPBS and the suspensions were collected in 15 ml falcons. After centrifugation for 10 min at 1400 rcf at 4°C the supernatants were discarded. The pellets were resuspended in 1x RIPA lysis buffer supplemented with 1x complete mini EDTA free protease inhibitors from 50x stock solution and transferred to 1.5 ml Eppendorf tubes. The suspensions were incubated for 30 min on ice being flicked every 10 min. After centrifugation at 13000 rpm for 30 min at 4°C, the supernatant was collected in new 1.5 ml Eppendorf tubes.

The protein concentrations were measured by Bradford assay. The samples were diluted in water (1:20-1:40 depending on the size of the cell pellet). For calculation of the protein concentrations, a standard range (7.5 mg/ml, 5 mg/ml, 2.5 mg/ml, 1 mg/ml, 0.75 mg/ml, 0.5 mg/ml and 0.25 mg/ml) was diluted 1:10 and included in the Bradford assay. The diluted samples and diluted standards were measured using the Bradford reagent (1:5 diluted). The concentration of the proteins was measured at a wavelength of 280 nm using the SPECTROstar® *Nano* spectrophotometer. For analysis in ELISA, lysates were stored at -80°C until use. 5x DTT loading buffer was added to the samples to reduce disulfide bonds for Western blotting. Afterwards, the proteins were denatured for 10 min at 99°C. The samples were stored at -20°C until use.

### 6.1.2. SDS-polyacrylamide Gel Electrophoresis (SDS-PAGE)

To separate the proteins according to their molecular weight, sodium dodecyl sulfate polyacrylamide gel electrophoresis (SDS-PAGE) was used. Therefore, proteins were negatively charged due to the binding of SDS (sodium dodecyl sulfate) and loaded on SDS gels consisting of a stacking and a separating gel.

| Separating gel (8-12%) | Stacking gel (5%) |
|---|---|
| 1.5 M Tris, pH 8.8 | 0.5 M Tris, pH 6.8 |
| 8-12% Acrylamide-Bis (29:1) | 5% Acrylamide-Bis (29:1) |
| 0.1% SDS | 0.1% SDS |
| 0.1% APS | 0.1% APS |
| 0.08% TEMED | 0.16% TEMED |

25-100 µg of the total protein lysates were loaded on the SDS gel. The estimation of

molecular protein weight was realized by loading PageRuler Prestained Protein Ladder. For the electrophoresis the 1x SDS running buffer was used. The initial voltage was set at 80 V for 20 min and afterwards increased to 120 V for separating the proteins. The run was stopped according to the marker.

### 6.1.3. Western Blot

To detect the proteins of interest, the electrophoretic transfer in a Mini Trans-Blot© Cell on the PVDF membrane (0.45 µm) was performed. Therefore, the membrane (Amersham™ Hybond™ P. 0.45 PVDF, Cytiva, Buckinghamshire) was activated by incubating in 100% methanol and afterwards washed in water for a few minutes before being dipped in the transfer buffer. The assembly of the sandwich was done as shown in Fig.6.1.3.1

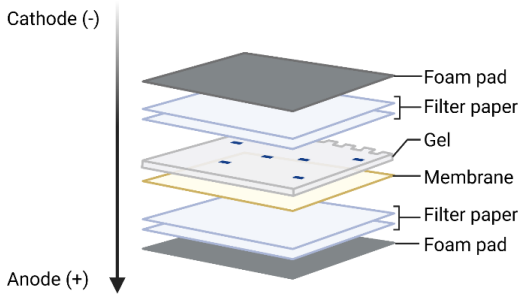


**Fig. 6.1.3.1 Assembly of sandwich Western Blot**. To transfer the proteins separated by electrophoresis to the membrane the SDS-gel and membrane were assembled in a sandwich including filter paper and foam pad. The proteins were blotted on the membrane by applying voltage (created with BioRender.com).

Blotting of the proteins on the membrane was performed at 4°C for 1 h at 400 mA in a Bio-Rad Mini Trans-Blot Cell 153BR chamber. Afterwards, to prevent unspecific protein binding, the membrane was incubated in 5 % milk powder (in 1x TBST) or 5 % BSA (in 1x TBST) for 1 h at room temperature. Due to the marker, the membrane could be cut to detect several proteins simultaneously. For the detection of the proteins of interest, primary antibodies were chosen and diluted in 5% milk (in TBST) or in 2.5% BSA (in TBST) and incubated with the membrane over night at 4°C with agitation. Afterwards, the membrane was washed three times for 10 min at room temperature in 1x TBST. In the next step, the membrane was incubated with the HRP-conjugated secondary antibody diluted 1:10,000 in 5% milk/TBST or 2.5% BSA/TBST for 1h at room temperature with agitation and washed afterwards three times for 10 min in 1x TBST.

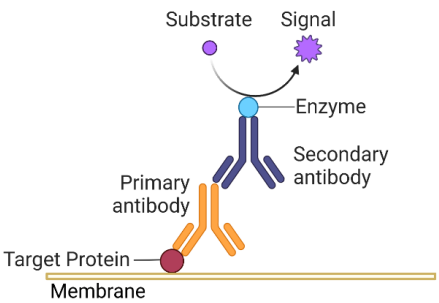


**Fig. 6.1.3.2 Principle of protein detection in Western Blot**. To detect and visualize the protein of interest first the membrane was incubated with a primary antibody binding to the target protein. Afterwards, secondary antibodies were used which were HRP- coupled. For visualisation of the protein of interest, ECL substrate used to enable the detection of luminescence signals (created with BioRender.com).

After the membrane was incubated with enhanced chemiluminescent reaction solution (ECL), it was exposed to X-ray films. So, the luminescence signal could be detected. The visualization was achieved by the CURIX 60 developer machine.

## 6.2. Proteomics

### 6.2.1. Sample preparation

To analyse the cells by proteomics, cells were treated and harvested at defined time points by scratching in 1 mL 1 x PBS. The suspension was collected and centrifuged at 1400 rpm for 10 min at 4°C. The supernatant was discarded. Afterwards, one volume cell pellet was resuspended in five volumes of lysis buffer and incubated for 30 min on ice. Subsequent sonification was performed at 70% output 3x 10 s at 4°C with 30 s rest in between (0.5 s on 0.5 s off setting, put sample in ice-water bath). The residual cell debris was removed by centrifugation at 13.300 rpm for 1 h at 4°C [270]. The protein concentration was determined by Bradford assay. For later use, the samples were stored at – 80°C.

### 6.2.2. Mass spectrometry analysis

Prepared samples were handed to the mass spectrometry core facility of the DKFZ for analyses. Briefly, samples were digested in solution with Lyc-C and Trypsin in an 8 M Urea buffer and subsequently desalted using Sep-Pak cartridges. The desalted eluates have further been analyzed by LC-MS/MS measurement.

Resulting peptides were loaded on a cartridge trap column, which was packed with Acclaim PepMap300 C18, 5 µm, 300Å wide pore (Thermo Scientific). Their separation was performed via a gradient from 3% to 40% ACN on a nanoEase MZ Peptide analytical column (300Å, 1.7 µm, 75 µm x 200 mm, Waters™) using a 150 min MS-method. Eluted peptides were analyzed by an online coupled Orbitrap Exploris 480 mass spectrometer. Samples were measured in data-dependent acquisition mode (DDA).

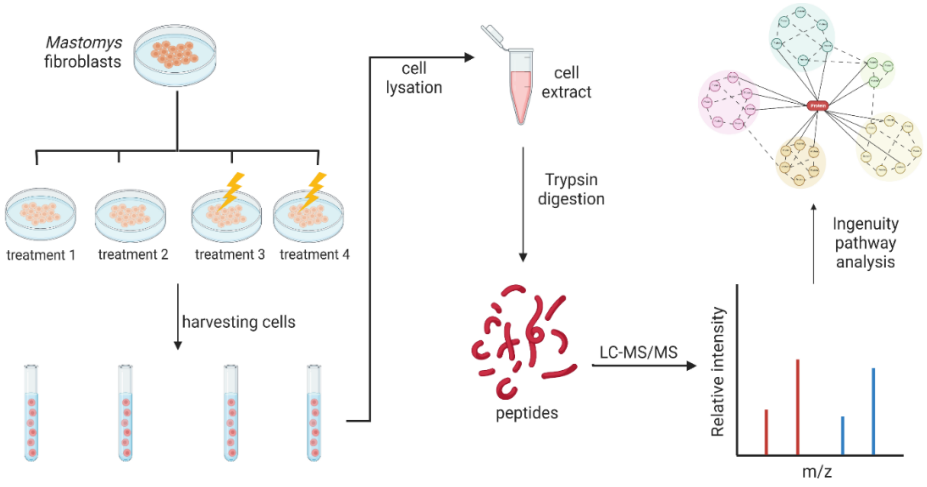


**Fig. 6.2.2 General workflow for mass spec analysis**. *Mastomys* fibroblasts are treated according to experimental setup and harvested by scratching. Cells are lysed according to core facility's suggestions. Afterwards, cells are handed in to the core facility where trypsin digestion followed by mass spec analyses is performed. Results can be investigated by using IPA (ingenuity pathway analysis) (created with BioRender.com).

### 6.2.3. Data processing and analysis

Using MaxQuant (version 1.6.14.0)[138], all raw files were processed, and MS/MS spectra were searched against mouse proteins from UniProt. False discovery rates for peptide and protein identification were set to 1%. For further statistical analyses label free quantification (LFQ) values were extracted from the data. Using the Limma package in R/Bioconductor [271], differentially regulated proteins were determined by first fitting a linear model and afterwards using empirical Bayesian methods. Proteins with a p-value < 0.05 and |FoldChange| > 1.5 were considered as differentially regulated. Proteins were annotated using the KEGG database[272-274] and relevant pathways were extracted.

## 6.3. Cultivation and treatment of cells

### 6.3.1. Cultivation of mammalian cell lines

Mammalian cell lines were cultivated at 37°C and 5 % $CO_2$. All cell lines were regularly tested for contamination with *Mycoplasma spp.. via* PCR.
*Mastomys* fibroblast (MaFi) cell lines were cultivated in DMEM (low glucose, 1 g/L) supplemented with 1% Penicillin/ Streptavidin, 1% L-Glutamine and 10% fetal bovine serum (FBS).
Murine 308 keratinocytes were cultured in 4x Minimal Essential Medium (MEM) with additional 1% L-glutamin and 1% penicillin/streptomycin. Passaging of the cells was started by removing the medium and washing once with 1x DPBS. The cells were incubated with 1-2 ml of 0.25% trypsin-EDTA at 37°C until getting detached. The trypsin-EDTA was neutralized by adding medium containing 10% FBS. The cell suspension was collected in a 15 ml or 50 ml Falcon tube and centrifuged for 3 min at 350 g. Supernatants were discarded and the cell pellets were resuspended in fresh medium. Afterwards, cells were passaged in a ratio from 1:10 to 1:20.

To determine the number of cells, 1 µl of the cell suspension was mixed with 19 µl of 0.25% trypan blue. The cells were counted with the Neubauer counting chamber under the microscope. The cell number was calculated as followed:

$$cell\ number\ per\ ml = \frac{counted\ number\ of\ cells}{number\ of\ squares}\ x\ 20\ x\ 10^4$$

### 6.3.2. Cryopreservation of cells

To store cells over a longer period, cells were detached from cell culture dishes as described above. Instead of resuspending the cells in fresh media, cells were resuspended in 1 ml Cryo medium and transferred to a 1.5 ml cryotube. The tubes were put in a CoolCell® SV2 device and directly stored at -80°C for at least 24 h before the cryotubes were transferred to the nitrogen tank for long storage. For defrosting the frozen cells, the cryotube was held in a 37°C warm water bath until the cell suspension was thawn. The suspension was transferred into a 15 ml Falcon tube containing 1:1 mix of 1x DPBS and growth medium. After centrifugation for 4 min at 350 g, the cell pellet was resuspended in growth medium and seeded in cell culture dishes or flasks.

### 6.3.3. Transfection of *Mastomys* fibroblasts

For transfection of *Mastomys* fibroblasts, 1,5 x $10^5$ cells were seeded in 6 cm cell culture dished in growth medium. Cells were incubated overnight.
The plasmids, the cells should be transfected with, were diluted in an appropriate volume of Opti-MEM and Turbofect (1:2 µg DNA:µl Turbofect) or PEI (1:3 µg DNA:µl PEI). The solution was vortexed for at least 30 sec and incubated at room temperature for 15-20 min. Before adding this transfection solution to the cells, the growth medium was removed and replaced by DMEM without additional supplements. Cells were incubated with the transfection mix for 24 h before harvesting.

### 6.3.4. Isolation of macrophages from *Mastomys coucha*

#### Isolation of macrophages from bone marrow

For the isolation of macrophages, the bone marrow needed to be isolated from the *Mastomys*' bones (Fig. 6.3.4). Therefore, animals were put under anaesthesia with isoflurane before being sacrificed by cervical dislocation. The tibiae and femora were removed and cleaned from meat and tissue. Afterwards, both ends of the tibiae and femora were cut off by using a scalpel. Using a 20 ml syringe with a 20G cannula, the bone barrow was washed out with DMEM (complemented with 10% FCS, 1% L-Glutamin, 1% Penicillin/ Streptavidin). The solution was collected in a 10 cm cell culture dish. After collecting the bone marrow from all bones, the suspension was transferred to a 50 ml falcon tube and spined for 10 min at 4°C at 1400 rpm. Next, the supernatant was discarded, and the remaining pellet was resuspended in ACK lysis buffer to remove the red blood cells. After incubation for 5 min at room temperature, 30 ml DMEM containing 10% FCS, 1% L-Glutamin and 1% Penicillin/ Streptavidin were added following centrifugation for 10 min at 4°C at 1400 rpm. The supernatant was discarded. The pellet was resuspended in appropriate volume of complete DMEM with additional M-CSF (final concentration: 1 µg/ml). The cells were grown in 6 well plates on cover slips overnight. The next day, medium was removed carefully and fresh medium containing M-CSF was added. The medium was changed every day until only adherent cells were left (up to 7 days). The cells were then fixed, and immune fluorescence staining performed to proof the presence of macrophages.

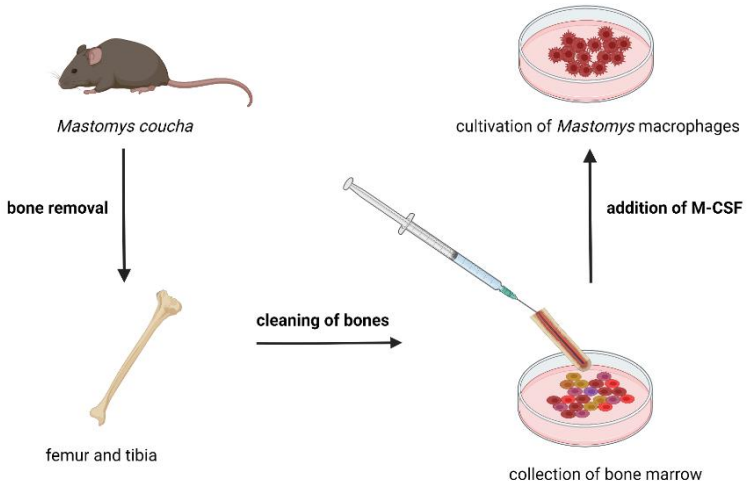


**Fig. 6.3.4 Scheme of macrophage isolation from *Mastomys* bone marrow**. Animals were sacrificed by cervical dislocation before bones from the legs were removed. After cleaning from tissue, bones were opened, and the bone marrow was rinsed out. Adding M-CSF to the growth media, macrophages were isolated (created with BioRender.com).

### Isolation of peritoneal macrophages

Not only from the bone marrow but also from peritoneum macrophages can be gained. Therefore, *Mastomys* animals were put under anaesthesia with isoflurane and sacrificed by cervical dislocation. Afterwards, the animals were put on their back on a board and all four limps were pinned down. Next, the animals were wet with ethanol. To get access to the peritoneum, the skin was cut open without damaging the peritoneum. Afterwards, 8 ml medium (RPMI 1640, supplemented with 10% FCS, 1% L-Glutamin, 1% Penicillin/ Streptavidin) was injected into the peritoneum using a canula. The peritoneum was shaken carefully using forceps without damaging it. Next, a fresh canula and syringe were used to remove the medium from the peritoneum. The suspension was collected in a 15 ml falcon tube and spined for 10 min at 1200 rpm at 4°C. The supernatant was discarded, and the cell pellet was resuspended in fresh supplemented RPMI 1640 medium. Cells were seeded on 6 well plates and incubated until they got adherent.

## 6.3.5. UV irradiation of cells

To investigate the influence of UVB light on cell mechanisms, 1.5x $10^5$ *Mastomys* fibroblasts or 2x $10^5$ murine 308 keratinocytes were seeded in 6 cm dishes. After incubation overnight, the medium was removed, and the cells were washed once with 1x DPBS. The cell culture dishes were placed inverted without lids on the UV table (UV 181 BL). 308 keratinocytes were irradiated with 50 mJ/cm$^2$, while *Mastomys* fibroblasts (MaFi191, MaFi191 R266C and MaFi132) were treated with a dose of 20 mJ/cm$^2$. To ensure that the desired dose was applied, a UV detector (Variocontrol, Spectrum: TL06) was used. After reaching the intended dose, growth medium was added and depending on the experiment, HB-EGF was added to the growth medium in defined concentrations. The cells were incubated and harvested at defined time points for protein lysis or RNA extraction.

## 6.3.6. Immunofluorescence staining

For the detection of proteins of interest by fluorescence, cells were seeded in 6 cm dishes on 12 mm glass coverslips. At defined time points, the cover slips were transferred to a 12 well plate (one cover slip per well) containing cold 1x PBS to wash the media off. Afterwards, the PBS was carefully removed, and the cells were fixed in 4% PFA in PBS for 10 min at room temperature. The PFA was carefully removed, and the cells washed once with cold PBS. The coverslips were stored at 4°C in PBS until use.

For the detection of proteins located in the cells, the cells were permeabilized by incubation with 0.05% Triton-X® 100 in PBS for 5 min at room temperature. Unspecific binding of antibodies was blocked by incubating the cells with 1% BSA in PBS for 1 h at room temperature. The primary antibodies were correspondingly diluted in 1% BSA in PBS and incubated with the cells at 4°C over night. Afterwards, cells were washed three times for 10 min with cold PBS and incubated with secondary antibodies diluted 1:1000 in 1% BSA in PBS for 1h at room temperature in the dark. After washing three times in PBS the cells were incubated with DAPI (0.3 µg/ml in PBS) for 5 min at room temperature in the dark. After washing three times in PBS, the stained cells were once rinsed with dd$H_2O$ to remove salts and directly mounted on glass slides in a drop of Dako Faramount Aqueous Mounting Medium and dried in the dark until harden.

The visualization was achieved by the Keyence BIOREVO BZ-9000 microscope or the confocal Olympus FluoView FV1000.

#### Quantification of γH2AX foci

To quantify the number of γH2AX foci, a macro based on Image J and provided by the DKFZ microscope core facility was used.

## 6.4. Isolation and cloning of nucleic acids

### 6.4.1. RNA extraction and reverse transcription (RT)

For the analysis of the mRNA levels in our cells, RNA was isolated and transcribed into cDNA. The RNA extraction was performed by using the RNeasy® Mini kit (Qiagen) according to manufacturer's protocol. To ensure that the samples remained DNA free, DNase digestion was done as described in the manufacturer's protocol (TURBO DNA-free™ kit, ThermoFisher Scientific). Afterwards, the concentration of RNA was measured by using the Plate reader Synergy 2 (BioTek®, Bad Friedrichshall).
For the PCR reaction, the mRNA needed to be transcribed into cDNA. Therefore, the following mix was used including 1 µg of RNA:

| Component | Volume [µl] |
|---|---|
| $H_2O$ (RNase-free) | 11.5-x |
| Oligo-dT Primer (200 µM) | 1.0 |
| RNA (1 µg) | x |
| Total volume | 12,5 |

The mix was incubated for 5 min at 65°C and afterwards put directly on ice. For the final reaction, the following reaction mix was prepared and added:

| Component | Volume [µl] |
|---|---|
| 5 x RT Buffer | 4.0 |
| dNTP (10 mM) | 2.0 |
| Ribolock RI | 0.5 |
| RevertAid RT or $ddH_2O$ | 1.0 |
| Total volume | 7.5 |

To ensure that genomic DNA is not detected in the qPCR analyses, for each sample a reaction mix without RevertAid RT but $ddH_2O$ was prepared (-RT samples). The reaction mix was incubated for 1h at 42°C, followed by an incubation step of 10 min at 70°C. Samples were kept at -20°C before being analysed in qPCR reaction.

### 6.4.2. Quantitative PCR analysis

To determine the levels of mRNA in our cells, the quantitative real-time PCR was performed. For the PCR reaction the iTaq™ Universal SYBR Supermix was used as below:

| Reagent | Volume/ amount |
|---|---|
| iTaq™ Universal SYBR Supermix | 7.5 µl |
| Primer Mix (forward + reverse, 20 µM) | 0.5 µl |
| cDNA | 5 ng |
| $ddH_2O$ | to 15 µl |

The reactions were performed in technical duplicates using the following cycle program:

| Temperature | Time | |
|---|---|---|
| 95°C | 10 min | |
| 95 °C<br>60 °C<br>Plate read | 15 s<br>1 min | 40 cycles |
| 95 °C | 1 min | |
| 60 °C | 1 min | |
| 65 °C | 31 s | |
| 65 °C<br>+ 0.5 °C/cycle<br>Ramp 0.5 °C/s<br>Plate read | 5 s | 60 cycles |

The amplification of the cDNA was performed in the Thermal Cycler C1000™. In each run, the corresponding -RT samples were included. The fluorescent signals were detected by the CFX96 Touch Real-Time PCR detection system.

### 6.4.3. Agarose gel electrophoresis

To separate DNA fragments according to their size, agarose gel electrophoresis was used. Therefore gels (1 to 2% agarose in 1x TAE buffer) were mixed with 0.05 µg/µl ethidium bromide to visualize DNA fragments. As marker, 1 kb DNA ladder was included in the analysis. The detection was performed by exposing the gel to UV light at 260 nm in chamber.

### 6.4.4. Construction of expression plasmids

At first, primers were designed binding to the coding DNA sequences of the proteins. For *Mastomys* proteins, primers were designed using the sequences of mouse or rat. As template, the complete cDNA from cells or animal tissue were used. After amplification, the products were cloned into the pJET vector. Therefore, the CloneJET kit was used, and cloning was performed according to manufacturer's protocol. After sequencing, the PCR product was verified by alignment to the expected sequence. As backbone for expression of the proteins, the pPK-CMV-E3 vector was used.

#### Amplification of the insert

For amplification of the insert (CDS of the respective gene), plasmids were designed containing restriction sites at the 5' were designed. Additionally, the forward primers were designed containing a Kozak consensus sequence upstream to the start codon as initiation site for protein translation. Since antibodies for *Mastomys* proteins were not commercially available, a HA-tag was included, fused to the protein due to cloned CDS without stop codon. For amplification, the following reaction mix was used:

| Component | Volume [µl] |
|---|---:|
| 2x Master Mix GC Buffer | 12.5 |
| Primer mix (forw. + rev.) (20 µM) | 1.0 |
| cDNA (ca. 10 ng) | 0.5 |
| dd$H_2O$ | add to 25 |

The PCR was performed with the following conditions:

| Temperature | Time | |
|---|---|---|
| 98°C | 2 min | |
| 98 °C<br>X °C | 30 s<br>25 s | 32 cycles |
| 72 °C | Y s | |
| 72 °C | 2 min | |

For X, the primer-dependent annealing temperature was used, and Y (elongation time) was calculated based on the length on the insert with 15 s/ 1kb.

### Digestion of PCR products and vector backbone by restriction enzymes

For ligation of the PCR product into the vector, the vector and the reaction mix after PCR were digested 1.5 h at 37°C. Therefore, the following mix was used:

| Component | Vector | Insert |
|---|---|---|
| 10x FD Green Buffer | 3.0 µl | 3.0 µl |
| Enzyme I | 1.0 µl | 1.0 µl |
| Enzyme II | 1.0 µl | 1.0 µl |
| Insert | - | 25 µl |
| Vektor 2-3 µg | X µl | - |
| Alkaline Phosphatase (Fermentas) | 1.0 µl | - |
| ddH2O | to 30 µl | - |
| Total volume | 30 µl | 30 µl |

The enzymes were heat inactivated for 5 min at 80°C. In the next step, the linearized vector was dephosphorylated using 1 U of FastAP Thermosensitive Alkaline Phosphatase. The vector was incubated for 1 h at 37°C.
The enzyme was inactivated at 65°C for 10 min after addition of DNA Loading dye (1% SDS, 100 mM EDTA). Vector and insert were purified by agarose gel electrophoresis. The specific bands were cut out and DNA was extracted from the gel using the Aquick Gel Extraction Kit according to manufacturer's protocol. The DNA concentrations were measured using the Synergy2 reader.

### Ligation of the final construct

For successful ligation, a molar ration of 1:3 (insert to vector) was calculated as followed:

$$insert\ [ng] = \frac{insert\ (bp)}{vector\ (bp)}\ x\ vector\ [ng]\ x\ 3$$

The ligation mix was set up using the following mix:

| Component | Ligation mix |
|---|---|
| 10x Ligase Buffer | 1.0 µl |
| Vector (x ng/µl) => 50 ng | xx µl |
| Insert (xxx ng/µl) Verd. => 51,8 ng | xx µl |
| T4 Ligase | 0.5 µl |
| ddH2O | add to 10 µl |

The mix was incubated at 16°C over night and afterwards stored at -20°C.

### 6.4.5. Transformation of chemically competent bacteria

For transformation, 25-50 µl chemically competent *E. coli* (TOP10) were thawed on ice. 3 ml of the ligation reaction were added and mixed carefully. Afterwards, the suspension was incubated for 30 min on ice before performing a heat shock for 40 s at 42°C on a ThermoMixer. The suspension was incubated for 1 min on ice and before the addition of 250 µl SOC medium. After agitation for 1 h at 37°C, 75 ml of the transformed *E. coli* were plated on agar plates supplemented with the respective antibiotic. Plates were incubated at 37°C over night.

### 6.4.6. Isolation and multiplication of expression plasmids

After successful transformation, single colonies were picked from the plates (usually 5-10) and transferred into 5 ml LB medium supplemented with the respective antibiotic. The suspension was incubated with agitation at 37°C for 12-18h. 2 ml of the suspension were used to perform colony PCR using primers complementary to the vector backbone. For positive clones, 2 ml of the corresponding bacteria suspension was centrifuged for 10 min at 4°C. The supernatant was discarded, and the plasmid was extracted from the cell pellet using the QIAprep® Spin Miniprep kit according to manufacturer's protocol. The DNA concentration was measured by using the Synergy2 reader before sequencing of the plasmid (GATC, Konstanz).
For longer storage, to 700 µl of bacteria suspension containing the plasmid 300 µl glycerol was added and transferred into 1.5 ml safe lock tubes. If large amounts of the plasmid were needed, 500 ml of the cell suspension were transferred into 150 ml LB medium containing the respective antibiotic and incubated at 37°C over night. The plasmid was extracted by using the QIAGEN® Plasmid Midi kit according to manufacturer's protocol. DNA was resuspended in 50-200 µl TE buffer and the concentration was determined by using the Synergy2 reader.

## 6.5. Animal experiments

### 6.5.1. Animal housing

A naturally MnPV-infected *Mastomys coucha* colony was bred at the Zentrum für Präklinische Forschung (ZPF) at the DKFZ. The cages were individually ventilated (IVC) with a temperature from 22 to 24°C and 55% relative humidity. Animals were fed using mouse breeding diet and water *ad libitum*. Animals were observed during their lifetime and sacrificed due to tumour growth, health issues or for experimental purpose. All animal experiments were performed with the permission of the responsible Animal Ethics Committee (Regional Council of Karlsruhe, Germany; File No 35-9185.81/G289/15 and 35-9185.81/G65/21). All *Mastomys coucha* at the DKFZ were housed and handled in compliance with German and European statutes. A virus free *Mastomys coucha* colony was bred at Janvier labs in France under similar conditions.

### 6.5.2. Vaccination and experimental infection

For immunization of *Mastomys coucha*, 150 ml of the respective antigen solution were injected subcutaneously in a skin fold of the neck. Vaccination was performed four times in a bi-weekly cycle. Two weeks after last immunization, the animals were experimentally infected. Therefore, animals were put under anaesthesia (3% isoflurane). The back was shaved and superficially scratched in longitudinal and transverall direction with tattoo needles. Afterwards, 30 µl MnPV-induced papilloma extract, which contained infectious MnPV virions [256], were applied. For taking blood samples, animals were put under anaesthesia before puncturing the submandibular vein.
For vaccination, the different antigens were injected in a final volume of 150 µl and using different adjuvants:

| Antigen | Injected amount | Adjuvant |
|---|---|---|
| MnPV L1-VLPs [**256**] | 10 µg | 50% Sigma Adjuvant System (SAS)<br>+ 1 x PBS adjusted to 150 µl |
| HPV16 RG1-VLPs [**254**] | 10 µg | 50 µg Monophosphoryl-Lipid A (MPLA)<br>+ 500 µg Alhydrogel adjuvant 2%<br>+ 1 x PBS adjusted to 150 µl |
| CUT-PANHPVAX [**255**] | 20 µg | 50% AddaVax<br>+ 1 x PBS adjusted to 150 µl |

The PBS control group was injected with PBS and 50% AddaVax only.

## 6.6. Collection and Analysis of Animal Tissue Samples

### 6.6.1. Determination of viral load

To define the viral load of the respective animals, hair samples were collected by plucking with forceps from three random positions from the back area. For extraction of the DNA the Chelex resin-based method was used. The hair was digested overnight in 150 µl Chelex risin (5% w/v in water; 100-200 mesh) supplemented with 2 mg proteinase K at 56°C and 300 rpm. The next day, the suspension was mixed by vortexing for 10 sec before incubation for 8 min at 99°C. Afterwards, the suspension was again vortexed or 10 sec and centrifuged at 12,000xg for 3 min. The supernatant was collected into a new tube and stored at -20°C. To determine the viral load qPCR was performed as described before using 1 µl of the collected supernatant. Using primers for the detection of MnPV-L1 gene (MnPV-L1 forw and MnPV-L1 rev from previous study [256]) and β-globin (β-globin forw and β-globin rev also from previous study [256]) the number of input cell equivalents was determined. Samples were analysed in duplicates and the MnPV DNA copy number was calculated by including standards containing MnPV and β-globulin plasmids. Viral load defined as the number of MnPV genomes per two β-globin copies.

### 6.6.2. Histological Samples of skin samples

To identify the proteins of interest in *Mastomys* skin, the animals were first put under anaesthesia with isoflurane. Afterwards, they were sacrificed by cervical dislocation. A scalpel was used to cut out part of the skin of the shaved back. After separating the skin from the animal's back, the skin was sliced into pieces and skin pieces were impaled on cork and incubated in 4% formalin for at least 24h at 4°C. In the next step, tissue samples were embedded in paraffin blocks and sliced in sections of 3 µm by the light microscopy core facility, DKFZ.

### 6.6.3. Hematoxylin-eosin (HE) Staining

Before performing immunohistochemistry (IHC), the tissue sections were stained with hematoxylin-eosin to identify the different compartments of the skin. To remove the paraffin, tissue samples were incubated two times in xylol for 10 min at room temperature and afterwards rehydrated with 100% ethanol for 5 min, 96% ethanol for 5 min, 70% ethanol for 5 min and finally incubated for 10 min in PBS. Afterwards, the samples were stained for 2 min with hetamoxylin. After rinsing with tab water for 5 min, staining with eosin for 30 s were performed before incubation with a graded ethanol series and finally incubated in xylene. The skin samples were mounted and covered with coverslips. Images were taken using the Keyence BZ-9000 microscope. The HE stainings were kindly provided by the light microscopy core facility, DKFZ.

### 6.6.4. Tissue Staining

For the detection of defined proteins in the tissue sections of the animals, immunofluorescence was used. Tissue sections were deparaffinised as described above before starting the heat-induced epitope retrieval by boiling the samples in EDTA (pH 9) or citrate (pH 6) for 10 min in a steam pot. After cooling down in the steam pot, the samples were incubated in 1x PBS for 5 min at room temperature, before blocking unspecific by incubation with 5% goat serum in 1x PBS for 1 h at room temperature. The primary antibodies were diluted in 1% goat serum in PBS. After removing the blocking solution, the primary antibodies were added on the tissue samples and incubated over night at 4°C. The next day, the samples were washed for 5 min in 1x PBS. Afterwards, the corresponding secondary antibodies tagged to a fluorophore were diluted in 1% goat serum in 1x PBS and the skin samples were incubated with the solutions for 1h at room temperature in the dark. For detection of cell nuclei, the tissue sections were washed for 5 min in 1x PBS and incubated with DAPI for 5 min at room temperature. In a final step, the samples were washed two times for 5 min in 1x PBS before being dipped in water, being mounted and covered with coverslips. Images were taken using the Keyence BZ-9000 microscope.

## 6.7. Enzyme-linked Immunosorbent Assay (ELISA)

### 6.7.1. GST-capture ELISA

GST-capture ELISA were performed as described previously [275]. Briefly, the ELISA based on the chemical crosslik of glutathione to casein for using the indirect binding of the fusion protein via its N-terminal GST-tag. Fusion to the SV40-tag at the C-terminus allows the detection of the bound full-length fusion protein via KT3 [276]. Gluthathione-casein was diluted in 100 ml 50 mM carbonate buffer (pH 9.6) and a 96-well Polysorb Nunc-Immuno plate was coated with 200 ng/well overnight at 4 °C. The next day, the plate was blocked 1 h at 37°C with casein blocking buffer (CBB, 0.2% casein in PBST: 0.05% Tween-20 in PBS, 180 µl/well). The plate was incubated for 1 h at room temperature with bacterial lysate containing GST-antigen-SV40-tag fusion protein. To prevent unspecific binding, *Mastomys* sera were diluted 1:50 in CBB containing GST-SV40-tag and incubated for 1 h. After blocking, the ELISA plate was washed four times with 1 x PBS-T and the diluted *Mastomys* sera were added. The plate was incubated for 1 h at room temperature. After washing four times with 1 x PBS-T, 100 µl/well of HRP-conjugated goat anti-mouse IgG diluted 1:10,000 in CBB were added and incubated for 1 h at room temperature. For quantification of the bound antibodies, the plate was washed and incubated with 100 µl/well substrate buffer (0.1 µg/µl tetramethylbenzidine and 0.006% $H_2O_2$ in 100 mM sodium acetate, pH 6.0). After 8 min, the reaction was stopped by adding 50 µl/well of 1 M sulfuric acid. To measure the absorption at a wavelength of 450 nm, the SPECTROstar Nano plate reader was used. To calculate the reactivity of the serum against the antigen, the sera were tested in duplicates and calculations were performed subtracting the background GST-SV40-tag value from the respective antigen. All ELISAs were performed at least twice.

### 6.7.2. VLP-ELISA

For the detection of antibodies specifically binding to the surface of MnPV VLPs, VLP-ELISA was used as previously described [256]. Briefly, a 96-well Polysorb Nunc-Immuno plate was coated over night at 4°C with purified VLPs (100 ng/well) diluted in 50 mM carbonate buffer (pH 9.6). The next day, the plate was blocked with CBB (180 µl/well) for 1 h at 37°C. In the next step, serial dilutions of *Mastomys* sera were added to the plate and incubated for 1 h at room temperature. After washing the plate four times with 1 x PBS-T, the plate was incubated with HRP-conjugate goat anti-mouse IgG (1:10,000 in CBB, 100 µl/well) for 1 h at room temperature. After the final washing step, colorimetrically quantification was performed by incubating for 8 min with substrate buffer (100 µl/well). Through adding 50 µl/well of 1 M sulfuric acid, the enzyme reaction was stopped. The absorption was measured at a wavelength of 450 nm using the SPECTROstar Nano plate reader. Antibody titer represents the last reciprocal serum dilution above blank.

### 6.7.3. HB-EGF ELISA

In this work, a HB-EGF ELISA was performed according to the manufacturer's instructions (Mouse HB-EGF DuoSet ELISA, Cat. #: DY8239-05; R&D Systems). Briefly, the capture antibody was solved in PBS before coating a 96-well microplate with 100 µl per well. The plate was incubated over night at room temperature. To prepare the plate for the experiment, the plate was washed three times with 400 µl wash buffer. After the last washing step, remaining wash buffer was removed. To avoid unspecific binding, the plate was blocked with 300 µl block buffer for 1h at room temperature. The plate was washed again three times with wash buffer. Before adding 100 µl per sample per well, samples were diluted in appropriate reagent diluent. To define the concentration of HB-EGF in the samples, standards included in the kit were used. The plate was incubated for 2 h at room temperature. Afterwards, the plate was washed three times with wash buffer before adding 100 µl of the detection antibody diluted on reagent diluent per well and incubation for 2 h at room temperature. Next, the wash was repeated as previously described and the plate was incubated with 100 µl of Streptavidin-HRP per well for 20 min at room temperature. After the final wash, to each well 100 µl of substrate solution were added and incubated for 20 min at room temperature. To stop the reaction, a volume of 50 µl stop solution was added to each well and mixed by gently tapping the plate. The optical density was determined immediately at 450 nm by using the Plate Reader SPECTROstar Nano BMG (LABTECH, Ortenberg).

### 6.7.4. MnPV pseudovirion-based neutralisation assay (PBNA)

In the neutralisation assay, the reactivity of sera against pseudovirions (PsVs) is tested [277]. Therefore, animal sera were diluted in DMEM supplemented with 10% FCS and used for three-fold serial dilutions ranging from 1:100 to 1:1,968,300. 60 µl of the diluted sera were mixed with 40 µl of pseudovirions in a 96well cell culture plate and incubated for 15 min at room temperature. The pseudovirions used in this study contain a reporter plasmid encoding for Gaussia luciferase. In the next step, 2.5 x $10^5$ HeLaT cells/ml in a volume of 50 µl were seeded onto the pseudovirion suspension and cultured at 37°C for 48 h. For the measurement of the secreted luciferase, coelenterazine substrate and Gaussia glow juice (PJK, Biotech) were added according to manufacturer's protocol. After incubation for 15 min, the signal was measured using the Synergy 2

(BioTek). Samples were analysed in duplicates. The neutralisation titer represents the reciprocal of the highest dilution reducing the signal by at least 50%.
Pseudovirions used in this assay were produced and kindly provided by Dr. Rui Cao.

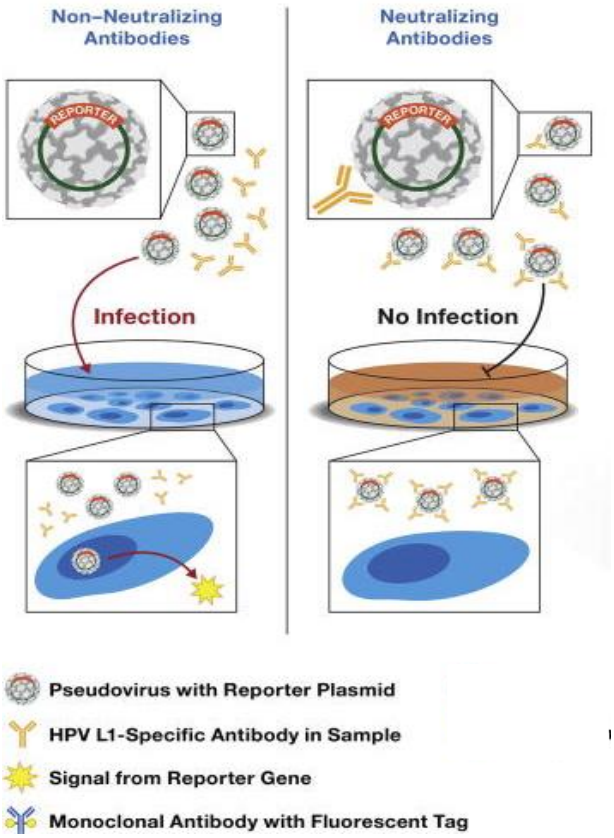


**Fig. 6.7.4 Schematical overview of pseudovirion-based neutralization assay.** This assay allows sensitive detection of neutralizing antibodies. Therefore, HeLaT cells are infected with pseudovirions which are formed by the major capsid protein L1 and the minor capsid protein L2. In the pseudovirions a reporter gene (coding for Gaussia luciferase) is encapsulated. By infecting the HeLaT cells with those pseudovirions, the cells secret Gaussia luciferase to the medium and allows measurement of the activity of the luciferase. In the presence of neutralizing antibodies, the HeLaT cells are prevented from being infected. The figure is adapted and modified from [277].

# 7. Supplemental data

## 7.1. MaFi191

**Suppl. table 1 List of significantly (p <0.05) up- or down- regulated proteins upon γ-irradiation in MaFi191 cells.**

| Gene name | Protein name | p-value | $Log_2FC$ γ-irradiated cells vs ctrl cells |
|---|---|---|---|
| *Taf1* | Transcription factor IID | 0.005 | 1.3 |
| *Ikbkb* | Inhibitor of nuclear factor kappa B kinase subunit beta | 0.040 | 1.1 |
| *Plxna1* | Plexin A1 | 0.040 | 1.0 |
| *Jup* | plakoglobin | 0.005 | 1.0 |
| *Bcas2* | Breast carcinoma-amplified sequence 2 | 0.027 | 1.0 |
| *Tbc1d2* | TBC1 domain family member 2 | 0.008 | 0.9 |
| *Nbea* | Neurobeachin | 0.029 | 0.9 |
| *Pcyox1l* | Prenylcysteine oxidase 1 like | 0.048 | 0.9 |
| *Acot8* | Acyl-coenzyme A thioesterase 8 | 0.030 | 0.8 |
| *Cemip* | Cell migration-inducing protein | 0.026 | 0.8 |
| *Sbno1* | Strawberry notch homolog 1 | 0.043 | -0.7 |
| *Ints12* | Integrator complex subunit 12 | 0.041 | -0.8 |
| *Rad51* | RAD51 | 0.007 | -0.8 |
| *Ykt6* | YKT6 V-SNARE Protein | 0.012 | -0.8 |
| *Akr1c13* | Aldo-keto reductase family 1, member C13 | 0.033 | -0.8 |
| *Qtrtd1* | Queuine TRNA-ribosyltransferase catalytic subunit 1 | 0.026 | -0.9 |
| *Rps8* | 40S ribosomal protein S8 | 0.042 | -1.0 |
| *Nnmt* | Nicotinamide N-methyltransferase | 0.004 | -1.1 |
| *Ccdc115* | Coiled-coil domain containing 115 | 0.007 | -1.2 |

**Suppl. table 2 List of significantly (p <0.05) down- or up-regulated proteins upon UVB-irradiation in MaFi191 cells.**

| Gene name | Protein name | p-value | $Log_2FC$ UVB-irradiated cells vs ctrl cells |
|---|---|---|---|
| *Anxa8* | Annexin A8 | 0.008 | 1.7 |
| *Bcas2* | Breast carcinoma-amplified sequence 2 | 0.015 | 1.3 |
| *H2-Q6* | Histocompatibility 2, Q region locus 6 | 0.011 | 1.3 |
| *Akr1c19* | aldo-keto reductase family 1, member C19 | 0.009 | 1.2 |
| *Atp5d* | ATP synthase subunit delta | 0.031 | 1.1 |
| *Otud6b* | OTU domain containing 6B | 0.028 | 1.0 |
| *Pcyox1l* | Prenylcysteine oxidase 1 like | 0.019 | 0.9 |
| *Dhrs1* | Dehydrogenase 1 | 0.020 | 0.9 |
| *Nelfb* | Negative elongation factor complex member B | 0.008 | 0.9 |
| *Mnat1* | Menage a trois 1 | 0.033 | 0.7 |
| *Thbs1* | Thrombospondin 1 | 0.014 | -0.7 |
| *Nnmt* | Nicotinamide N-methyltransferase | 0.014 | -1.2 |
| *Ints12* | Integrator complex subunit 12 | 0.038 | -1.2 |
| *Arfgef2* | Brefeldin A-inhibited guanine nucleotide-exchange protein 2 | 0.011 | -1.4 |
| *Sufu* | SUFU negative regulator of hedgehog signalling | 0.003 | -1.4 |
| *Col5a1* | Collagen type V alpha 1 chain | 0.011 | -1.4 |
| *Col1a2* | Collagen type I alpha 2 chain | 0.013 | -1.4 |
| *Cfdp1* | Craniofacial development protein 1 | 0.012 | -1.5 |
| *Col5a2* | Collagen type V alpha 2 chain | 0.009 | -1.6 |
| *Cemip* | Cell migration-inducing protein | 0.001 | -2.1 |

**Suppl. table 3 List of significantly (p <0.05) up- or down-regulated proteins upon HB-EGF treatment in MaFi191 cells.**

| Gene name | Protein name | p-value | $Log_2FC$ HB-EGF treated cells vs ctrl cells |
|---|---|---|---|
| *Bcas2* | Breast carcinoma-amplified sequence 2 | 0.012 | 1.2 |
| *Tbc1d2* | TBC1 domain family member 2A | 0.009 | 1.0 |
| *Akr1c19* | Aldo-keto reductase family 1, member C19 | 0.018 | 1.0 |
| *Mapkapk2* | MAPK activated protein kinase 2 | 0.009 | 0.9 |
| *Dlgap5* | DLG associated protein 5 | 0.019 | 0.8 |
| *Imp3* | Insulin-like growth factor II mRNA-binding protein 3 | 0.012 | 0.8 |
| *Slc1a5* | Solute carrier family 1 member 5 | 0.009 | 0.8 |
| *Gtf2e2* | General transcription factor IIE subunit 2 | 0.027 | 0.8 |
| *Jup* | Plakoglobin | 0.009 | 0.8 |
| *Ikbkb* | Inhibitor of nuclear factor kappa B kinase subunit beta | 0.035 | 0.8 |
| *Hk2* | Hexokinase 2 | 0.038 | -0.5 |
| *Wdr43* | WD repeat domain 43 | 0.042 | -0.5 |
| *Xpot* | Exportin-T | 0.047 | -0.5 |
| *Prep* | Prolyl endopeptidase | 0.011 | -0.5 |
| *Sgta* | Small glutamine rich tetratricopeptide repeat co-chaperone alpha | 0.008 | -0.6 |
| *Fam129b* | Fam129B | 0.024 | -0.6 |
| *Nampt* | Nicotinamide phosphoribosyltransferase | 0.021 | -0.6 |
| *Xpo5* | Exportin-5 | 0.037 | -0.6 |
| *Rasa1* | RAS p21 protein activator 1 | 0.009 | -0.6 |
| *Tnfaip2* | Tumor necrosis factor, alpha-induced protein 2 | 0.029 | -0.6 |

**Suppl. table 4 List of significantly (p <0.05) down- or up-regulated proteins upon HB-EGF treatment in γ-irradiated MaFi191 cells.**

| Gene name | Protein name | p-value | $Log_2FC$ HB-EGF treated γ-irradiated cells vs γ-irradiated cells |
|---|---|---|---|
| *Rpia* | Ribose 5-phosphate isomerase A | 0.001 | 1.5 |
| *Serpinb10* | Serpin Family B Member 10 | 0.006 | 1.3 |
| *S100a10* | S100 calcium binding protein A10 | 0.005 | 1.2 |
| *Ptpn14* | Protein tyrosine phosphatase, non-receptor type 14 | 0.016 | 0.9 |
| *Mnat1* | Menage a trois 1 | 0.026 | 0.9 |
| *Akr1c13* | Aldo-keto reductase family 1, member C13 | 0.014 | 0.9 |
| *Diap1* | Diaphanous related formin 1 | 0.021 | 0.8 |
| *Ubxn6* | UBX domain protein 6 | 0.007 | 0.8 |
| *Pea15* | Proliferation and apoptosis adaptor protein 15A | 0.047 | 0.8 |
| *Akr1b10* | Aldo-keto reductase family 1, member B10 | 0.008 | 0.8 |
| *Fam129b* | Fam129B | 0.015 | -0.5 |
| *Sbno1* | Strawberry notch 1 | 0.034 | -0.5 |
| *Qtrtd1* | Queuine TRNA-ribosyltransferase accessory subunit 1 | 0.046 | -0.5 |
| *Mtap* | Methylthioadenosine phosphorylase | 0.011 | -0.5 |
| *Oxsr1* | Oxidative-stress responsive 1 | 0.034 | -0.6 |
| *Impa2* | Inositol Monophosphatase 2 | 0.023 | -0.6 |
| *Ppid* | Peptidylprolyl isomerase D | 0.021 | -0.6 |
| *Cbx1* | Chromobox 1 | 0.049 | -0.6 |
| *Gnai3* | Guanine nucleotide binding protein (G protein), alpha inhibiting 3 | 0.044 | -0.6 |
| *Plac8* | Placenta specific 8 | 0.040 | -0.6 |

**Suppl. table 5 List of significantly (p <0.05) up- or down-regulated proteins upon HB-EGF treatment in UVB-irradiated MaFi191 cells.**

| Gene name | Protein name | p-value | $Log_2FC$ HB-EGF treated UVB-irradiated cells vs UVB-irradiated cells |
|---|---|---|---|
| *Tmem2* | Transmembrane protein 2 | $1.40*10^{-7}$ | 4.3 |
| *Eef1d* | Eukaryotic Translation Elongation Factor 1 Delta | $3.47*10^{-9}$ | 3.0 |
| *Bsdc1* | BSD domain-containing protein 1 | $4.95*10^{-8}$ | 2.5 |
| *Impa2* | Inositol monophosphatase 2 | $9.96*10^{-8}$ | 2.2 |
| *Wdr81* | WD repeat-containing protein 81 | 0.0005 | 2.0 |
| *Tjap1* | Tight junction-associated protein 1 | $3.27*10^{-9}$ | 1.8 |
| *Slc48a1* | Heme transporter HRG1 | 0.022 | 1.5 |
| *Mmp10* | Stromelysin-2 | 0.008 | 1.4 |
| *Agk* | Acylglycerol kinase, mitochondrial | 0.039 | 0.9 |
| *Tjp2* | Tight junction protein ZO-2 | 0.027 | 0.9 |
| *Zbtb7a* | Zinc finger and BTB domain-containing protein 7A | 0.036 | -1.2 |
| *Taf1* | Transcription initiation factor TFIID subunit 1 | 0.024 | -1.2 |
| *Cnst* | Consortin | 0.017 | -1.5 |
| *Sidt2* | SID1 transmembrane family member 2 | 0.009 | -1.1 |
| *Zbtb7a* | Zinc finger and BTB domain-containing protein 7A | 0.036 | -1.2 |
| *Col5a1* | Collagen alpha-1(V) chain | 0.009 | -1.4 |
| *Col5a2* | Collagen alpha-2(V) chain | 0.044 | -1,5 |
| *Ppil1* | Peptidyl-prolyl cis-trans isomerase-like 1 | 0.002 | -1.7 |
| *Rxrb* | Retinoic acid receptor RXR-beta | 0.0003 | -1,8 |
| *Hist1h3a* | Histone H3.1 | $3.79*10^{-9}$ | -3,2 |

## 7.2. MaFi191 R266C

**Suppl. table 6 List of significantly (p <0.05) down- or up-regulated proteins upon γ-irradiation in MaFi191 R266C cells.**

| Gene name | Protein name | p-value | $Log_2FC$ γ-irradiated cells vs ctrl cells |
|---|---|---|---|
| *Snrpd1* | Small nuclear ribonucleoprotein D1 | 0.013 | 2.5 |
| *Plekhg5* | Pleckstrin homology and RhoGEF domain xontaining G5 | $1.76*10^{-9}$ | 1.6 |
| *Rps29* | Ribosomal protein S29 | 0.001 | 1.5 |
| *Pebp1* | Phosphatidylethanolamine binding protein 1 | 0.001 | 1.5 |
| *Guk1* | Guanylate kinase 1 | $8.83*10^{-9}$ | 1.2 |
| *Cox5a* | Cytochrome c oxidase subunit 5A | 0.008 | 1.2 |
| *Rps15* | Ribosomal protein S15 | 0.009 | 1.2 |
| *Sdf2* | Stromal cell derived factor 2 | 0.001 | 1.2 |
| *Top2a* | DNA topoisomerase II alpha | 0.0002 | 1.1 |
| *Sf3b5* | Splicing factor 3b, subunit 5 | 0.0002 | 1.1 |
| *Golt1b* | Golgi transport 1B | 0.048 | -0.7 |
| *Atpif1* | ATPase inhibitory factor 1 | 0.002 | -0.7 |
| *Serpinc1* | Antithrombin | 0.042 | -0.7 |
| *Ogdhl* | Oxoglutarate dehydrogenase L | 0.010 | -0.7 |
| *Plp2* | Proteolipid protein 2 | 0.023 | -0.8 |
| *Rpl19* | Ribosomal protein L19 | 0.033 | -0.8 |
| *Irgq* | Immunity related GTPase Q | 0.038 | -0.9 |
| *Rpl6* | Ribosomal protein L6 | 0.002 | -1.0 |
| *E4f1* | E4F transcription factor 1 | 0.021 | -1.1 |
| *Hist1h1d* | Histone H1.3 | 0.019 | -1.4 |

**Suppl. table 7 List of significantly (p <0.05) down- or up-regulated proteins upon UVB-irradiation in MaFi191 R266C cells.**

| Gene name | Protein name | p-value | $Log_2FC$ UVB-irradiated cells vs ctrl cells |
|---|---|---|---|
| *H3f3c* | H3 histone, family 3C | $5.57*10^{-7}$ | 2.6 |
| *Gm10320* | SEC61 translocon subunit beta | 0.001 | 2.4 |
| *Plekhg5* | Pleckstrin homology and RhoGEF domain containing G5 | $4.88*10^{-7}$ | 2.1 |
| *Snrpd1* | Small nuclear ribonucleoprotein D1 | 0.028 | 2.0 |
| *Ptgs1* | Prostaglandin-endoperoxide synthase 1 | $1.91*10^{-9}$ | 1.6 |
| *H1f0* | H1.0 linker histone | 0.005 | 1.6 |
| *Smco4* | Single-pass membrane protein with coiled-coil domains 4 | 0.0003 | 1.5 |
| *Rps29* | Ribosomal protein S29 | 0.002 | 1.3 |
| *Uck1* | Uridine-cytidine kinase 1 | 0.0002 | 1.3 |
| *Trp53* | Transformation related protein 53 | $9.37*10^{-8}$ | 1.2 |
| *Mnat1* | Menage a trois 1 | 0.030 | 1.0 |
| *Thbs1* | Thrombospondin 1 | 0.0001 | -1.0 |
| *Exoc6b* | Exocyst complex component 6 | 0.0002 | -1.1 |
| *Slc4a4* | Solute carrier family 4, member 4 | $3.83*10^{-9}$ | -1.2 |
| *Col5a1* | Collagen, type V, alpha 1 | $1.14*10^{-9}$ | -1.2 |
| *App* | Amyloid beta (A4) precursor protein | $1.06*10^{-}$ | -1.2 |
| *Il6st* | Interleukin 6 signal transducer | $5.75*10^{-9}$ | -1.2 |
| *Col12a1* | Collagen type XII alpha 1 chain | $5.67*10^{-8}$ | -1.4 |
| *Itga11* | Integrin alpha 11 | $9.24*10^{-8}$ | -1.5 |
| *Tgfbr2* | Transforming growth factor, beta receptor II | $3.44*10^{-9}$ | -1.6 |
| *Cemip* | Cell migration inducing protein | 0.009 | -3.4 |

**Suppl. table 8 List of significantly (p <0.05) down- or up-regulated proteins upon HB-EGF treatment in MaFi191 R266C cells.**

| Gene name | Protein name | p-value | $Log_2FC$ HB-EGF treated cells vs ctrl cells |
|---|---|---|---|
| *Hist1h1b* | Histone H1.5 | 0.002 | 2.6 |
| *Plekhg5* | Pleckstrin homology and RhoGEF domain containing G5 | $1.11*10^{-9}$ | 2.1 |
| *Akap8l* | A-kinase anchoring protein 8 like | 0.003 | 1.5 |
| *H1f0* | H1.0 linker histone | 0.023 | 1.4 |
| *Acta2* | Smooth muscle actin alpha 2 | 0.025 | 1.3 |
| *Cks2* | CDC28 protein kinase regulatory subunit 2 | 0.0008 | 1.3 |
| *Guk1* | Guanylate kinase 1 | 0.0003 | 1.2 |
| *Ccdc124* | Coiled-coil domain containing 124 | 0.001 | 1.2 |
| *Hint1* | Histidine triad nucleotide binding protein 1 | 0.020 | 1.1 |
| *Rrp7a* | Ribosomal RNA processing 7 homolog A | 0.003 | 1.1 |
| *Sh3bgrl* | SH3 domain binding glutamate rich protein like | 0.049 | -0.5 |
| *Rps19* | Ribosomal protein S19 | 0.039 | -0.5 |
| *Eif1ad* | Eukaryotic translation initiation factor 1A domain containing | 0.033 | -0.5 |
| *Fam129b* | Fam129B | 0.041 | -0.5 |
| *Serpinb6a* | Serpin family B member 6 | 0.041 | -0.5 |
| *Pfas* | Phosphoribosylformylglycinamidine synthase | 0.047 | -0.5 |
| *Fnbp1l* | Formin binding protein 1-like | 0.034 | -0.5 |
| *Rbpj* | Recombination signal binding protein | 0.048 | -0.5 |
| *Crabp1* | Cellular retinoic acid binding protein 1 | 0.029 | -0.5 |
| *Arpc5l* | Actin related protein 2/3 complex subunit 5 like | 0.029 | -0.5 |

**Suppl. table 9 List of significantly ( p <0.05) down- or up-regulated proteins upon HB-EGF treatment in γ-irradiated MaFi191 R266C cells.**

| Gene name | Protein name | p-value | $Log_2FC$ HB-EGF treated γ-irradiated cells vs γ-irradiated cells |
|---|---|---|---|
| *Tlk1* | Tousled like kinase 1 | 0.002 | 1.6 |
| *Tle3* | Transducin-like enhancer of split 3 | 0.001 | 1.4 |
| *Irgq* | Immunity related GTPase Q | 0.006 | 1.3 |
| *Polr3f* | Polymerase III polypeptide F | $7.76*10^{-9}$ | 1.2 |
| *Cdc20* | Cell division cycle 20 | 0.002 | 1.1 |
| *Atg2b* | Autophagy related 2B | 0.005 | 0.9 |
| *Tmsb10* | Thymosin beta 10 | 0.001 | 0.8 |
| *Fosl1* | Fos-like antigen 1 | 0.025 | 0.8 |
| *Uba52* | Ubiquitin A-52 residue ribosomal protein fusion product 1 | 0.003 | 0.8 |
| *Eif4ebp1* | Eukaryotic translation initiation factor 4E binding protein 1 | 0.009 | 0.8 |
| *Cdk1* | Cyclin-dependent kinase 1 | 0.044 | -0.2 |
| *Eif5a* | Eukaryotic translation initiation factor 5A | 0.045 | -0.2 |
| *Peak1* | Pseudopodium enriched atypical kinase 1 | 0.043 | -0.2 |
| *Ptpn12* | Protein tyrosine phosphatase non-receptor type 12 | 0.028 | -0.2 |
| *Psmb6* | Proteasome 20S subunit beta 6 | 0.045 | -0.2 |
| *Itga5* | Integrin alpha 5 | 0.037 | -0.2 |
| *Tulp3* | Tubby-like protein 3 | 0.033 | -0.2 |
| *Noc4l* | Nucleolar complex associated 4 homolog | 0.048 | -0.2 |
| *Rnf20* | Ring finger protein 20 | 0.049 | -0.2 |
| *Add1* | Adducin 1 | 0.031 | -0.2 |

**Suppl. table 10 List of significantly (p <0.05) up- or down-regulated proteins upon HB-EGF treatment in UVB-irradiated MaFi191 R266C cells.**

| Gene name | Protein name | p-value | $Log_2FC$ HB-EGF treated γ-irradiated cells vs γ-irradiated cells |
|---|---|---|---|
| *Nol7* | Nucleolar protein 7 | 0.022 | 1.2 |
| *Atp5me* | ATP synthase membrane subunit E | 0.022 | 1.1 |
| *Amot* | Angiomotin | 0.046 | 1.0 |
| *Iah1* | Isoamyl acetate-hydrolyzing esterase 1 homolog | 0.005 | 0.8 |
| *Tgfbr2* | Transforming growth factor, beta receptor II | 0.011 | 0.8 |
| *Ndfip1* | Nedd4 family interacting protein 1 | 0.005 | 0.7 |
| *Junb* | Jun B proto-oncogene | 0.009 | 0.7 |
| *Mob1a* | MOB kinase activator 1A | 0.001 | 0.7 |
| *S100a6* | Calcium binding protein A6 | 0.031 | 0.6 |
| *Ajuba* | Ajuba | 0.009 | 0.6 |
| *Rasa1* | RAS p21 protein activator 1 | 0.015 | -0.3 |
| *Atg5* | Autophagy related 5 | 0.014 | -0.3 |
| *Ampd2* | Adenosine monophosphate deaminase 2 | 0.042 | -0.4 |
| *Rilpl1* | Rab interacting lysosomal protein-like 1 | 0.034 | -0.4 |
| *Elmo2* | Engulfment and cell motility 2 | 0.026 | -0.4 |
| *Ncbp2* | Nuclear cap binding protein subunit 2 | 0.037 | -0.4 |
| *Olfml3* | Olfactomedin like 3 | 0.016 | -0.4 |
| *Fntb* | Farnesyltransferase | 0.004 | -0.4 |
| *Fhl3* | Four and a half LIM domains 3 | 0.033 | -0.4 |
| *Apoa1bp* | Apolipoprotein A 1 | 0.039 | -0.4 |

## 7.3. MaFi132

**Suppl. table 11 List of significantly (p <0.05) up- or down-regulated proteins upon γ-irradiation in MaFi132 cells.**

| Gene name | Protein name | p-value | $Log_2FC$ γ-irradiated cells vs ctrl cells |
|---|---|---|---|
| *Slc9a1* | Solute carrier family 9, member 1 | 0.013 | 3.0 |
| *Rfk* | Riboflavin kinase | 0.031 | 1.2 |
| *Znf668* | Zinc finger protein 668 | 0.006 | 1.1 |
| *Pole* | Polymerase, epsilon | 0.049 | 1.1 |
| *Ccdc134* | Coiled-coil domain containing 134 | 0.011 | 1.0 |
| *Lamtor4* | Late endosomal/lysosomal adaptor, MAPK and MTOR activator 4 | 0.032 | 1.0 |
| *Ccs* | Copper chaperone for superoxide dismutase | 0.028 | 0.8 |
| *Loxl2* | Lysyl oxidase like 2 | 0.008 | 0.8 |
| *Nop14* | Nucleolar protein 14 | 0.001 | 0.8 |
| *Apoe* | Apolipoprotein E | 0.011 | 0.8 |
| *Med1* | Mediator complex subunit 1 | 0.047 | -0.4 |
| *Vprbp* | VPRBP | 0.048 | -0.5 |
| *Cetn2* | Centrin 2 | 0.031 | -0.6 |
| *Eif2b1* | Eukaryotic translation initiation factor 2B subunit alpha | 0.013 | -0.6 |
| *Ccnh* | Cyclin H | 0.049 | -0.6 |
| *Spag7* | Sperm associated antigen 7 | 0.021 | -0.7 |
| *Tarbp2* | AR DNA binding protein | 0.008 | -0.7 |
| *Nolc1* | Nucleolar and coiled-body phosphoprotein 1 | 0.033 | -0.8 |
| *Tjap1* | Tight junction associated protein 1 | 0.036 | -1.1 |
| *Srd5a3* | Steroid 5 alpha-reductase 3 | 0.002 | -1.1 |

**Suppl. table 12 List of significantly (p <0.05) up- or down-regulated proteins in UVB-irradiated MaFi132 cells.**

| Gene name | Protein name | p-value | $Log_2FC$ UVB-irradiated cells vs ctrl cells |
|---|---|---|---|
| *Slc9a1* | Solute carrier family 9, member 1 | 0.013 | 1.9 |
| *Cd63* | CD63 | 0.031 | 1.6 |
| *Orc3* | Origin recognition complex, subunit 3 | 0.006 | 1.5 |
| *Arhgef2* | Rho/Rac guanine nucleotide exchange factor 2 | 0.049 | 1.5 |
| *Mgea5* | Meningioma Expressed Antigen 5 | 0.011 | 1.3 |
| *Tomm5* | Translocase of outer mitochondrial membrane 5 | 0.032 | 1.2 |
| *Rabif* | RAB interacting factor | 0.028 | 1.2 |
| *Szt2* | SZT2 | 0.008 | 1.1 |
| *Otulin* | OTU Deubiquitinase | 0.001 | 1.1 |
| *Dsp* | Desmoplakin | 0.011 | 0.9 |
| *Thbs1* | Thrombospondin 1 | 0.001 | -0.8 |
| *Nrp1* | Neuropilin 1 | 0.014 | -0.8 |
| *Ptprk* | Protein tyrosine phosphatase, receptor type, K | 0.023 | -0.9 |
| *Col3a1* | Collagen, type III, alpha 1 | 0.012 | -0.9 |
| *Uck1* | Uridine-cytidine kinase 1 | 0.001 | -0.9 |
| *Exoc4* | Exocyst complex component 4 | 0.0004 | -1.0 |
| *Mycbp2* | MYC Binding Protein 2 | 0.0004 | -1.1 |
| *Col5a2* | Collagen type V, alpha 2 | 0.001 | -1.3 |
| *Col5a1* | Collagen type V, alpha 1 | 0.0004 | -1.4 |
| *Col12a1* | Collagen type XII, alpha 1 | 0.0003 | -1.5 |

**Suppl. table 13 List of significantly (p <0.05) down- or up-regulated proteins upon HB-EGF treatment in MaFi132 cells.**

| Gene name | Protein name | p-value | $Log_2FC$ HB-EGF treated cells vs ctrl cells |
|---|---|---|---|
| *Phf2* | PHD finger protein 2 | 0.021 | 3.1 |
| *Slc9a1* | Solute carrier family 9 member A1 | 0.022 | 2.0 |
| *Arhgef2* | Arhgef2 | 0.001 | 1.8 |
| *Orc3* | Origin recognition complex subunit 3 | 0.011 | 1.2 |
| *Rpl26* | Ribosomal protein L26 | 0.006 | 1.0 |
| *Szt2* | SZT2 | 0.023 | 1.0 |
| *Ptgs2* | Prostaglandin-endoperoxide synthase 2 | 0.019 | 1.0 |
| *Rabif* | RAB Interacting Factor | 0.007 | 1.0 |
| *Stxbp5* | Syntaxin binding protein 5 | 0.004 | 1.0 |
| *Ak6* | Adenylate kinase 6 | 0.012 | 0.9 |
| *Eif3g* | Eukaryotic translation initiation factor 3 subunit G | 0.049 | -0.3 |
| *Sec23b* | SEC23 homolog B | 0.028 | -0.3 |
| *Surf2* | Surfeit 2 | 0.041 | -0.3 |
| *Smyd2* | SET and MYND domain containing 2 | 0.030 | -0.3 |
| *Hsph1* | Heat shock protein family H member 1 | 0.036 | -0.3 |
| *Tuba1b* | Tubulin alpha 1b | 0.037 | -0.3 |
| *Tsnax* | Translin associated factor X | 0.022 | -0.4 |
| *Cfdp1* | Craniofacial development protein 1 | 0.046 | -0.4 |
| *Smek1* | Protein phosphatase 4 regulatory subunit 3A | 0.015 | -0.4 |
| *Fam169a* | Family with sequence similarity 169 member A | 0.025 | -0.4 |

**Suppl. table 14 List of significantly (p <0.05) down- or up-regulated proteins upon HB-EGF treatment in γ-irradiated MaFi132 cells.**

| Gene name | Protein name | p-value | $Log_2FC$ HB-EGF treated γ-irradiated cells vs γ-irradiated cells |
|---|---|---|---|
| *Orc3* | Origin recognition complex, subunit 3 | 0.039 | 1.4 |
| *Ptgs2* | Prostaglandin-endoperoxide synthase 2 | 0.036 | 1.3 |
| *Fry1* | FRY like transcription coactivator | 0.0002 | 1.2 |
| *Eif2d* | Eukaryotic translation initiation factor 2D | 0.025 | 1.2 |
| *Polr3e* | RNA polymerase III subunit E | 0.039 | 1.1 |
| *Mmp3* | Matrox metalloproteinase 3 | 0.0 | 0.7 |
| *Hltf* | Helicase like transcription factor | 0.013 | 1.0 |
| *Nop9* | NOP9 nucleolar protein | 0.012 | 0.8 |
| *Usp38* | Ubiquitin specific peptidase 38 | 0.008 | 0.8 |
| *Cmss1* | Cms1 ribosomal small subunit homolog | 0.004 | 0.7 |
| *Elmo2* | Engulfment and cell motility 2 | 0.019 | -0.4 |
| *Ntan1* | N-Terminal asparagine amidase | 0.025 | -0.4 |
| *Ehd3* | EH domain containing 3 | 0.038 | -0.4 |
| *Git1* | GIT ArfGAP 1 | 0.037 | -0.4 |
| *Pdcd2* | Programmed cell death 2 | 0.037 | -0.4 |
| *Nt5c3a* | 5'-Nucleotidase, cytosolic IIIA | 0.042 | -0.4 |
| *Ric8a* | RIC8 guanine nucleotide exchange factor A | 0.013 | -0.4 |
| *Tfap2a* | Transcription factor AP-2 alpha | 0.044 | -0.4 |
| *Ppp3ca* | Protein phosphatase 3 catalytic subunit alpha | 0.032 | -0.5 |
| *Gorasp1* | Golgi reassembly stacking protein 1 | 0.049 | -0.5 |

**Suppl. table 15 List of significantly (p <0.05) up- or down-regulated proteins upon HB-EGF treatment in UVB-irradiated MaFi132 cells.**

| Gene name | Protein name | p-value | $Log_2FC$ HB-EGF treated UVB-irradiated cells vs UVB-irradiated cells |
|---|---|---|---|
| *Mmp3* | Matrix metalloproteinase 3 | $3.09*10^{-8}$ | 2.7 |
| *Gm10320* | Predicted pseudogene 10320 | 0.0019 | 2.1 |
| *Slc7a5* | Solute carrier family 7, member 5 | 0.0002 | 1.8 |
| *Prdx6b* | Peroxiredoxin 6B | 0.002 | 1.7 |
| *Arg2* | Arginase type II | 0.0008 | 1.7 |
| *Tln2* | Talin 2 | $2.22*10^{-9}$ | 1.7 |
| *Cd63* | CD63 | 0.023 | 1.5 |
| *Cdc27* | Cell division cycle 27 | 0.0001 | 1.5 |
| *Slc38a2* | Solute carrier family 38, member 2 | 0.0003 | 1.4 |
| *Cetn3* | Centrin 3 | $9.61*10^{-9}$ | 1.4 |
| *Fam91a1* | Family with sequence similarity 91 member A1 | 0.045 | -0.4 |
| *Smad2* | SMAD family member 2 | 0.039 | -0.4 |
| *Ipo5* | Importin 5 | 0.049 | -0.4 |
| *Pwp2* | Periodic tryptophan protein 2 | 0.048 | -0.4 |
| *Ahsa1* | Activator of heat shock 90kDa protein ATPase homolog 1 | 0.043 | -0.4 |
| *Lypla1* | Lysophospholipase 1 | 0.034 | -0.4 |
| *Ube2e3* | Ubiquitin conjugating enzyme E2 E3 | 0.041 | -0.4 |
| *Bop1* | Block of proliferation 1 | 0.043 | -0.4 |
| *Hsph1* | Heat shock protein family H member 1 | 0.048 | -0.4 |
| *Idh3g* | Isocitrate dehydrogenase 3 gamma | 0.037 | -0.4 |

# 8. References


1. Torre, L.A., et al., *Global Cancer Incidence and Mortality Rates and Trends—An Update.* Cancer Epidemiology, Biomarkers & Prevention, 2016. **25**(1): p. 16-27.
2. Iranzo, J., I. Martincorena, and E.V. Koonin, *Cancer-mutation network and the number and specificity of driver mutations.* Proc Natl Acad Sci U S A, 2018. **115**(26): p. E6010-e6019.
3. Prior, I.A., F.E. Hood, and J.L. Hartley, *The Frequency of Ras Mutations in Cancer.* Cancer Res, 2020. **80**(14): p. 2969-2974.
4. Zhang, C., et al., *Gain-of-function mutant p53 in cancer progression and therapy.* J Mol Cell Biol, 2020. **12**(9): p. 674-687.
5. Chang, M.T., et al., *Identifying recurrent mutations in cancer reveals widespread lineage diversity and mutational specificity.* Nat Biotechnol, 2016. **34**(2): p. 155-63.
6. van den Bulk, J., E.M. Verdegaal, and N.F. de Miranda, *Cancer immunotherapy: broadening the scope of targetable tumours.* Open Biol, 2018. **8**(6).
7. Malone, E.R., et al., *Molecular profiling for precision cancer therapies.* Genome Med, 2020. **12**(1): p. 8.
8. Furue, H., *[Chemotherapy cancer treatment during the past sixty years].* Gan To Kagaku Ryoho, 2003. **30**(10): p. 1404-11.
9. Allen, C., S. Her, and D.A. Jaffray, *Radiotherapy for Cancer: Present and Future.* Adv Drug Deliv Rev, 2017. **109**: p. 1-2.
10. Galluzzi, L., et al., *Classification of current anticancer immunotherapies.* Oncotarget, 2014. **5**(24): p. 12472-508.
11. Sterner, R.C. and R.M. Sterner, *CAR-T cell therapy: current limitations and potential strategies.* Blood Cancer J, 2021. **11**(4): p. 69.
12. Sellars, M.C., C.J. Wu, and E.F. Fritsch, *Cancer vaccines: Building a bridge over troubled waters.* Cell, 2022. **185**(15): p. 2770-2788.
13. Lewandowska, A.M., et al., *Environmental risk factors for cancer – review paper.* Annals of Agricultural and Environmental Medicine, 2019. **26**(1): p. 1-7.
14. de Martel, C., et al., *Global burden of cancer attributable to infections in 2018: a worldwide incidence analysis.* The Lancet Global Health, 2020. **8**(2): p. e180-e190.
15. Read, S.A. and M.W. Douglas, *Virus induced inflammation and cancer development.* Cancer Lett, 2014. **345**(2): p. 174-81.
16. Boshart, M., et al., *A new type of papillomavirus DNA, its presence in genital cancer biopsies and in cell lines derived from cervical cancer.* EMBO J, 1984. **3**(5): p. 1151-7.
17. Dürst, M., et al., *A papillomavirus DNA from a cervical carcinoma and its prevalence in cancer biopsy samples from different geographic regions.* Proc Natl Acad Sci U S A, 1983. **80**(12): p. 3812-5.
18. Institute, N.C. *HPV and Cancer*. 2022.
19. Brianti, P., E. De Flammineis, and S.R. Mercuri, *Review of HPV-related diseases and cancers.* New Microbiol, 2017. **40**(2): p. 80-85.
20. Robert-Koch-Institute. *Humane Papillomviren*. 2018.
21. Scarth, J.A., et al., *The human papillomavirus oncoproteins: a review of the host pathways targeted on the road to transformation.* J Gen Virol, 2021. **102**(3).
22. Richards, R.M., et al., *Cleavage of the papillomavirus minor capsid protein, L2, at a furin consensus site is necessary for infection.* Proc Natl Acad Sci U S A, 2006. **103**(5): p. 1522-7.
23. Chandrachud, L.M., et al., *Vaccination of cattle with the N-terminus of L2 is necessary and sufficient for preventing infection by bovine papillomavirus-4.* Virology, 1995. **211**(1): p. 204-8.
24. Bastien, N. and A.A. McBride, *Interaction of the papillomavirus E2 protein with mitotic chromosomes.* Virology, 2000. **270**(1): p. 124-34.

25. Snijders, P.J., et al., *Human papillomavirus (HPV) type 16 and 33 E6/E7 region transcripts in tonsillar carcinomas can originate from integrated and episomal HPV DNA.* J Gen Virol, 1992. **73 ( Pt 8)**: p. 2059-66.
26. Kessis, T.D., et al., *Expression of HPV16 E6 or E7 increases integration of foreign DNA.* Oncogene, 1996. **13**(2): p. 427-31.
27. Moody, C.A. and L.A. Laimins, *Human papillomavirus oncoproteins: pathways to transformation.* Nature Reviews Cancer, 2010. **10**(8): p. 550-560.
28. Murakami, I., et al., *Roles for E1-independent replication and E6-mediated p53 degradation during low-risk and high-risk human papillomavirus genome maintenance.* PLoS Pathog, 2019. **15**(5): p. e1007755.
29. Li, X. and P. Coffino, *High-risk human papillomavirus E6 protein has two distinct binding sites within p53, of which only one determines degradation.* J Virol, 1996. **70**(7): p. 4509-16.
30. Wallace, N.A., K. Robinson, and D.A. Galloway, *Beta human papillomavirus E6 expression inhibits stabilization of p53 and increases tolerance of genomic instability.* J Virol, 2014. **88**(11): p. 6112-27.
31. Heck, D.V., et al., *Efficiency of binding the retinoblastoma protein correlates with the transforming capacity of the E7 oncoproteins of the human papillomaviruses.* Proc Natl Acad Sci U S A, 1992. **89**(10): p. 4442-6.
32. Hwang, E.S., T. Nottoli, and D. Dimaio, *The HPV16 E5 protein: expression, detection, and stable complex formation with transmembrane proteins in COS cells.* Virology, 1995. **211**(1): p. 227-33.
33. Griffin, L.L., F.R. Ali, and J.T. Lear, *Non-melanoma skin cancer.* Clinical Medicine, 2016. **16**(1): p. 62-65.
34. Didona, D., et al., *Non Melanoma Skin Cancer Pathogenesis Overview.* Biomedicines, 2018. **6**(1).
35. Kim, D.P., K.J.B. Kus, and E. Ruiz, *Basal Cell Carcinoma Review.* Hematol Oncol Clin North Am, 2019. **33**(1): p. 13-24.
36. Waldman, A. and C. Schmults, *Cutaneous Squamous Cell Carcinoma.* Hematol Oncol Clin North Am, 2019. **33**(1): p. 1-12.
37. Akgul, B., J.C. Cooke, and A. Storey, *HPV-associated skin disease.* J Pathol, 2006. **208**(2): p. 165-75.
38. Weissenborn, S.J., et al., *Intrafamilial transmission and family-specific spectra of cutaneous betapapillomaviruses.* J Virol, 2009. **83**(2): p. 811-6.
39. de Villiers, E.M., *Cross-roads in the classification of papillomaviruses.* Virology, 2013. **445**(1-2): p. 2-10.
40. Deau, M.C., M. Favre, and G. Orth, *Genetic heterogeneity among human papillomaviruses (HPV) associated with epidermodysplasia verruciformis: evidence for multiple allelic forms of HPV5 and HPV8 E6 genes.* Virology, 1991. **184**(2): p. 492-503.
41. Yamashita, T., et al., *Biological and biochemical activity of E7 genes of the cutaneous human papillomavirus type 5 and 8.* Oncogene, 1993. **8**(9): p. 2433-41.
42. Ferreira, D.A., et al., *A "hit-and-run" affair – A possible link for cancer progression in virally driven cancers.* Biochimica et Biophysica Acta (BBA) - Reviews on Cancer, 2021. **1875**(1): p. 188476.
43. Yang, W., *Surviving the sun: repair and bypass of DNA UV lesions.* Protein Sci, 2011. **20**(11): p. 1781-9.
44. Moldovan, G.L., et al., *DNA polymerase POLN participates in cross-link repair and homologous recombination.* Mol Cell Biol, 2010. **30**(4): p. 1088-96.
45. Jeggo, P.A. and M. Löbrich, *DNA double-strand breaks: their cellular and clinical impact?* Oncogene, 2007. **26**(56): p. 7717-9.
46. Lechner, M.S. and L.A. Laimins, *Inhibition of p53 DNA binding by human papillomavirus E6 proteins.* J Virol, 1994. **68**(7): p. 4262-73.

47. White, E.A., et al., *Comprehensive analysis of host cellular interactions with human papillomavirus E6 proteins identifies new E6 binding partners and reflects viral diversity.* J Virol, 2012. **86**(24): p. 13174-86.
48. Accardi, R., et al., *Skin human papillomavirus type 38 alters p53 functions by accumulation of deltaNp73.* EMBO Rep, 2006. **7**(3): p. 334-40.
49. Lavin, M.F. and N. Gueven, *The complexity of p53 stabilization and activation.* Cell Death Differ, 2006. **13**(6): p. 941-50.
50. Wendel, S.O. and N.A. Wallace, *Loss of Genome Fidelity: Beta HPVs and the DNA Damage Response.* Front Microbiol, 2017. **8**: p. 2250.
51. Caldeira, S., et al., *The E6 and E7 proteins of the cutaneous human papillomavirus type 38 display transforming properties.* J Virol, 2003. **77**(3): p. 2195-206.
52. Parkin, J. and B. Cohen, *An overview of the immune system.* Lancet, 2001. **357**(9270): p. 1777-89.
53. Beutler, B., *Innate immunity: an overview.* Mol Immunol, 2004. **40**(12): p. 845-59.
54. Vesely, M.D., et al., *Natural innate and adaptive immunity to cancer.* Annu Rev Immunol, 2011. **29**: p. 235-71.
55. Bonilla, F.A. and H.C. Oettgen, *Adaptive immunity.* J Allergy Clin Immunol, 2010. **125**(2 Suppl 2): p. S33-40.
56. Ouwehand, K., et al., *CCL5 and CCL20 mediate immigration of Langerhans cells into the epidermis of full thickness human skin equivalents.* Eur J Cell Biol, 2012. **91**(10): p. 765-73.
57. Sperling, T., et al., *Human papillomavirus type 8 interferes with a novel C/EBPβ -mediated mechanism of keratinocyte CCL20 chemokine expression and Langerhans cell migration.* PLoS Pathog, 2012. **8**(7): p. e1002833.
58. Zhou, Q., K. Zhu, and H. Cheng, *Toll-like receptors in human papillomavirus infection.* Arch Immunol Ther Exp (Warsz), 2013. **61**(3): p. 203-15.
59. Hasan, U.A., et al., *TLR9 expression and function is abolished by the cervical cancer-associated human papillomavirus type 16.* J Immunol, 2007. **178**(5): p. 3186-97.
60. Miller, L.S., *Toll-like receptors in skin.* Adv Dermatol, 2008. **24**: p. 71-87.
61. Fitzgerald, K.A. and J.C. Kagan, *Toll-like Receptors and the Control of Immunity.* Cell, 2020. **180**(6): p. 1044-1066.
62. Vandermark, E.R., et al., *Human papillomavirus type 16 E6 and E 7 proteins alter NF-kB in cultured cervical epithelial cells and inhibition of NF-kB promotes cell growth and immortalization.* Virology, 2012. **425**(1): p. 53-60.
63. Niebler, M., et al., *Post-translational control of IL-1β via the human papillomavirus type 16 E6 oncoprotein: a novel mechanism of innate immune escape mediated by the E3-ubiquitin ligase E6-AP and p53.* PLoS Pathog, 2013. **9**(8): p. e1003536.
64. Groves, I.J. and N. Coleman, *Pathogenesis of human papillomavirus-associated mucosal disease.* J Pathol, 2015. **235**(4): p. 527-38.
65. Athanasiou, A., et al., *HPV vaccination and cancer prevention.* Best Practice & Research Clinical Obstetrics & Gynaecology, 2020. **65**: p. 109-124.
66. Arbyn, M., et al., *Prophylactic vaccination against human papillomaviruses to prevent cervical cancer and its precursors.* Cochrane Database Syst Rev, 2018. **5**(5): p. Cd009069.
67. Pogoda, C.S., R.B. Roden, and R.L. Garcea, *Immunizing against Anogenital Cancer: HPV Vaccines.* PLoS Pathog, 2016. **12**(5): p. e1005587.
68. Einstein, M.H., et al., *Comparison of the immunogenicity and safety of Cervarix and Gardasil human papillomavirus (HPV) cervical cancer vaccines in healthy women aged 18-45 years.* Hum Vaccin, 2009. **5**(10): p. 705-19.
69. Breitburd, F., et al., *Immunization with viruslike particles from cottontail rabbit papillomavirus (CRPV) can protect against experimental CRPV infection.* J Virol, 1995. **69**(6): p. 3959-63.

70. Roden, R.B.S., et al., *Minor Capsid Protein of Human Genital Papillomaviruses Contains Subdominant, Cross-Neutralizing Epitopes.* Virology, 2000. **270**(2): p. 254-257.
71. Pastrana, D.V., et al., *Cross-neutralization of cutaneous and mucosal Papillomavirus types with anti-sera to the amino terminus of L2.* Virology, 2005. **337**(2): p. 365-372.
72. Gambhira, R., et al., *Protection of rabbits against challenge with rabbit papillomaviruses by immunization with the N terminus of human papillomavirus type 16 minor capsid antigen L2.* J Virol, 2007. **81**(21): p. 11585-92.
73. Jagu, S., et al., *Vaccination with multimeric L2 fusion protein and L1 VLP or capsomeres to broaden protection against HPV infection.* Vaccine, 2010. **28**(28): p. 4478-86.
74. Christensen, N.D., et al., *The open reading frame L2 of cottontail rabbit papillomavirus contains antibody-inducing neutralizing epitopes.* Virology, 1991. **181**(2): p. 572-9.
75. Gambhira, R., et al., *A protective and broadly cross-neutralizing epitope of human papillomavirus L2.* J Virol, 2007. **81**(24): p. 13927-31.
76. Karanam, B., et al., *Developing vaccines against minor capsid antigen L2 to prevent papillomavirus infection.* Immunol Cell Biol, 2009. **87**(4): p. 287-99.
77. Schellenbacher, C., et al., *Efficacy of RG1-VLP vaccination against infections with genital and cutaneous human papillomaviruses.* J Invest Dermatol, 2013. **133**(12): p. 2706-2713.
78. Caldeira Jdo, C., et al., *Immunogenic display of diverse peptides, including a broadly cross-type neutralizing human papillomavirus L2 epitope, on virus-like particles of the RNA bacteriophage PP7.* Vaccine, 2010. **28**(27): p. 4384-93.
79. Tumban, E., et al., *A pan-HPV vaccine based on bacteriophage PP7 VLPs displaying broadly cross-neutralizing epitopes from the HPV minor capsid protein, L2.* PLoS One, 2011. **6**(8): p. e23310.
80. Schaper, I.D., et al., *Development of skin tumors in mice transgenic for early genes of human papillomavirus type 8.* Cancer Res, 2005. **65**(4): p. 1394-400.
81. Marcuzzi, G.P., et al., *Spontaneous tumour development in human papillomavirus type 8 E6 transgenic mice and rapid induction by UV-light exposure and wounding.* J Gen Virol, 2009. **90**(Pt 12): p. 2855-2864.
82. Hufbauer, M., et al., *Human papillomavirus mediated inhibition of DNA damage sensing and repair drives skin carcinogenesis.* Mol Cancer, 2015. **14**: p. 183.
83. Dong, W., et al., *Skin hyperproliferation and susceptibility to chemical carcinogenesis in transgenic mice expressing E6 and E7 of human papillomavirus type 38.* J Virol, 2005. **79**(23): p. 14899-908.
84. Hardin, A., et al., *Comparative Genomic Characterization of the Multimammate Mouse Mastomys coucha.* Molecular biology and evolution, 2019. **36**.
85. Davis, D.H.S.H., R.B.; Mcneill, D.; Meyer, K.F., *Serological survey of plague in rodents and other small mammals in kenya.* . Trans. R. Soc. Trop. Med. Hyg, 1968: p. 62, 838–861.
86. Müller, H. and L. Gissmann, *Mastomys natalensis papilloma virus (MnPV), the causative agent of epithelial proliferations: characterization of the virus particle.* J Gen Virol, 1978. **41**(2): p. 315-23.
87. Kruppa, T.F., et al., *Mastomys natalensis or Mastomys coucha. Correct species designation in animal experiments.* Trop Med Parasitol, 1990. **41**(2): p. 219-20.
88. Robbins, C.B., J.W. Krebs, Jr., and K.M. Johnson, *Mastomys (rodentia: muridae) species distinguished by hemoglobin pattern differences.* Am J Trop Med Hyg, 1983. **32**(3): p. 624-30.
89. Smit, A.A. and H.F. Van der Bank, *Isozyme and allozyme markers distinguishing two morphologically similar, medically important Mastomys species (Rodentia: Muridae).* BMC Genet, 2001. **2**: p. 15.
90. Rudolph, R.M., H., *Induktion von epidermalem Tumorwachstum in der Haut von Mastomys natalensis durch Übertragung virushaltigen Tumorgewebes eines Plattenepithelkarzinoms.* Zentralblatt für Veterinärmedizin Reihe B, 1976: p. 23, 143–150.

91. Hasche, D., et al., *The interplay of UV and cutaneous papillomavirus infection in skin cancer development.* PLoS Pathog, 2017. **13**(11): p. e1006723.
92. Pickering, C.R., et al., *Mutational Landscape of Aggressive Cutaneous Squamous Cell Carcinoma.* Clinical Cancer Research, 2014. **20**(24): p. 6582-6592.
93. Olivier, M., M. Hollstein, and P. Hainaut, *TP53 mutations in human cancers: origins, consequences, and clinical use.* Cold Spring Harb Perspect Biol, 2010. **2**(1): p. a001008.
94. Missero, C. and D. Antonini, *Crosstalk among p53 family members in cutaneous carcinoma.* Experimental Dermatology, 2014. **23**(3): p. 143-146.
95. Hasche, D., et al., *Establishment of an Immortalized Skin Keratinocyte Cell Line Derived from the Animal Model Mastomys coucha.* PLoS One, 2016. **11**(8): p. e0161283.
96. Higashiyama, S., et al., *A heparin-binding growth factor secreted by macrophage-like cells that is related to EGF.* Science, 1991. **251**(4996): p. 936-9.
97. Sabbah, D.A., R. Hajjo, and K. Sweidan, *Review on Epidermal Growth Factor Receptor (EGFR) Structure, Signaling Pathways, Interactions, and Recent Updates of EGFR Inhibitors.* Curr Top Med Chem, 2020. **20**(10): p. 815-834.
98. Seeger, M.A. and A.S. Paller, *The Roles of Growth Factors in Keratinocyte Migration.* Adv Wound Care (New Rochelle), 2015. **4**(4): p. 213-224.
99. Kuo, D., et al., *HBEGF(+) macrophages in rheumatoid arthritis induce fibroblast invasiveness.* Sci Transl Med, 2019. **11**(491).
100. Mathay, C., et al., *Heparin-Binding EGF-Like Growth Factor Is Induced by Disruption of Lipid Rafts and Oxidative Stress in Keratinocytes and Participates in the Epidermal Response to Cutaneous Wounds.* Journal of Investigative Dermatology, 2008. **128**(3): p. 717-727.
101. Miyata, K., et al., *Regulatory Mechanisms of the HB-EGF Autocrine Loop in Inflammation, Homeostasis, Development and Cancer.* Anticancer Research, 2012. **32**(6): p. 2347.
102. Izumi, Y., et al., *A metalloprotease-disintegrin, MDC9/meltrin-gamma/ADAM9 and PKCdelta are involved in TPA-induced ectodomain shedding of membrane-anchored heparin-binding EGF-like growth factor.* Embo j, 1998. **17**(24): p. 7260-72.
103. Lemjabbar, H. and C. Basbaum, *Platelet-activating factor receptor and ADAM10 mediate responses to Staphylococcus aureus in epithelial cells.* Nature Medicine, 2002. **8**(1): p. 41-46.
104. Sahin, U., et al., *Distinct roles for ADAM10 and ADAM17 in ectodomain shedding of six EGFR ligands.* J Cell Biol, 2004. **164**(5): p. 769-79.
105. Dao, D.T., et al., *Heparin-Binding Epidermal Growth Factor-Like Growth Factor as a Critical Mediator of Tissue Repair and Regeneration.* Am J Pathol, 2018. **188**(11): p. 2446-2456.
106. Abraham, J.A., et al., *Heparin-binding EGF-like growth factor: characterization of rat and mouse cDNA clones, protein domain conservation across species, and transcript expression in tissues.* Biochem Biophys Res Commun, 1993. **190**(1): p. 125-33.
107. Vinante, F. and A. Rigo, *Heparin-binding epidermal growth factor-like growth factor/diphtheria toxin receptor in normal and neoplastic hematopoiesis.* Toxins (Basel), 2013. **5**(6): p. 1180-1201.
108. Chen, X., et al., *Induction of Heparin-binding EGF-like Growth Factor Expression during Myogenesis: ACTIVATION OF THE GENE BY MyoD AND LOCALIZATION OF THE TRANSMEMBRANE FORM OF THE PROTEIN ON THE MYOTUBE SURFACE *.* Journal of Biological Chemistry, 1995. **270**(31): p. 18285-18294.
109. Harding, P.A., et al., *Characterization of the gene encoding murine heparin-binding epidermal growth factor-like growth factor.* Gene, 1996. **169**(2): p. 291-292.
110. Nakagawa, T., et al., *Amino-terminal Processing of Cell Surface Heparin-binding Epidermal Growth Factor-like Growth Factor Up-regulates Its Juxtacrine but Not Its Paracrine Growth Factor Activity*.* Journal of Biological Chemistry, 1996. **271**(48): p. 30858-30863.

111. Yan, Y., K. Shirakabe, and Z. Werb, *The metalloprotease Kuzbanian (ADAM10) mediates the transactivation of EGF receptor by G protein–coupled receptors.* The Journal of Cell Biology, 2002. **158**: p. 221 - 226.
112. Nanba, D., et al., *Proteolytic release of the carboxy-terminal fragment of proHB-EGF causes nuclear export of PLZF.* J Cell Biol, 2003. **163**(3): p. 489-502.
113. Blotnick, S., et al., *T lymphocytes synthesize and export heparin-binding epidermal growth factor-like growth factor and basic fibroblast growth factor, mitogens for vascular cells and fibroblasts: differential production and release by CD4+ and CD8+ T cells.* Proc Natl Acad Sci U S A, 1994. **91**(8): p. 2890-94.
114. Geiger-Maor, A., et al., *Macrophages Regulate the Systemic Response to DNA Damage by a Cell Nonautonomous Mechanism.* Cancer Res, 2015. **75**(13): p. 2663-73.
115. Farahnak, S., et al., *HB-EGF Synthesized by CD4 T Cells Modulates Allergic Airway Eosinophilia by Regulating IL-5 Synthesis.* J Immunol, 2019. **203**(1): p. 39-47.
116. Singh, B., G. Carpenter, and R. Coffey, *EGF receptor ligands: recent advances [version 1; peer review: 3 approved].* F1000Research, 2016. **5**(2270).
117. Naglich, J.G., et al., *Expression cloning of a diphtheria toxin receptor: Identity with a heparin-binding EGF-like growth factor precursor.* Cell, 1992. **69**(6): p. 1051-1061.
118. Bazley, L.A. and W.J. Gullick, *The epidermal growth factor receptor family.* Endocr Relat Cancer, 2005. **12 Suppl 1**: p. S17-27.
119. Rodemann, H.P., K. Dittmann, and M. Toulany, *Radiation-induced EGFR-signaling and control of DNA-damage repair.* Int J Radiat Biol, 2007. **83**(11-12): p. 781-91.
120. Ang, K.K., et al., *Impact of epidermal growth factor receptor expression on survival and pattern of relapse in patients with advanced head and neck carcinoma.* Cancer Res, 2002. **62**(24): p. 7350-6.
121. Das, A.K., et al., *Somatic mutations in the tyrosine kinase domain of epidermal growth factor receptor (EGFR) abrogate EGFR-mediated radioprotection in non-small cell lung carcinoma.* Cancer Res, 2007. **67**(11): p. 5267-74.
122. Fiano, V., et al., *PAkt, cyclin D1 and p27/Kip.1 in glioblastomas with and without EGFR amplification and PTEN mutation.* Anticancer Res, 2004. **24**(5a): p. 2643-7.
123. Park, C.M., et al., *Ionizing radiation enhances matrix metalloproteinase-2 secretion and invasion of glioma cells through Src/epidermal growth factor receptor-mediated p38/Akt and phosphatidylinositol 3-kinase/Akt signaling pathways.* Cancer Res, 2006. **66**(17): p. 8511-9.
124. Toledano-Katchalski, H., et al., *Protein tyrosine phosphatase epsilon inhibits signaling by mitogen-activated protein kinases.* Mol Cancer Res, 2003. **1**(7): p. 541-50.
125. Toulany, M., M. Baumann, and H.P. Rodemann, *Stimulated PI3K-AKT signaling mediated through ligand or radiation-induced EGFR depends indirectly, but not directly, on constitutive K-Ras activity.* Mol Cancer Res, 2007. **5**(8): p. 863-72.
126. Ravid, T., et al., *Epidermal growth factor receptor activation under oxidative stress fails to promote c-Cbl mediated down-regulation.* J Biol Chem, 2002. **277**(34): p. 31214-9.
127. Fortini, P. and E. Dogliotti, *Base damage and single-strand break repair: mechanisms and functional significance of short- and long-patch repair subpathways.* DNA Repair (Amst), 2007. **6**(4): p. 398-409.
128. Demin, A.A., et al., *XRCC1 prevents toxic PARP1 trapping during DNA base excision repair.* Mol Cell, 2021. **81**(14): p. 3018-3030.e5.
129. Nicolai, S., et al., *DNA repair and aging: the impact of the p53 family.* Aging (Albany NY), 2015. **7**(12): p. 1050-65.
130. Lequin, R.M., *Enzyme immunoassay (EIA)/enzyme-linked immunosorbent assay (ELISA).* Clin Chem, 2005. **51**(12): p. 2415-8.
131. Kurien, B.T. and R.H. Scofield, *Western blotting.* Methods, 2006. **38**(4): p. 283-93.

132. Yates Iii, J.R., *A century of mass spectrometry: from atoms to proteomes.* Nature Methods, 2011. **8**(8): p. 633-637.
133. Gillet, L.C., A. Leitner, and R. Aebersold, *Mass Spectrometry Applied to Bottom-Up Proteomics: Entering the High-Throughput Era for Hypothesis Testing.* Annual Review of Analytical Chemistry, 2016. **9**(1): p. 449-472.
134. Fenn, J.B., et al., *Electrospray Ionization for Mass Spectrometry of Large Biomolecules.* Science, 1989. **246**(4926): p. 64-71.
135. Makarov, A., *Electrostatic Axially Harmonic Orbital Trapping: A High-Performance Technique of Mass Analysis.* Analytical Chemistry, 2000. **72**(6): p. 1156-1162.
136. De Hoffmann, E. and V. Stroobant, *Mass spectrometry: principles and applications*. 2007: John Wiley & Sons.
137. Sinitcyn, P., J.D. Rudolph, and J. Cox, *Computational Methods for Understanding Mass Spectrometry–Based Shotgun Proteomics Data.* Annual Review of Biomedical Data Science, 2018. **1**(1): p. 207-234.
138. Cox, J. and M. Mann, *MaxQuant enables high peptide identification rates, individualized p.p.b.-range mass accuracies and proteome-wide protein quantification.* Nat Biotechnol, 2008. **26**(12): p. 1367-72.
139. Cox, J., et al., *Accurate proteome-wide label-free quantification by delayed normalization and maximal peptide ratio extraction, termed MaxLFQ.* Mol Cell Proteomics, 2014. **13**(9): p. 2513-26.
140. Dai, D.F., et al., *Global proteomics and pathway analysis of pressure-overload-induced heart failure and its attenuation by mitochondrial-targeted peptides.* Circ Heart Fail, 2013. **6**(5): p. 1067-76.
141. Gatto, L. and A. Christoforou, *Using R and Bioconductor for proteomics data analysis.* Biochim Biophys Acta, 2014. **1844**(1 Pt A): p. 42-51.
142. Tyanova, S., et al., *The Perseus computational platform for comprehensive analysis of (prote)omics data.* Nat Methods, 2016. **13**(9): p. 731-40.
143. Aguilan, J.T., K. Kulej, and S. Sidoli, *Guide for protein fold change and p-value calculation for non-experts in proteomics.* Mol Omics, 2020. **16**(6): p. 573-582.
144. Ren, Z., W.-L. Du, and X. Wen, *The Psychological Effects of Digital Companies' Employees during the Phase of COVID-19 Pandemic Extracted from Online Employee Reviews.* Sustainability, 2022.
145. Volman, Y., et al., *DNA damage alters EGFR signaling and reprograms cellular response via Mre-11.* Scientific Reports, 2022. **12**(1): p. 5760.
146. Madeira, F., et al., *Search and sequence analysis tools services from EMBL-EBI in 2022.* Nucleic Acids Res, 2022. **50**(W1): p. W276-9.
147. Luo, S., et al., *Synergistic effects of acitretin and narrow-band UVB on inducing the expression of heparin-binding epidermal-growth-factor-like growth factor in normal human keratinocytes.* Arch Dermatol Res, 2007. **299**(8): p. 409-13.
148. Stanley, E.R., D.M. Chen, and H.S. Lin, *Induction of macrophage production and proliferation by a purified colony stimulating factor.* Nature, 1978. **274**(5667): p. 168-70.
149. Hamilton, J.A., et al., *Stimulation of macrophage plasminogen activator activity by colony-stimulating factors.* J Cell Physiol, 1980. **103**(3): p. 435-45.
150. Yotsumoto, F., et al., *Validation of HB-EGF and amphiregulin as targets for human cancer therapy.* Biochemical and Biophysical Research Communications, 2008. **365**(3): p. 555-561.
151. Ramani, T., et al., *Cytokines: The Good, the Bad, and the Deadly.* Int J Toxicol, 2015. **34**(4): p. 355-65.
152. Bernard, J.J., R.L. Gallo, and J. Krutmann, *Photoimmunology: how ultraviolet radiation affects the immune system.* Nature Reviews Immunology, 2019. **19**(11): p. 688-701.

153. Grandjean-Laquerriere, A., et al., *Differential regulation of TNF-α, IL-6 and IL-10 in UVB-irradiated human keratinocytes via cyclic AMP/protein kinase A pathway.* Cytokine, 2003. **23**(4): p. 138-149.
154. Tang, S.C., et al., *Topical application of glycolic acid suppresses the UVB induced IL-6, IL-8, MCP-1 and COX-2 inflammation by modulating NF-κB signaling pathway in keratinocytes and mice skin.* J Dermatol Sci, 2017. **86**(3): p. 238-248.
155. de Vos, S., et al., *Post-transcriptional regulation of interleukin-6 gene expression in human keratinocytes by ultraviolet B radiation.* J Invest Dermatol, 1994. **103**(1): p. 92-6.
156. Raziyeva, K., et al., *Immunology of Acute and Chronic Wound Healing.* Biomolecules, 2021. **11**(5).
157. Kupper, T.S., et al., *Human keratinocytes contain mRNA indistinguishable from monocyte interleukin 1 alpha and beta mRNA. Keratinocyte epidermal cell-derived thymocyte-activating factor is identical to interleukin 1.* J Exp Med, 1986. **164**(6): p. 2095-100.
158. Korhonen, E., et al., *Only IL-1β release is inflammasome-dependent upon ultraviolet B irradiation although IL-18 is also secreted.* Faseb j, 2020. **34**(5): p. 6437-6448.
159. Leverkus, M., et al., *Post-transcriptional regulation of UV induced TNF-alpha expression.* J Invest Dermatol, 1998. **110**(4): p. 353-7.
160. Singh, S., D. Anshita, and V. Ravichandiran, *MCP-1: Function, regulation, and involvement in disease.* Int Immunopharmacol, 2021. **101**(Pt B): p. 107598.
161. Behfar, S., et al., *A brief look at the role of monocyte chemoattractant protein-1 (CCL2) in the pathophysiology of psoriasis.* Cytokine, 2018. **110**: p. 226-231.
162. Wang, Y., et al., *Nonredundant roles of keratinocyte-derived IL-34 and neutrophil-derived CSF1 in Langerhans cell renewal in the steady state and during inflammation.* Eur J Immunol, 2016. **46**(3): p. 552-9.
163. Hogan, A.D. and A.W. Burks, *Epidermal Langerhans' cells and their function in the skin immune system.* Ann Allergy Asthma Immunol, 1995. **75**(1): p. 5-10; quiz 10-2.
164. Mah, L.J., A. El-Osta, and T.C. Karagiannis, *γH2AX: a sensitive molecular marker of DNA damage and repair.* Leukemia, 2010. **24**(4): p. 679-686.
165. Engeland, K., *Cell cycle regulation: p53-p21-RB signaling.* Cell Death Differ, 2022. **29**(5): p. 946-960.
166. el-Deiry, W.S., et al., *WAF1/CIP1 is induced in p53-mediated G1 arrest and apoptosis.* Cancer Res, 1994. **54**(5): p. 1169-74.
167. Broude, E.V., et al., *p21 (CDKN1A) is a negative regulator of p53 stability.* Cell Cycle, 2007. **6**(12): p. 1468-71.
168. Chen, J., *The Cell-Cycle Arrest and Apoptotic Functions of p53 in Tumor Initiation and Progression.* Cold Spring Harb Perspect Med, 2016. **6**(3): p. a026104.
169. Chatterjee, N. and G.C. Walker, *Mechanisms of DNA damage, repair, and mutagenesis.* Environ Mol Mutagen, 2017. **58**(5): p. 235-263.
170. Zhang, X., M. Yin, and J. Hu, *Nucleotide excision repair: a versatile and smart toolkit.* Acta Biochim Biophys Sin (Shanghai), 2022. **54**(6): p. 807-819.
171. Alexa, M., A. Hasenburg, and M.J. Battista, *The TCGA Molecular Classification of Endometrial Cancer and Its Possible Impact on Adjuvant Treatment Decisions.* Cancers (Basel), 2021. **13**(6).
172. Casey, L. and N. Singh, *POLE, MMR, and MSI Testing in Endometrial Cancer: Proceedings of the ISGyP Companion Society Session at the USCAP 2020 Annual Meeting.* Int J Gynecol Pathol, 2021. **40**(1): p. 5-16.
173. Bruhn, C., et al., *The essential function of the MRN complex in the resolution of endogenous replication intermediates.* Cell Rep, 2014. **6**(1): p. 182-95.
174. Chang, H.H.Y., et al., *Non-homologous DNA end joining and alternative pathways to double-strand break repair.* Nat Rev Mol Cell Biol, 2017. **18**(8): p. 495-506.

175. Howell, B.G., et al., *Microarray analysis of UVB-regulated genes in keratinocytes: downregulation of angiogenesis inhibitor thrombospondin-1.* J Dermatol Sci, 2004. **34**(3): p. 185-94.
176. Li, Y., et al., *Mouse skin-derived precursors alleviates ultraviolet B irradiation damage via early activation of TGF-β/Smad pathway by thrombospondin1.* Cell Cycle, 2020. **19**(4): p. 492-503.
177. Karimian, A., Y. Ahmadi, and B. Yousefi, *Multiple functions of p21 in cell cycle, apoptosis and transcriptional regulation after DNA damage.* DNA Repair (Amst), 2016. **42**: p. 63-71.
178. Malumbres, M., *Cyclin-dependent kinases.* Genome Biol, 2014. **15**(6): p. 122.
179. Isenberg, J.S. and D.D. Roberts, *THBS1 (thrombospondin-1).* Atlas Genet Cytogenet Oncol Haematol, 2020. **24**(8): p. 291-299.
180. Suzuki, M., et al., *Matrix metalloproteinase-3 releases active heparin-binding EGF-like growth factor by cleavage at a specific juxtamembrane site.* J Biol Chem, 1997. **272**(50): p. 31730-7.
181. Choi, D.H., et al., *A novel intracellular role of matrix metalloproteinase-3 during apoptosis of dopaminergic cells.* Journal of Neurochemistry, 2008. **106**(1): p. 405-415.
182. Malagón, T., et al., *Cross-protective efficacy of two human papillomavirus vaccines: a systematic review and meta-analysis.* The Lancet Infectious Diseases, 2012. **12**(10): p. 781-789.
183. Ahmels, M., et al., *Next generation L2-based HPV vaccines cross-protect against cutaneous papillomavirus infection and tumor development.* Front Immunol, 2022. **13**: p. 1010790.
184. Canali, E., et al., *A high-performance thioredoxin-based scaffold for peptide immunogen construction: proof-of-concept testing with a human papillomavirus epitope.* Sci Rep, 2014. **4**: p. 4729.
185. Ogun, S.A., et al., *The oligomerization domain of C4-binding protein (C4bp) acts as an adjuvant, and the fusion protein comprised of the 19-kilodalton merozoite surface protein 1 fused with the murine C4bp domain protects mice against malaria.* Infect Immun, 2008. **76**(8): p. 3817-23.
186. Day, P.M., et al., *A Human Papillomavirus (HPV) In Vitro Neutralization Assay That Recapitulates the In Vitro Process of Infection Provides a Sensitive Measure of HPV L2 Infection-Inhibiting Antibodies.* Clinical and Vaccine Immunology, 2012. **19**(7): p. 1075-1082.
187. Schiller, J.T., P.M. Day, and R.C. Kines, *Current understanding of the mechanism of HPV infection.* Gynecol Oncol, 2010. **118**(1 Suppl): p. S12-7.
188. Hasche, D. and F. Rösl, *Mastomys Species as Model Systems for Infectious Diseases.* Viruses, 2019. **11**(2).
189. Tang-Huau, T.L., et al., *Mastomys natalensis Has a Cellular Immune Response Profile Distinct from Laboratory Mice.* Viruses, 2021. **13**(5).
190. Tsai, C.J., et al., *Synonymous mutations and ribosome stalling can lead to altered folding pathways and distinct minima.* J Mol Biol, 2008. **383**(2): p. 281-91.
191. Moreira-Ramos, S., et al., *Synonymous mutations in the phosphoglycerate kinase 1 gene induce an altered response to protein misfolding in Schizosaccharomyces pombe.* Front Microbiol, 2022. **13**: p. 1074741.
192. Nagaraj, N.S., O.V. Singh, and N.B. Merchant, *Proteomics: a strategy to understand the novel targets in protein misfolding and cancer therapy.* Expert Rev Proteomics, 2010. **7**(4): p. 613-23.
193. Ridley, R.G., *Antibodies: A Laboratory Manual. Edited by Ed Harlow and David Lane. Cold Spring Harbor: Cold Spring Harbor Laboratory. New York. 1988. 726 pages. Paper $50.00. ISBN 0 87969 314 2.* Genetics Research, 1989. **54**(2): p. 161-161.
194. Pillai-Kastoori, L., A.R. Schutz-Geschwender, and J.A. Harford, *A systematic approach to quantitative Western blot analysis.* Anal Biochem, 2020. **593**: p. 113608.
195. Taylor, S.C., et al., *A Defined Methodology for Reliable Quantification of Western Blot Data.* Molecular Biotechnology, 2013. **55**(3): p. 217-226.

196. Peach, M., et al., *Solubilization of Proteins: The Importance of Lysis Buffer Choice*, in *Western Blotting: Methods and Protocols*, B.T. Kurien and R.H. Scofield, Editors. 2015, Springer New York: New York, NY. p. 49-60.
197. Miskiewicz, E.I. and D.J. MacPhee, *Lysis Buffer Choices Are Key Considerations to Ensure Effective Sample Solubilization for Protein Electrophoresis*, in *Electrophoretic Separation of Proteins: Methods and Protocols*, B.T. Kurien and R.H. Scofield, Editors. 2019, Springer New York: New York, NY. p. 61-72.
198. Janes, K.A., *An analysis of critical factors for quantitative immunoblotting.* Sci Signal, 2015. **8**(371): p. rs2.
199. Kulesz-Martin, M., et al., *Properties of carcinogen altered mouse epidermal cells resistant to calcium-induced terminal differentiation.* Carcinogenesis, 1983. **4**(11): p. 1367-1377.
200. Santarpia, L., S.M. Lippman, and A.K. El-Naggar, *Targeting the MAPK-RAS-RAF signaling pathway in cancer therapy.* Expert Opin Ther Targets, 2012. **16**(1): p. 103-19.
201. Kelso, A., *Cytokines: principles and prospects.* Immunol Cell Biol, 1998. **76**(4): p. 300-17.
202. Borish, L.C. and J.W. Steinke, *2. Cytokines and chemokines.* J Allergy Clin Immunol, 2003. **111**(2 Suppl): p. S460-75.
203. Bruunsgaard, H., M. Pedersen, and B.K. Pedersen, *Aging and proinflammatory cytokines.* Curr Opin Hematol, 2001. **8**(3): p. 131-6.
204. Chow, K.Y., et al., *A pivotal role for CXCL12 signaling in HPV-mediated transformation of keratinocytes: clues to understanding HPV-pathogenesis in WHIM syndrome.* Cell Host Microbe, 2010. **8**(6): p. 523-33.
205. Meuris, F., et al., *The CXCL12/CXCR4 Signaling Pathway: A New Susceptibility Factor in Human Papillomavirus Pathogenesis.* PLoS Pathog, 2016. **12**(12): p. e1006039.
206. Gardella, B., et al., *Cytokines and chemokines levels in primary HPV infection: a pilot study.* Acta Virol, 2021. **65**(1): p. 75-81.
207. Woodworth, C.D., *HPV innate immunity.* Front Biosci, 2002. **7**: p. d2058-71.
208. Williams, V.M., et al., *HPV-DNA integration and carcinogenesis: putative roles for inflammation and oxidative stress.* Future Virol, 2011. **6**(1): p. 45-57.
209. Boccardo, E., A.P. Lepique, and L.L. Villa, *The role of inflammation in HPV carcinogenesis.* Carcinogenesis, 2010. **31**(11): p. 1905-12.
210. Balkwill, F. and A. Mantovani, *Inflammation and cancer: back to Virchow?* Lancet, 2001. **357**(9255): p. 539-45.
211. Tampa, M., et al., *The Role of Beta HPV Types and HPV-Associated Inflammatory Processes in Cutaneous Squamous Cell Carcinoma.* J Immunol Res, 2020. **2020**: p. 5701639.
212. Fernandes, J.V., et al., *Link between chronic inflammation and human papillomavirus-induced carcinogenesis (Review).* Oncol Lett, 2015. **9**(3): p. 1015-1026.
213. Pacini, L., et al., *UV Radiation Activates Toll-Like Receptor 9 Expression in Primary Human Keratinocytes, an Event Inhibited by Human Papillomavirus 38 E6 and E7 Oncoproteins.* J Virol, 2017. **91**(19).
214. Jackson, R., S. Eade, and I. Zehbe, *An epithelial organoid model with Langerhans cells for assessing virus-host interactions.* Philos Trans R Soc Lond B Biol Sci, 2019. **374**(1773): p. 20180288.
215. Mehta, H., et al., *Inflammatory Skin Disorders: Monocyte-Derived Cells Take Center Stage.* Front Immunol, 2021. **12**: p. 691806.
216. Berres, M.L., M. Merad, and C.E. Allen, *Progress in understanding the pathogenesis of Langerhans cell histiocytosis: back to Histiocytosis X?* Br J Haematol, 2015. **169**(1): p. 3-13.
217. Wang, J.W., et al., *Roles of Fc Domain and Exudation in L2 Antibody-Mediated Protection against Human Papillomavirus.* J Virol, 2018. **92**(15).

218. Ginhoux, F. and S. Jung, *Monocytes and macrophages: developmental pathways and tissue homeostasis.* Nat Rev Immunol, 2014. **14**(6): p. 392-404.
219. Yang, J., et al., *Monocyte and macrophage differentiation: circulation inflammatory monocyte as biomarker for inflammatory diseases.* Biomark Res, 2014. **2**(1): p. 1.
220. Hassanshahi, A., et al., *Macrophage-Mediated Inflammation in Skin Wound Healing.* Cells, 2022. **11**(19).
221. Rodero, M.P. and K. Khosrotehrani, *Skin wound healing modulation by macrophages.* Int J Clin Exp Pathol, 2010. **3**(7): p. 643-53.
222. Rodero, M.P., et al., *Wound-associated macrophages control collagen 1α2 transcription during the early stages of skin wound healing.* Exp Dermatol, 2013. **22**(2): p. 143-5.
223. Fang, Y., et al., *Impaired cutaneous wound healing in granulocyte/macrophage colony-stimulating factor knockout mice.* Br J Dermatol, 2007. **157**(3): p. 458-65.
224. Kölgen, W., et al., *Epidermal langerhans cell depletion after artificial ultraviolet B irradiation of human skin in vivo: apoptosis versus migration.* J Invest Dermatol, 2002. **118**(5): p. 812-7.
225. Hibma, M.H., *The immune response to papillomavirus during infection persistence and regression.* Open Virol J, 2012. **6**: p. 241-8.
226. Kelvin, D.J., et al., *Interleukin 3 and cell cycle progression.* J Cell Physiol, 1986. **127**(3): p. 403-9.
227. Lovett, D.H. and A. Larsen, *Cell cycle-dependent interleukin 1 gene expression by cultured glomerular mesangial cells.* J Clin Invest, 1988. **82**(1): p. 115-22.
228. Engeland, K., *Cell cycle arrest through indirect transcriptional repression by p53: I have a DREAM.* Cell Death Differ, 2018. **25**(1): p. 114-132.
229. Halicka, H.D., et al., *Histone H2AX phosphorylation after cell irradiation with UV-B: relationship to cell cycle phase and induction of apoptosis.* Cell Cycle, 2005. **4**(2): p. 339-45.
230. Asaithamby, A. and D.J. Chen, *Cellular responses to DNA double-strand breaks after low-dose gamma-irradiation.* Nucleic Acids Res, 2009. **37**(12): p. 3912-23.
231. Deriano, L. and D.B. Roth, *Modernizing the nonhomologous end-joining repertoire: alternative and classical NHEJ share the stage.* Annual review of genetics, 2013. **47**: p. 433-55.
232. Mazumder, D.T., et al., *Head and Neck Squamous Cell Carcinoma: Prognosis using molecular approach.* Central European Journal of Biology, 2014. **9**.
233. Wang, X.S., et al., *DNA damage-induced phosphorylation of CtIP at a conserved ATM/ATR site T855 promotes lymphomagenesis in mice.* Proc Natl Acad Sci U S A, 2021. **118**(38).
234. Williams, R.S., et al., *Structural basis for phosphorylation-dependent signaling in the DNA-damage response.* Biochem Cell Biol, 2005. **83**(6): p. 721-7.
235. Mehta, K.P.M., et al., *CHK1 phosphorylates PRIMPOL to promote replication stress tolerance.* Sci Adv, 2022. **8**(13): p. eabm0314.
236. Bakkenist, C.J. and M.B. Kastan, *DNA damage activates ATM through intermolecular autophosphorylation and dimer dissociation.* Nature, 2003. **421**(6922): p. 499-506.
237. Williams, A.B. and B. Schumacher, *p53 in the DNA-Damage-Repair Process.* Cold Spring Harb Perspect Med, 2016. **6**(5).
238. Christmann, M. and B. Kaina, *Transcriptional regulation of human DNA repair genes following genotoxic stress: trigger mechanisms, inducible responses and genotoxic adaptation.* Nucleic Acids Res, 2013. **41**(18): p. 8403-20.
239. Huang, Y.W., et al., *Antiaging and smoothness-improving properties of farnesol-based facial masks on rat skin exposed to ultraviolet B.* J Cosmet Dermatol, 2020. **19**(2): p. 540-552.
240. Santivasi, W.L. and F. Xia, *Ionizing radiation-induced DNA damage, response, and repair.* Antioxid Redox Signal, 2014. **21**(2): p. 251-9.

241. Xue, L., et al., *Regulation of ATM in DNA double strand break repair accounts for the radiosensitivity in human cells exposed to high linear energy transfer ionizing radiation.* Mutat Res, 2009. **670**(1-2): p. 15-23.
242. Komaki, Y., et al., *Glucose starvation impairs NER and γ-H2AX after UVB irradiation.* Toxicol In Vitro, 2023. **86**: p. 105503.
243. D'Errico, M., et al., *Cell type and DNA damage specific response of human skin cells to environmental agents.* Mutat Res, 2007. **614**(1-2): p. 37-47.
244. Pines, A., et al., *Differential activity of UV-DDB in mouse keratinocytes and fibroblasts: impact on DNA repair and UV-induced skin cancer.* DNA Repair (Amst), 2009. **8**(2): p. 153-61.
245. Atanassov, B., et al., *Comparison of the global genomic and transcription-coupled repair rates of different lesions in human cells.* Z Naturforsch C J Biosci, 2004. **59**(5-6): p. 445-53.
246. Bian, L., et al., *MRE11-RAD50-NBS1 complex alterations and DNA damage response: implications for cancer treatment.* Mol Cancer, 2019. **18**(1): p. 169.
247. Qiu, S. and J. Huang, *MRN complex is an essential effector of DNA damage repair.* J Zhejiang Univ Sci B, 2021. **22**(1): p. 31-37.
248. Miller, M.A., et al., *Targeting autocrine HB-EGF signaling with specific ADAM12 inhibition using recombinant ADAM12 prodomain.* Sci Rep, 2015. **5**: p. 15150.
249. Carroll, M.J., et al., *M2 macrophages induce ovarian cancer cell proliferation via a heparin binding epidermal growth factor/matrix metalloproteinase 9 intercellular feedback loop.* Oncotarget, 2016. **7**(52).
250. Eichelbaum, K., et al., *Selective enrichment of newly synthesized proteins for quantitative secretome analysis.* Nat Biotechnol, 2012. **30**(10): p. 984-90.
251. Maurer, G., B. Tarkowski, and M. Baccarini, *Raf kinases in cancer–roles and therapeutic opportunities.* Oncogene, 2011. **30**(32): p. 3477-3488.
252. Gupta, G., R. Glueck, and P.R. Patel, *HPV vaccines: Global perspectives.* Hum Vaccin Immunother, 2017. **13**(6): p. 1-4.
253. Schellenbacher, C., R.B.S. Roden, and R. Kirnbauer, *Developments in L2-based human papillomavirus (HPV) vaccines.* Virus Res, 2017. **231**: p. 166-175.
254. Huber, B., et al., *A Chimeric 18L1-45RG1 Virus-Like Particle Vaccine Cross-Protects against Oncogenic Alpha-7 Human Papillomavirus Types.* PLoS ONE, 2015. **10**.
255. Mariz, F.C., et al., *A broadly protective vaccine against cutaneous human papillomaviruses.* NPJ Vaccines, 2022. **7**(1): p. 116.
256. Vinzón, S.E., et al., *Protective Vaccination against Papillomavirus-Induced Skin Tumors under Immunocompetent and Immunosuppressive Conditions: A Preclinical Study Using a Natural Outbred Animal Model.* PLOS Pathogens, 2014. **10**(2): p. e1003924.
257. Rubio, I., et al., *The N-terminal region of the human papillomavirus L2 protein contains overlapping binding sites for neutralizing, cross-neutralizing and non-neutralizing antibodies.* Virology, 2011. **409**(2): p. 348-59.
258. Bissett, S.L., A. Godi, and S. Beddows, *The DE and FG loops of the HPV major capsid protein contribute to the epitopes of vaccine-induced cross-neutralising antibodies.* Sci Rep, 2016. **6**: p. 39730.
259. Fleury, M.J., et al., *Identification of type-specific and cross-reactive neutralizing conformational epitopes on the major capsid protein of human papillomavirus type 31.* Arch Virol, 2006. **151**(8): p. 1511-23.
260. Olczak, P., et al., *RG2-VLP: a Vaccine Designed to Broadly Protect against Anogenital and Skin Human Papillomaviruses Causing Human Cancer.* J Virol, 2022. **96**(13): p. e0056622.
261. Pattyn, J., et al., *Infection and vaccine-induced HPV-specific antibodies in cervicovaginal secretions. A review of the literature.* Papillomavirus Res, 2019. **8**: p. 100185.

262. Wang, Y., et al., *Occurrence of newly discovered human polyomaviruses in skin of liver transplant recipients and their relation with squamous cell carcinoma in situ and actinic keratosis - a single-center cohort study.* Transpl Int, 2019. **32**(5): p. 516-522.
263. Vasiljević, N., et al., *Four novel human betapapillomaviruses of species 2 preferentially found in actinic keratosis.* J Gen Virol, 2008. **89**(Pt 10): p. 2467-2474.
264. Gutzmer, R., et al., *Actinic Keratosis and Cutaneous Squamous Cell Carcinoma.* Dtsch Arztebl Int, 2019. **116**(37): p. 616-626.
265. Rymsza, A., et al., *Expression of MCM2 as a Proliferative Marker in Actinic Keratosis and Cutaneous Squamous Cell Carcinoma.* In Vivo, 2022. **36**(3): p. 1245-1251.
266. Hanahan, D., *Studies on transformation of Escherichia coli with plasmids.* J Mol Biol, 1983. **166(4): p. 557-80.**
267. Towbin, H. *Towbin H, Staehelin T & Gordon J. Electrophoretic transfer of proteins frompolyacrylatnide gels to nitrocellulose sheets: procedure and some applications. Proc. Nat. Acad. Sd. USA 76:4350-4. 1979*. 2002.
268. Strickland, J.E., et al., *Development of murine epidermal cell lines which contain an activated rasHa oncogene and form papillomas in skin grafts on athymic nude mouse hosts.* Cancer Res, 1988. **48**(1): p. 165-9.
269. Sehr, P., et al., *High-throughput pseudovirion-based neutralization assay for analysis of natural and vaccine-induced antibodies against human papillomaviruses.* PLoS One, 2013. **8**(10): p. e75677.
270. Potel, C.M., et al., *Defeating Major Contaminants in Fe(3+)- Immobilized Metal Ion Affinity Chromatography (IMAC) Phosphopeptide Enrichment.* Mol Cell Proteomics, 2018. **17**(5): p. 1028-1034.
271. Ritchie, M.E., et al., *limma powers differential expression analyses for RNA-sequencing and microarray studies.* Nucleic Acids Res, 2015. **43**(7): p. e47.
272. Kanehisa, M., et al., *KEGG for taxonomy-based analysis of pathways and genomes.* Nucleic Acids Res, 2023. **51**(D1): p. D587-d592.
273. Kanehisa, M., *Toward understanding the origin and evolution of cellular organisms.* Protein Sci, 2019. **28**(11): p. 1947-1951.
274. Kanehisa, M. and S. Goto, *KEGG: kyoto encyclopedia of genes and genomes.* Nucleic Acids Res, 2000. **28**(1): p. 27-30.
275. Fu, Y., et al., *Expression of different L1 isoforms of Mastomys natalensis papillomavirus as mechanism to circumvent adaptive immunity.* Elife, 2020. **9**.
276. MacArthur, H. and G. Walter, *Monoclonal antibodies specific for the carboxy terminus of simian virus 40 large T antigen.* J Virol, 1984. **52**(2): p. 483-91.
277. Pinto, L.A., et al., *Immunogenicity of HPV prophylactic vaccines: Serology assays and their use in HPV vaccine evaluation and development.* Vaccine, 2018. **36**(32 Pt A): p. 4792-4799.

# 9. Appendix

## 9.1. Abbreviations

| | |
|---|---|
| ADAM(s) | a disintergin and metalloproteinase(s) |
| APCs | Antigen presenting cells |
| APS | Ammonium persulfate |
| ATM | Ataxia-telangiectasia mutated |
| ATR | Ataxia telangiectasia and Rad3 related |
| BCC | basal cell carcinoma |
| BER | Base excision repair |
| bp | Base pairs |
| CBB | Casein blocking buffer |
| CCL20 | chemokine (C-C motif) ligand 20 |
| CD | Cluster of differentiation |
| cDNA | complementary DNA |
| CDS | protein coding sequence |
| CER | complete early region |
| cm | Centimeter |
| CMV | Cytomegalovirus |
| $CO_2$ | carbon dioxide |
| CPD | cyclobutene pyrimidine dimer |
| CsA | Cyclosporine A |
| CSF-1 | colony-stimulating factor-1 |
| DCs | Dendritic cells |
| DDA | data-dependent acquisition |
| ddH2O | doubly distilled water |
| DEN | diethylnitrosamine |
| dKSFM | defined keratinocyte serum-free medium |
| DMEM | Dulbecco's modified Eagle's medium |
| DMSO | Dimethyl sulfoxide |
| DNA | Deoxyribonucleic acid |
| dNTP | Deoxynucleotide triphosphate |
| DPBS | Dublecco's phosphate buffered saline |
| DSB(s) | DNA double-strand break(s) |
| E | early |
| *E. coli* | *Escherichia coli* |
| ECL | Enhanced Chemiluminescence Substrate |
| EDTA | Ethylenediaminetetraacetic acid |
| EGF | epidermal growth factor |
| EGFP | Enhanced Green Fluorescent Protein |
| EGFR | epidermal growth factor receptor |
| EGTA | Ethylene glycol tetraacetic acid |
| ELISA | Enzyme-linked immunosorbent assay |
| ERK | extracellular signal-regulated kinase |
| FA | fanconi anaemia |
| FCS | fetal calf serum |
| GGR | global genome repair |

| | |
|---|---|
| Gln | Glutamine |
| GST | Glutathione S-transferase |
| Gy | Gray |
| h | Hour(s) |
| $H_2SO_4$ | Sulfuric acid |
| HA | Hemagglutinin |
| HB-EGF | heparin-binding epidermal growth factor-like factor |
| HBS | HEPES-buffered saline |
| HBSS | Hank's balanced salt solution |
| HE | Hematoxylin and eosin |
| HEPES | 4-(2-hydroxyethyl)-1-piperazine-ethanesulfonicacid |
| HPRT1 | Hypoxanthine phosphoribosyltransferase 1 |
| HPSG | Heparan sulfate proteoglycans |
| HPV(s) | Human papillomavirus(es) |
| HR | homologous recombination |
| HRP | Horseradish peroxidase |
| HSPG | heparan sulfate proteoglycans |
| HTLV-1 | human T-lymphotropic virus-1 |
| IARC | International Agency for Research on Cancer |
| IHC | Immunohistochemistry |
| IL | interleukin |
| kb | Kilobases |
| KCl | Potassium chloride |
| kDa | Kilodalton |
| Kera5 | *Mastomys* keratinocytes |
| $KH_2PO_4$ | Potassium dihydrogen phosphate |
| KSCC | keratinizing squamous cell carcinoma |
| KSCCs | keratinizing squamous cell carcinomas |
| KSHV | Kaposi's sarcoma herpesvirus |
| L | late |
| LB | lysogeny broth |
| LC | liquid chromatography |
| LCs | Langerhans cells |
| LFC | log fold change |
| M | Mol |
| mA | Miliampère |
| MaFi | *Mastomys* fibroblast |
| MCP-1 | Monocyte chemoattractant protein-1 |
| MCSF | macrophage colony stimulating factor |
| MEM | Minimum Essential Medium |
| $MgCl_2$ | Magnesium chloride |
| $MgSO_4$ | Magnesium sulfate |
| min | Minute(s) |
| $mJ/cm^2$ | Millijoule per square centimeter |
| ml | Milliliter |
| mM | Millimol |

| | |
|---|---|
| MnPV | *Mastomys natalensis* papilloma virus |
| mRNA | Messenger RNA |
| MS | mass spectrometry |
| $Na_2HPO_4$ | Sodium dihydrogen phosphate |
| NaCl | Sodium chloride |
| NaOH | Sodium hydroxide |
| NEAA | Non-essential amino acids |
| NER | nucleotide excision repair |
| NF-κB | Nucleotide excision repair |
| NHEJ | Non-homologous end-joining |
| nKSCC | non-keratinizing squamous cell carcinoma |
| nm | Nanometer |
| NMSC | non-melanoma skin cancer |
| NP-40 | Nonidet P-40 |
| ORF(s) | Open reading frame(s) |
| PAGE | Polyacrylamide gel electrophoresis |
| PAMP | pathogen-associated molecular pattern |
| PBS | Phosphate-buffered saline |
| PCR | Polymerase chain reaction |
| PFA | Paraformaldehyde |
| PV | Papillomavirus |
| PVDF | Polyvinylidene fluoride |
| qPCR | Quantitative polymerase chain reaction |
| Rb | Retinoblastom-Protein |
| RNA | Ribonucleic acid |
| ROS | Reactive oxygen species |
| rpm | rounds per minute |
| RT | Reverse transcription |
| SCC | Squamous cell carcinoma |
| SD | Standard deviation |
| SDS | Sodium dodecyl sulfate |
| sec | Second(s) |
| SEM | Standard error of the mean |
| SSBs | single strand breaks |
| TAE | Tris acetate EDTA |
| TBS | Tris-buffered saline |
| TBST | Tris-buffered saline + Tween20 |
| TEMED | Tetramethylethylenediamine |
| tg | transgenic |
| TLR | toll-like receptor |
| TMB | 3,3',5,5'-Tetramethylbenzidine |
| *TP53* | Tumor protein 53 |
| *Trp53* | Transformation related protein 53 |
| URR | upstream regulatory region |
| UV | Ultraviolet light |
| V | Volt |
| VLP | Virus-like particle |
| WHO | World Health Organisation |

| | |
|---|---|
| XRCC1 | X-ray repair cross-complementing protein 1 |
| µl | Microliter |
| µM | Micromol |
| µm | Micrometer |

## 9.2. Publications

Ahmels M, Mariz FC, Braspenning-Wesch I, Stephan S, Huber B, Schmidt G, Cao R, Müller M, Kirnbauer R, Rösl F, Hasche D. *Next generation L2-based HPV vaccines cross-protect against cutaneous papillomavirus infection and tumor development*. Front Immunol,13,1010790.

Hasche, D., Ahmels, M., Braspenning-Wesch, I., Stephan, S., Cao, R., Schmidt, G., Müller, M., & Rösl, F. (2022). *Isoforms of the Papillomavirus Major Capsid Protein Differ in Their Ability to Block Viral Spread and Tumor Formation*. Front Immunol, 13, 811094.

Nurjadi, D., Boutin, S., Schmidt, K., Ahmels, M., & Hasche, D. (2020). *Identification and Elimination of the Clinically Relevant Multi-Resistant Environmental Bacteria Ralstonia insidiosa in Primary Cell Culture.* Microorganisms, 8(10), 1599.

# 10. Danksagung

Ich bedanke mich insbesondere bei Prof. Dr. Frank Rösl für die Möglichkeit, ein spannendes Dissertationsthema zu bearbeiten zu dürfen und für die vielen spannenden Diskussion und kreativen Input. Zudem möchte ich mich bei Dr. Daniel Hasche für die Betreuung und Korrekturen bedanken, der das Labor mit viel Enthusiasmus und Motivation geleitet hat.
Besonderer Dank gilt auch den Mitgliedern meines TACs, Prof. Dr. Martin Müller und Prof. Dr. Baki Akgül, die mit ihren Ideen und Anregungen meine Doktorarbeit bereichert haben.

Ganz besonders bedanken möchte ich mich bei den TAs: Liebe Sonja, liebe Ilona, vielen Dank für all die Unterstützung, nicht nur bei der Durchführung und Hilfestellung bei Experimenten, sondern auch für Eure offenes Ohr und all die Lebensweisheiten, Kuchen und Kürbisse.

Liebe Regina, wir haben zwar nur kurz zusammengearbeitet, aber mit Deiner herzlichen und offenen Art habe ich eine sehr schwere Phase durchgestanden. Danke, dass Du mich und meine Launen ertragen hast und für die Unterstützung, wenn ich nicht mehr weiterwusste. Vielen Dank für die schönen Spaziergänge und lieben Worte.

Vielen, vielen Dank an Adela, Denise und Lina-Marie! Ihr habt mich motiviert, mich unterstützt und vorallem während der letzten Phase aufgebaut. Danke für all die schönen Kaffeestunden, Aperolabende und Sportsessions. Ohne Euch wäre die Zeit nicht so schön gewesen.

Vielen Dank für all die Gummibärchen und Kaffees, Max! Für die ganze Unterstützung, aufbauenden Worte und Neckereien, die mich motiviert und aufgebaut haben.

Zuletzt möchte ich meiner Familie danken: Ihr habt immer hinter mir gestanden, habt mich gepusht und mir mit Rat und Tat zur Seite gestanden. Ganz besonders möchte ich meiner Mama danken. Ohne Dich wäre ich nie so weit gekommen.